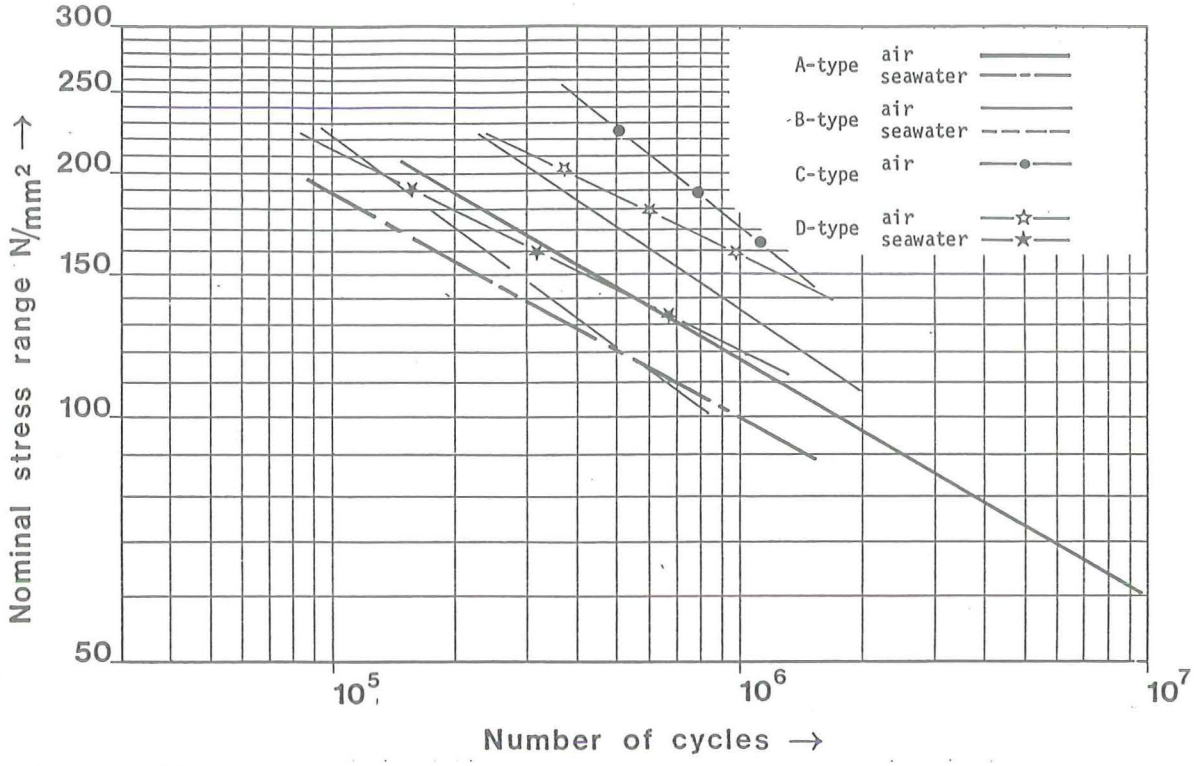

Fig. 2.2.38 Comparison of the test on the A-type, B-type, C-type and D-type 40 mm specimens.

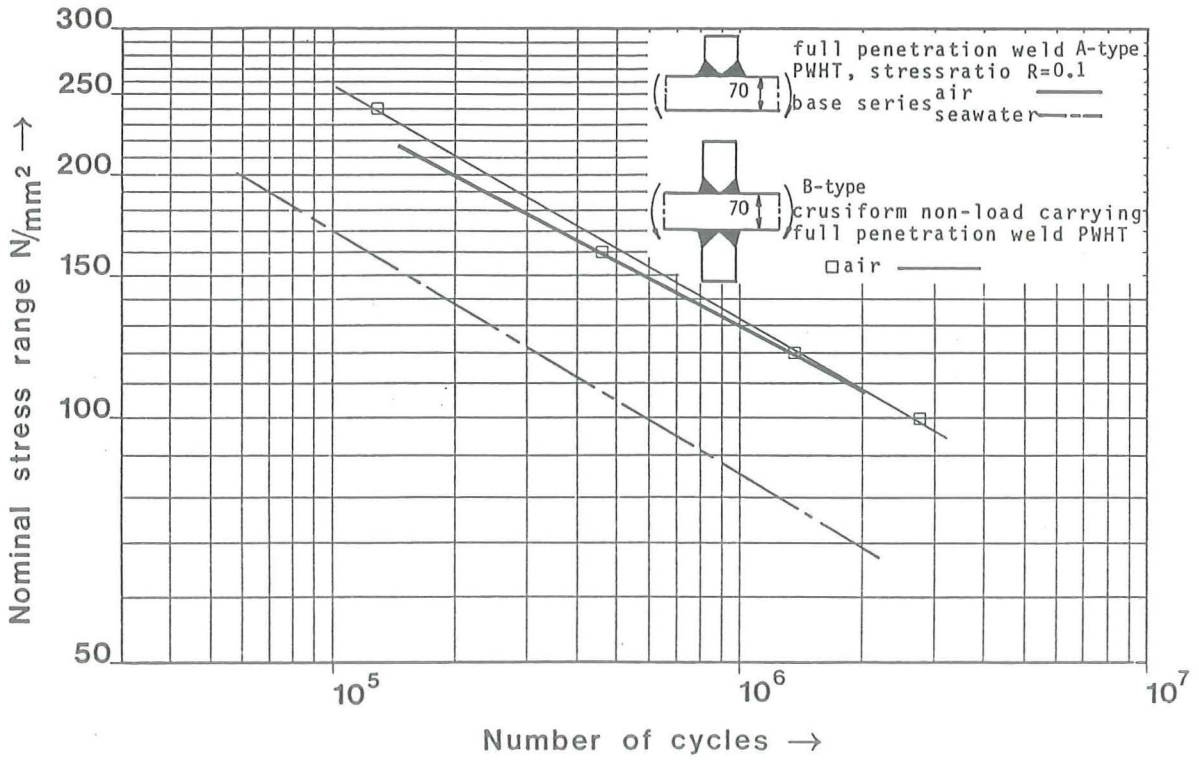

Fig. 2.2.39 Fatigue behaviour of 70 mm B-type specimens in air at a stress ratio R = 0.1.

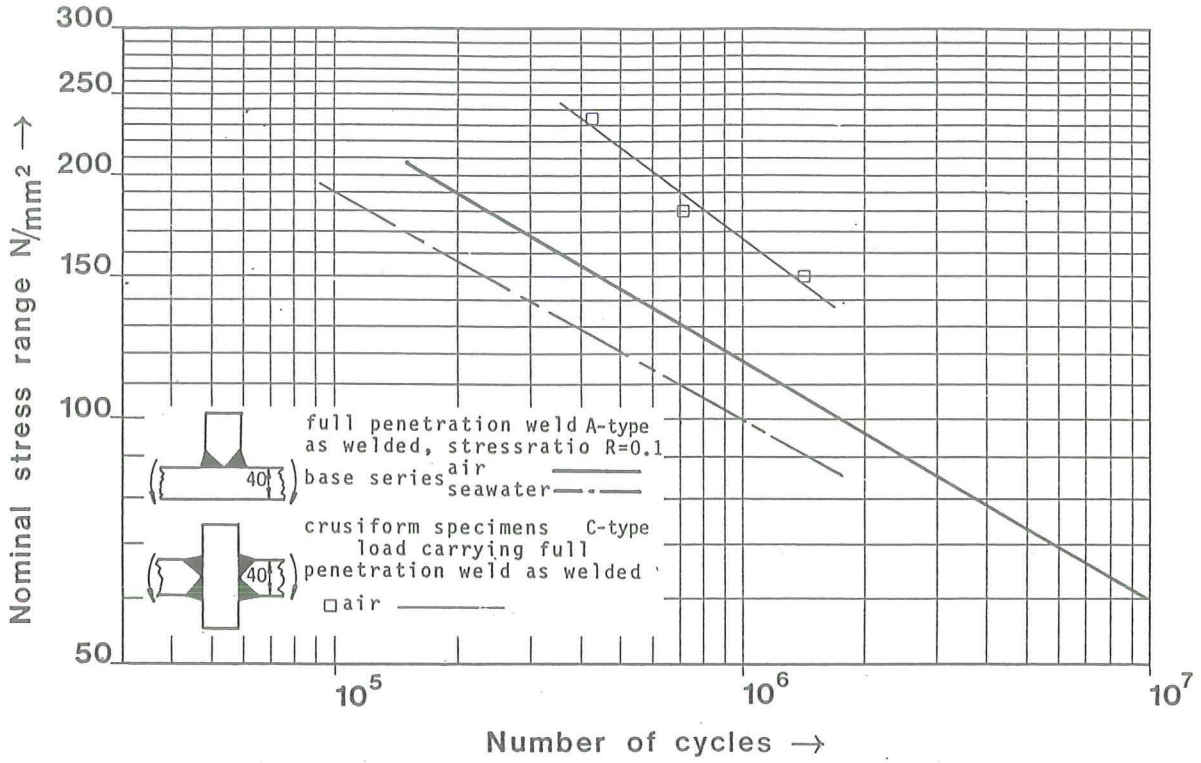

Fig. 2.2.36 Fatigue behaviour of 40 mm -type specimens in air at a stress ratio R = 0.1.

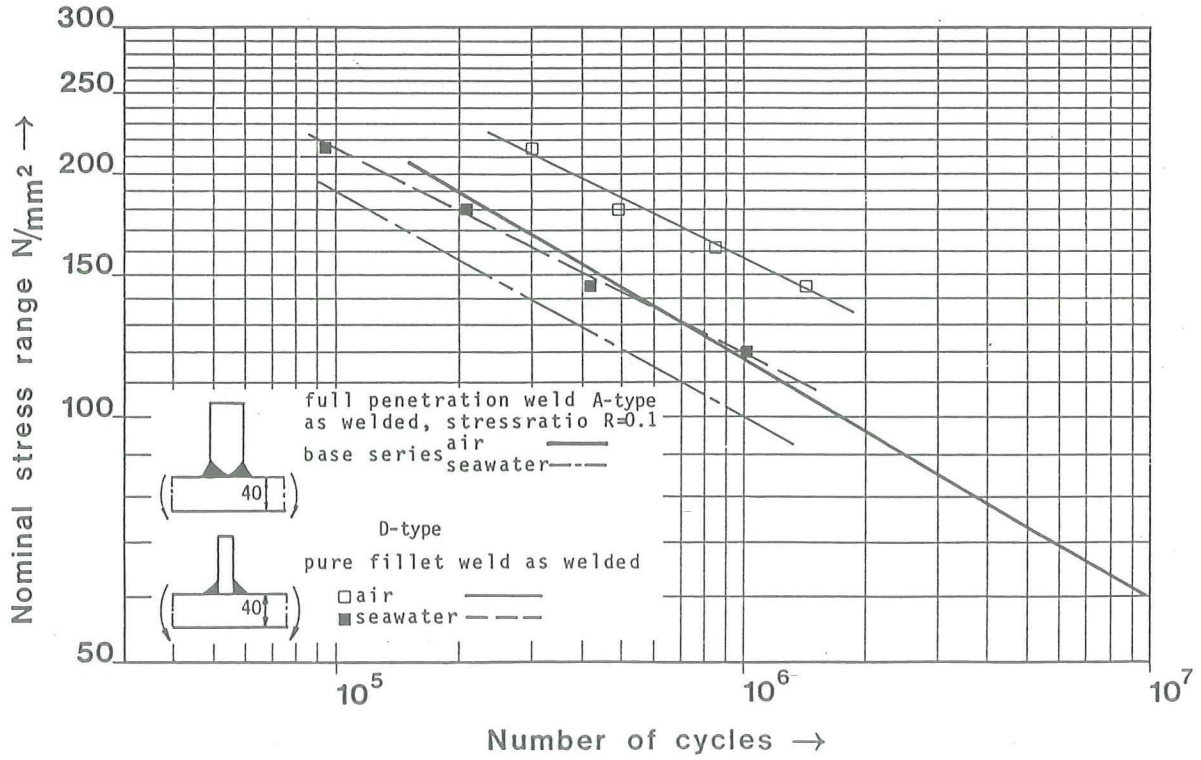

Fig. 2.2.37 Fatigue behaviour of 40 mm D-type specimens in air and seawater at a stress ratio R = 0.1.

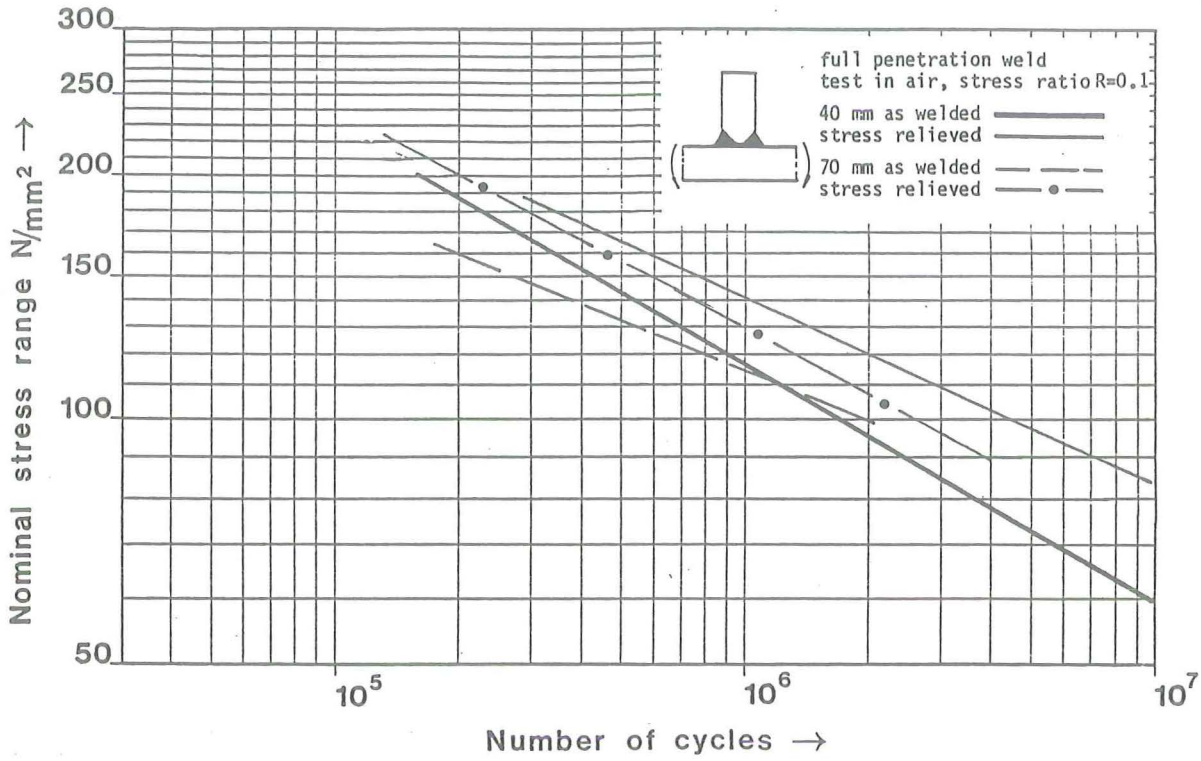

Fig. 2.2.34 Fatigue behaviour of 40 mm and 70 mm T-shape specimens (as welded and stress relieved) in air at a stress ratio R = 0.1.

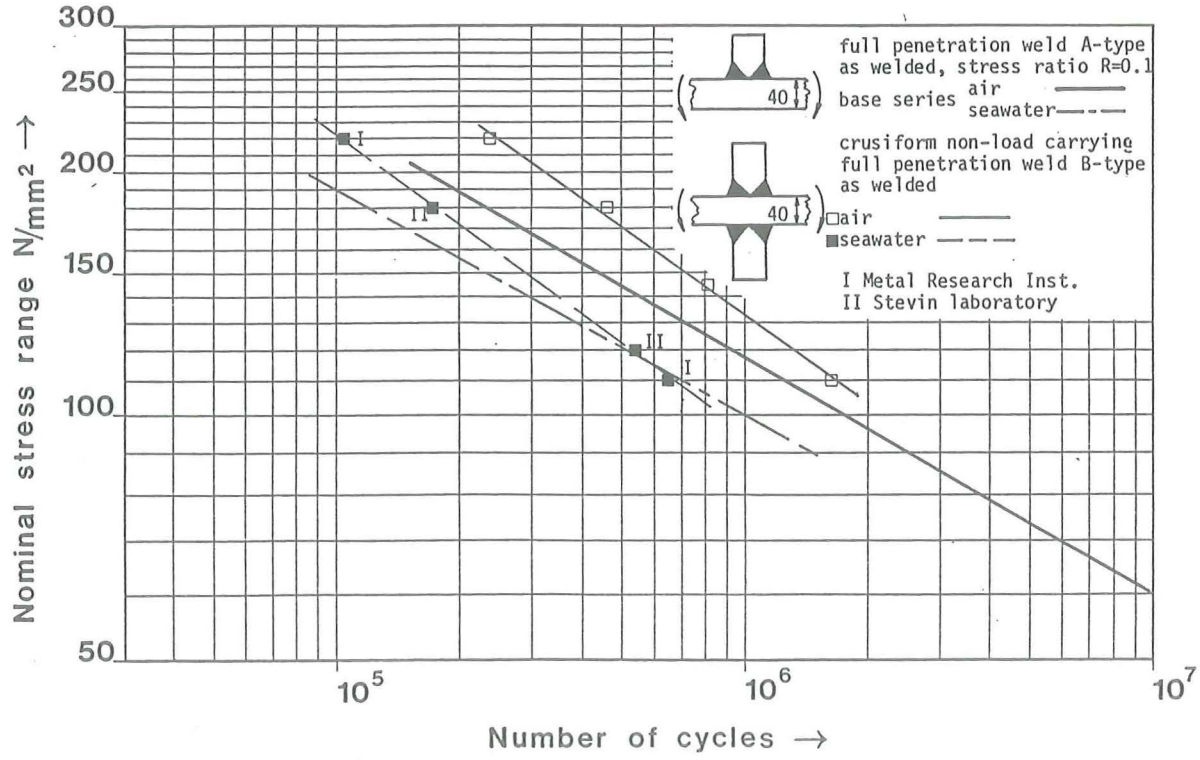

Fig. 2.2.35 Fatigue behaviour of 40 mm B-type specimens in air and seawater at a stress ratio R = 0.1.

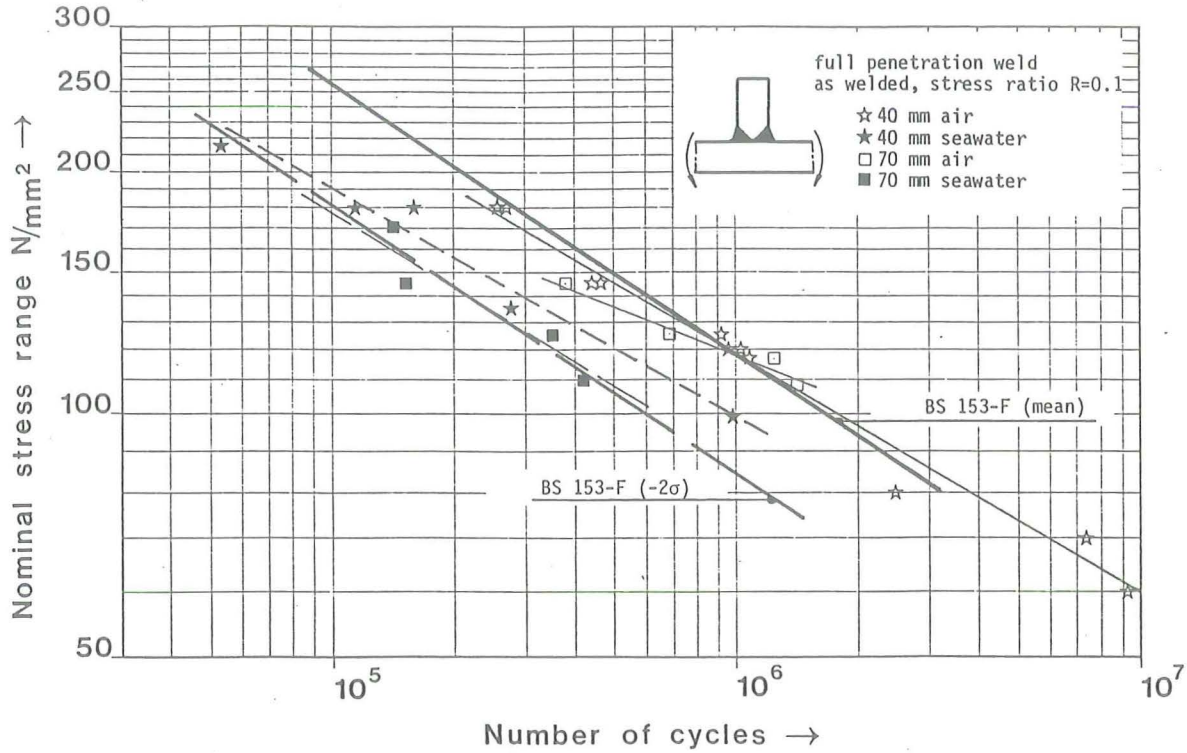

Fig. 2.2.32 Fatigue behaviour of 40 mm and 70 mm T-shape specimens (as welded) in air and seawater at a stress ratio R = 0.1.

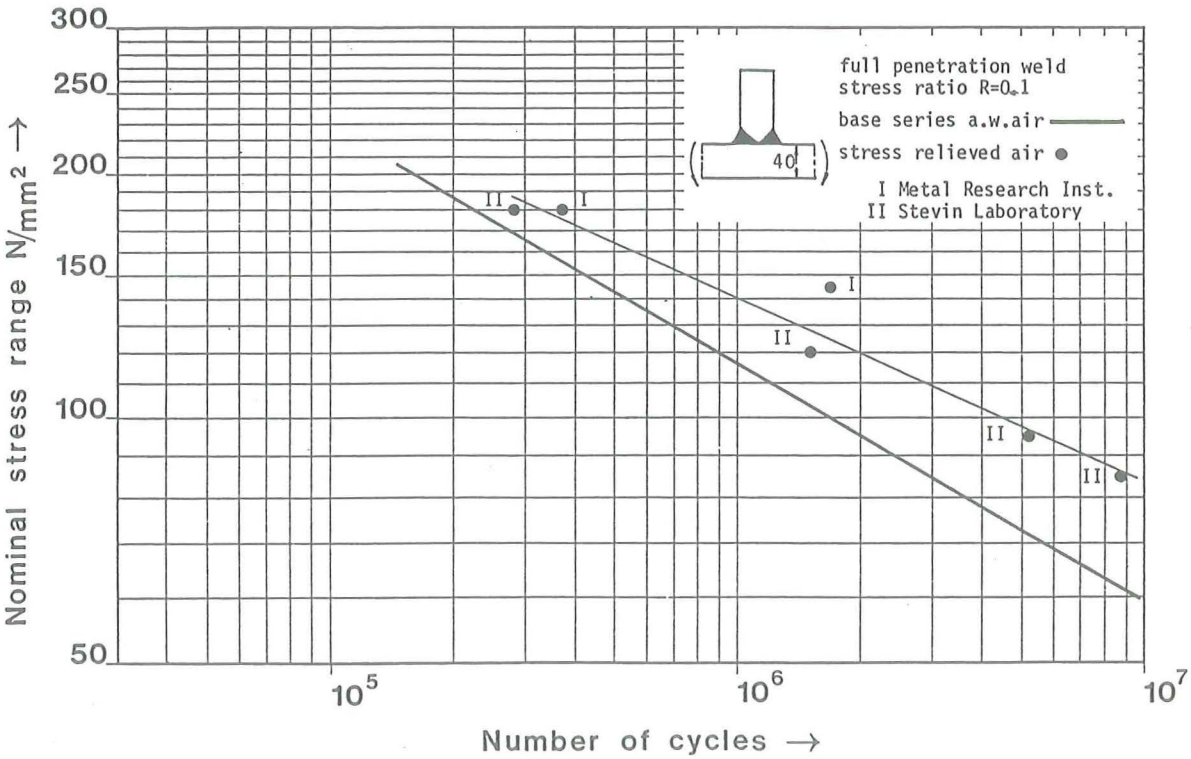

Fig. 2.2.33 Fatigue behaviour of 40 mm T-shape specimens (as welded and stress relieved) in air at a stress ratio R = 0.1.

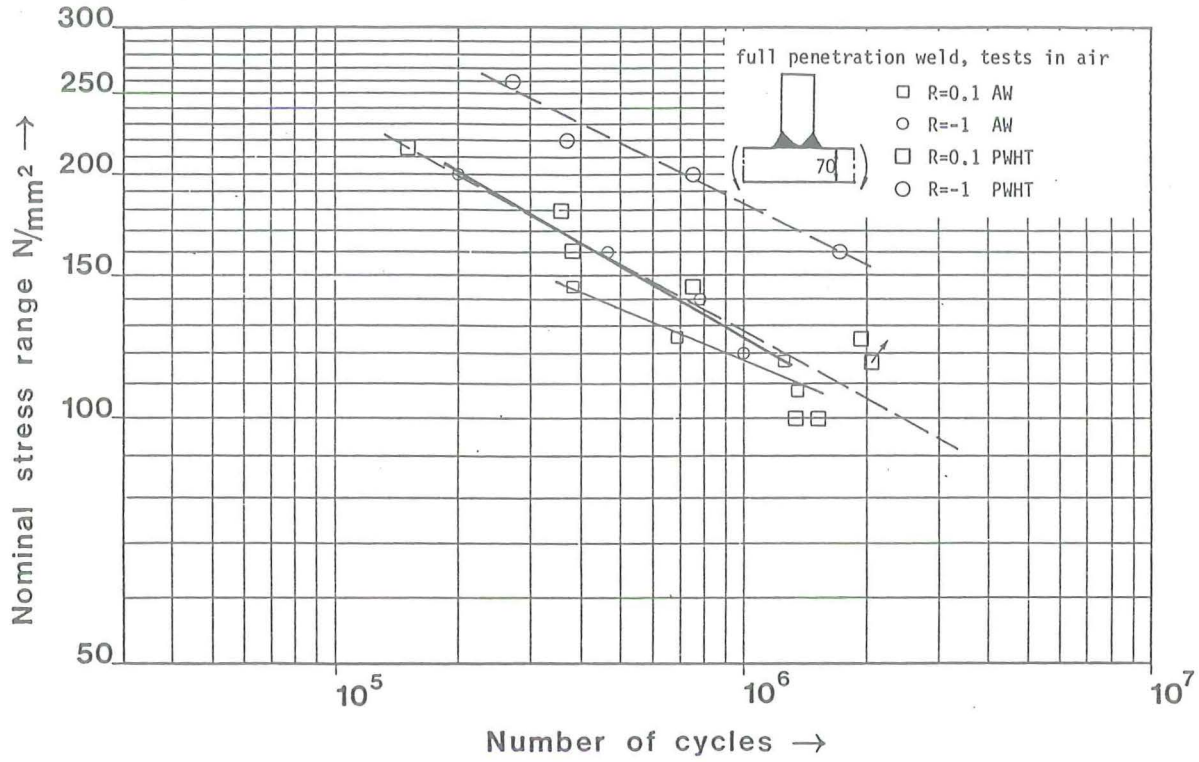

Fig. 2.2.30 Fatigue behaviour of 70 mm T-shape specimens (as welded and stress relieved) in air at stress ratios R = 0.1 and R = -1.

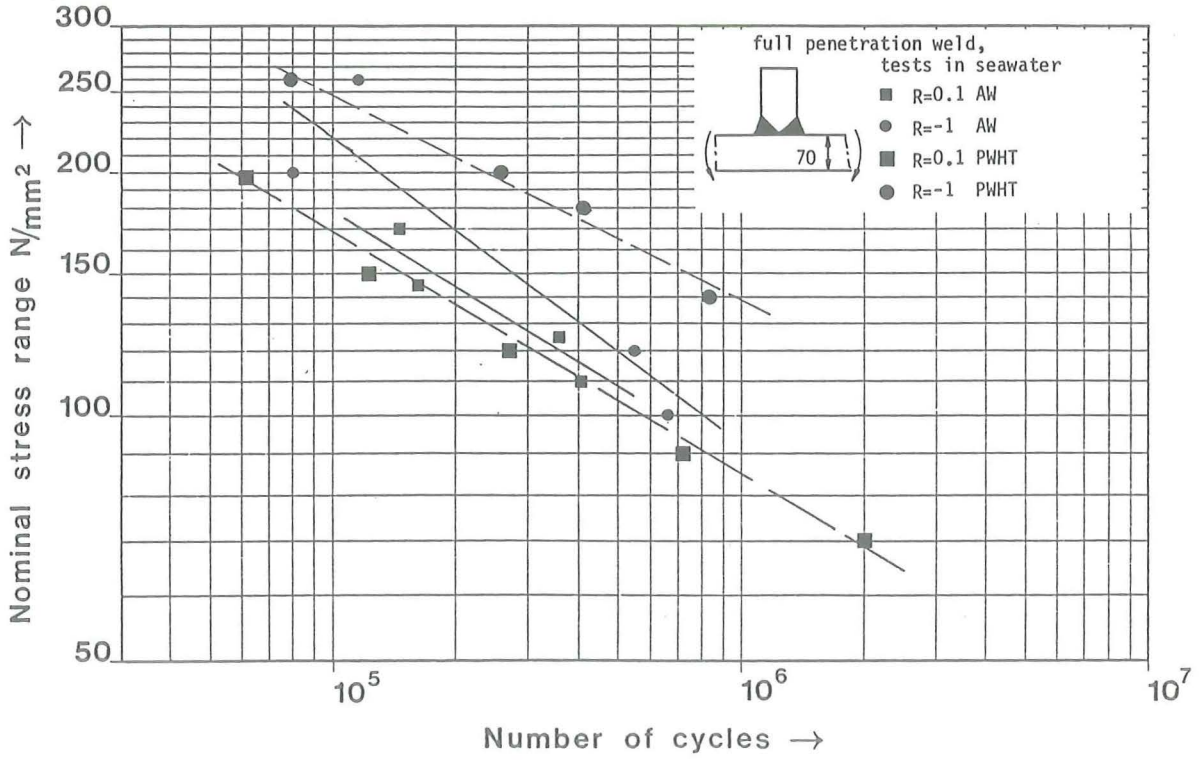

Fig. 2.2.31 Fatigue behaviour of 70 mm T-shape specimens (as welded and stress relieved) in seawater at stress ratios R = 0.1 and R = -1.

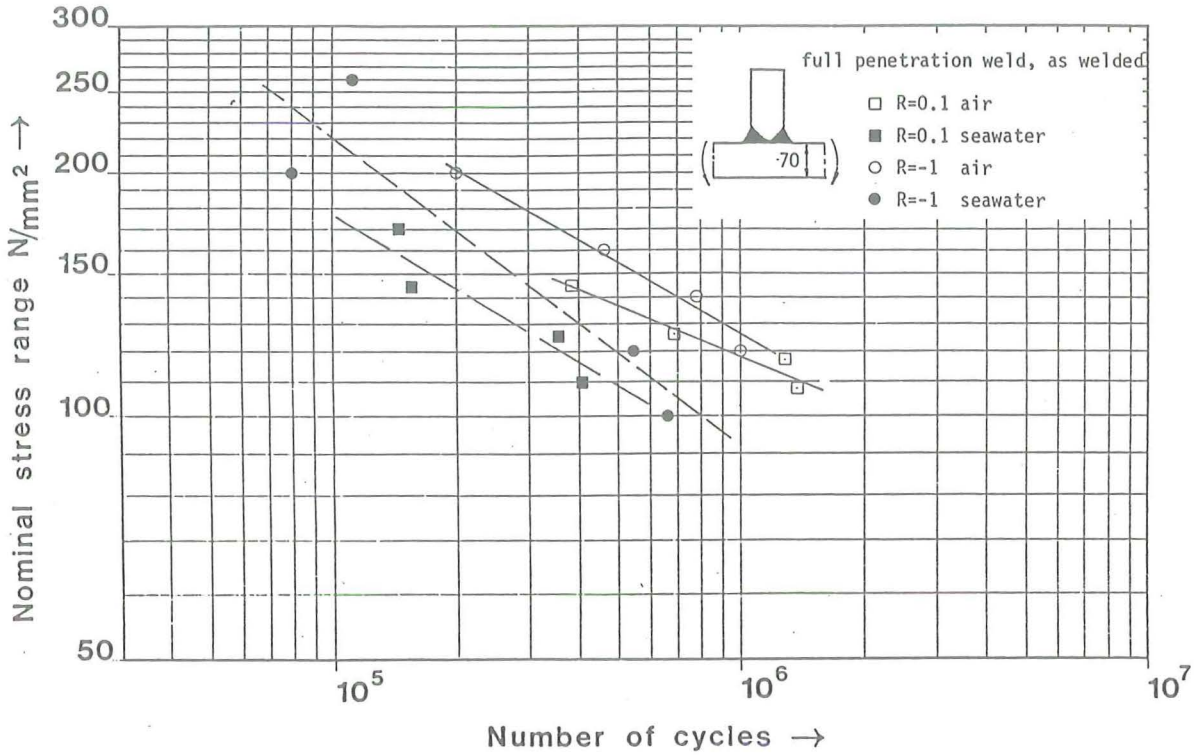

Fig. 2.2.28 Fatigue behaviour of 70 mm T-shape specimens (as welded) in air and seawater at stress ratios R = 0.1 and R = -1.

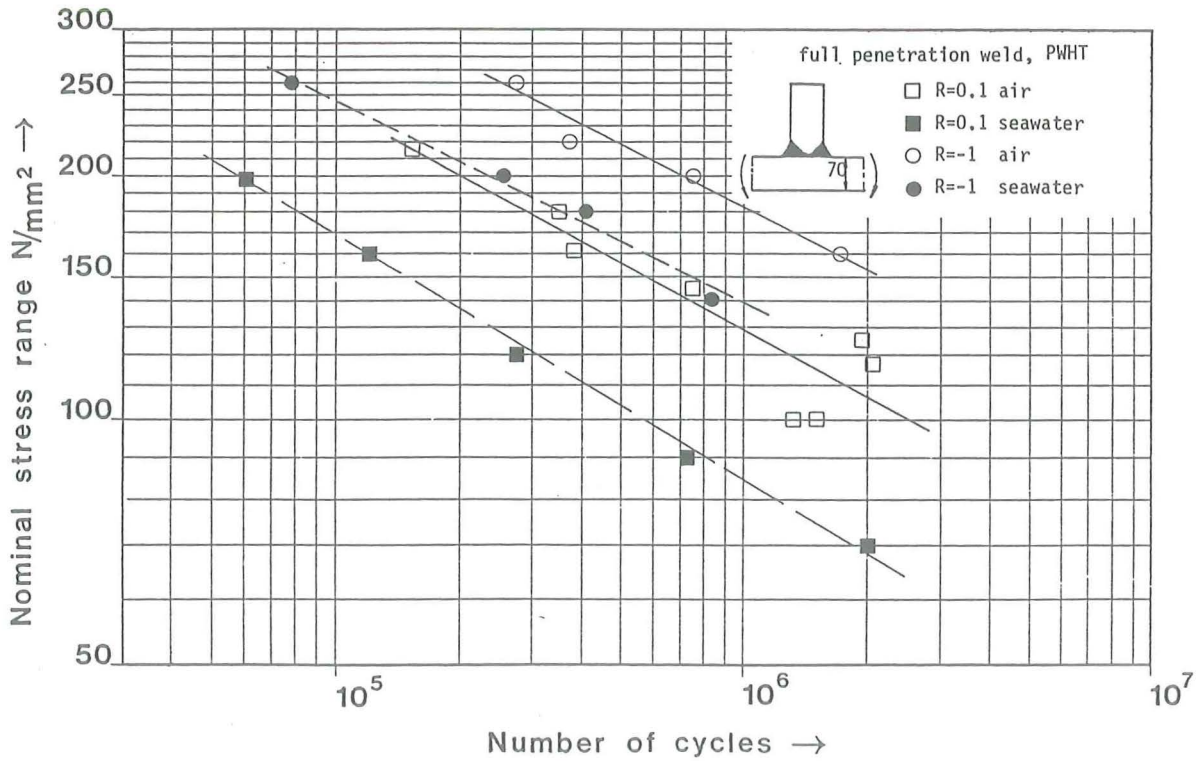

Fig. 2.2.29 Fatigue behaviour of 70 mm T-shape specimens (stress relieved) in air and seawater at stress ratios R = 0.1 and R = -1.

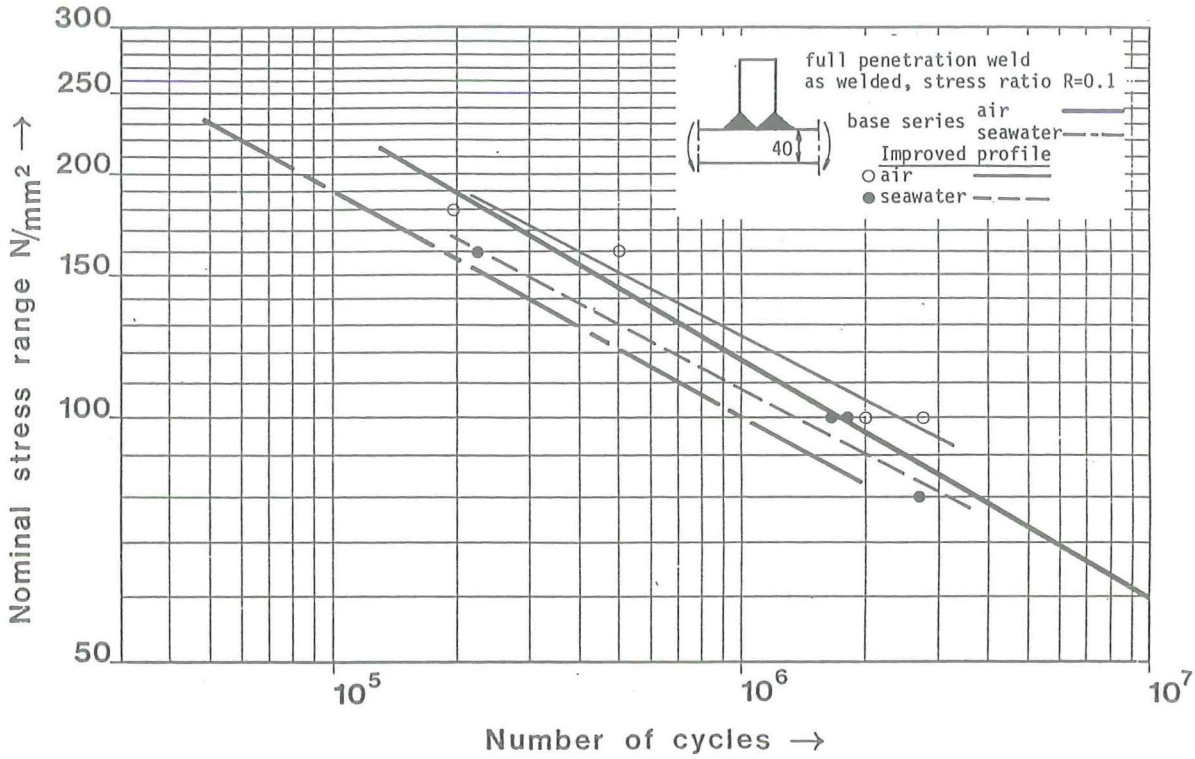

Fig. 2.2.26 Fatigue behaviour of 40 mm T-shape specimens (Improved profile) in air and seawater at a stress ratio R = 0.1.

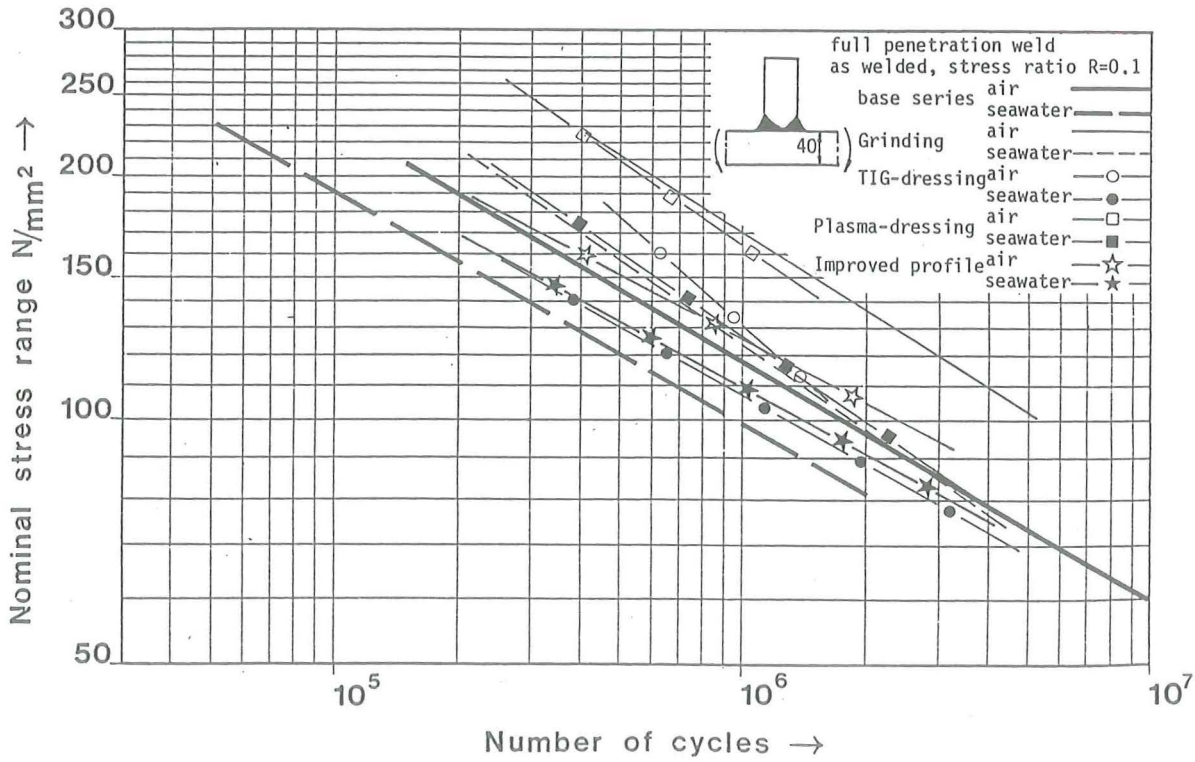

Fig. 2.2.27 Comparison of the four improvement techniques.

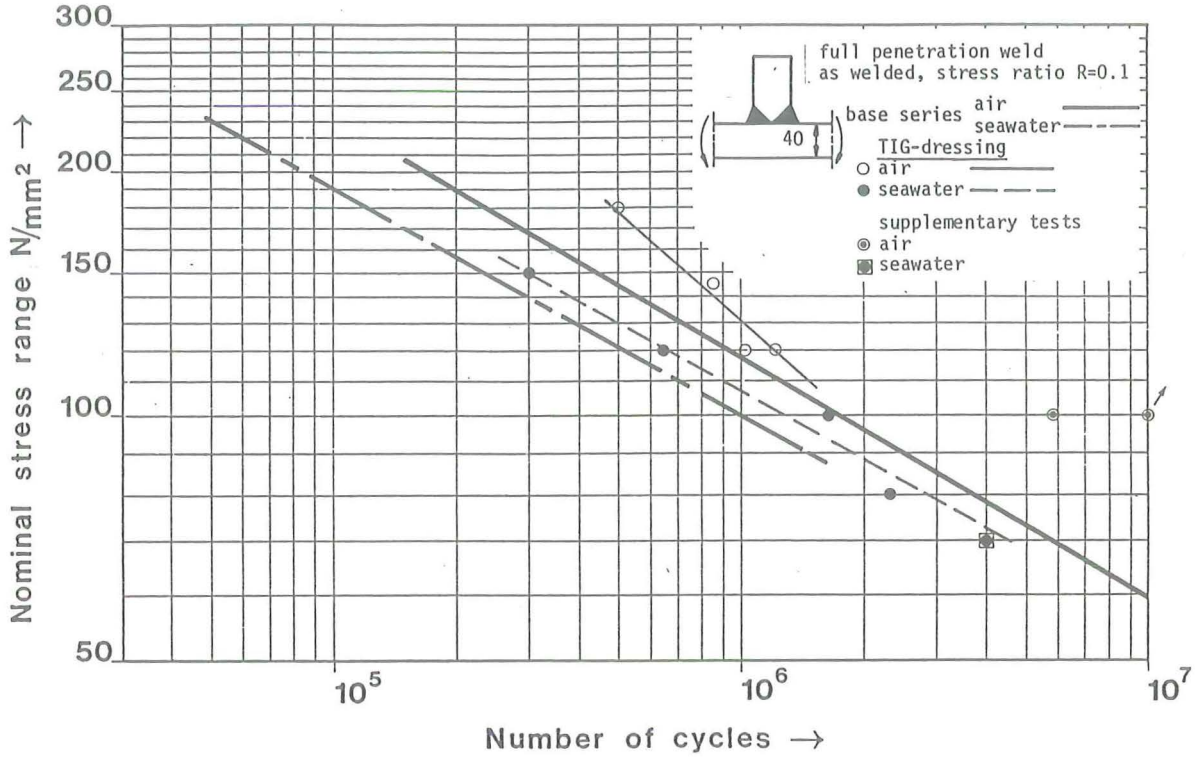

Fig. 2.2.24 Fatigue behaviour of 40 mm T-shape specimens (TIG dressing) in air and seawater at a stress ratio R = 0.1

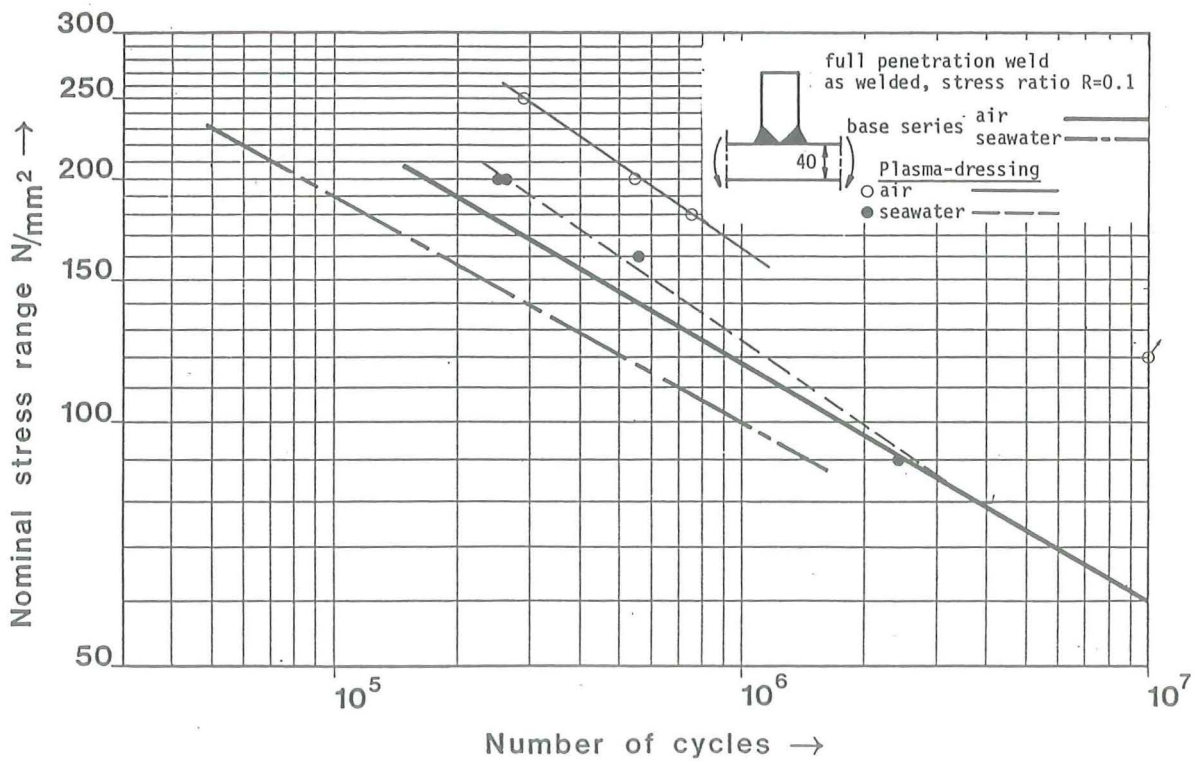

Fig. 2.2.25 Fatigue behaviour of 40 mm T-shape specimens (Plasma dressing) in air and seawater at a stress ratio R = 0.1.

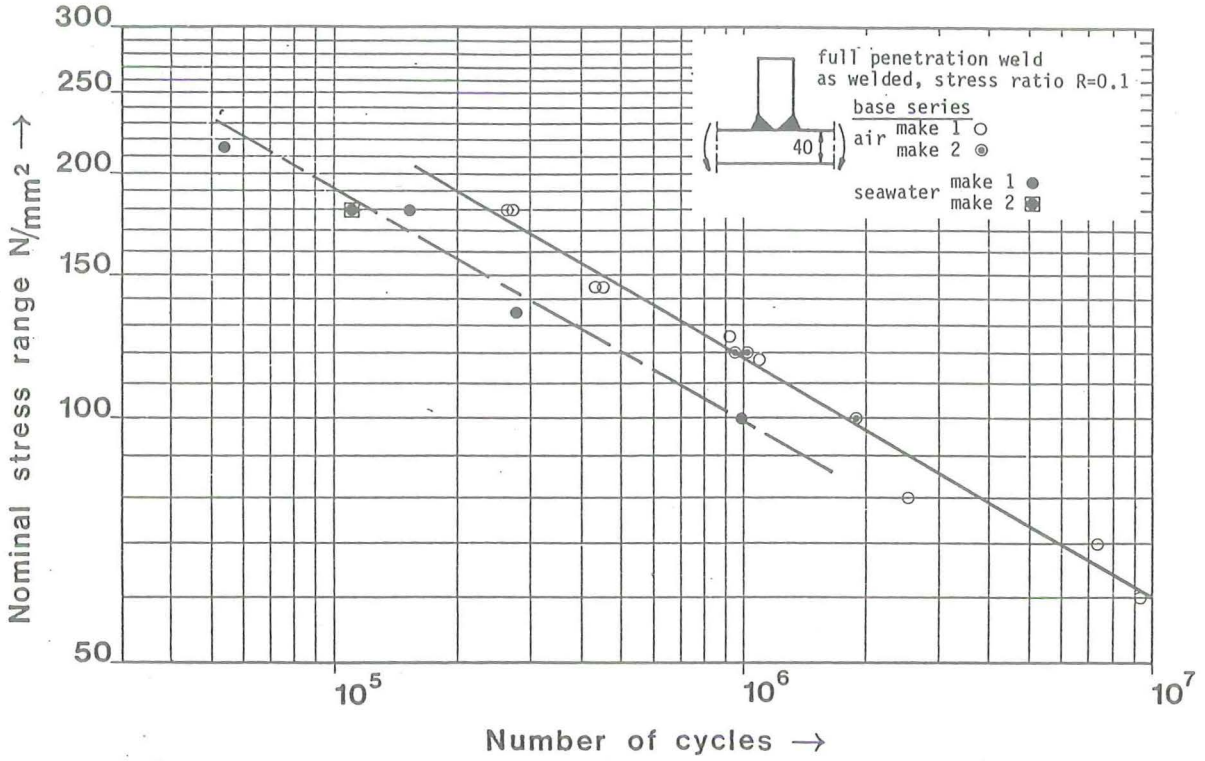

Fig. 2.2.22 Fatigue behaviour of 40 mm T-shape specimens as welded in air and seawater at a stress ratio of R = 0.1 (basic tests)

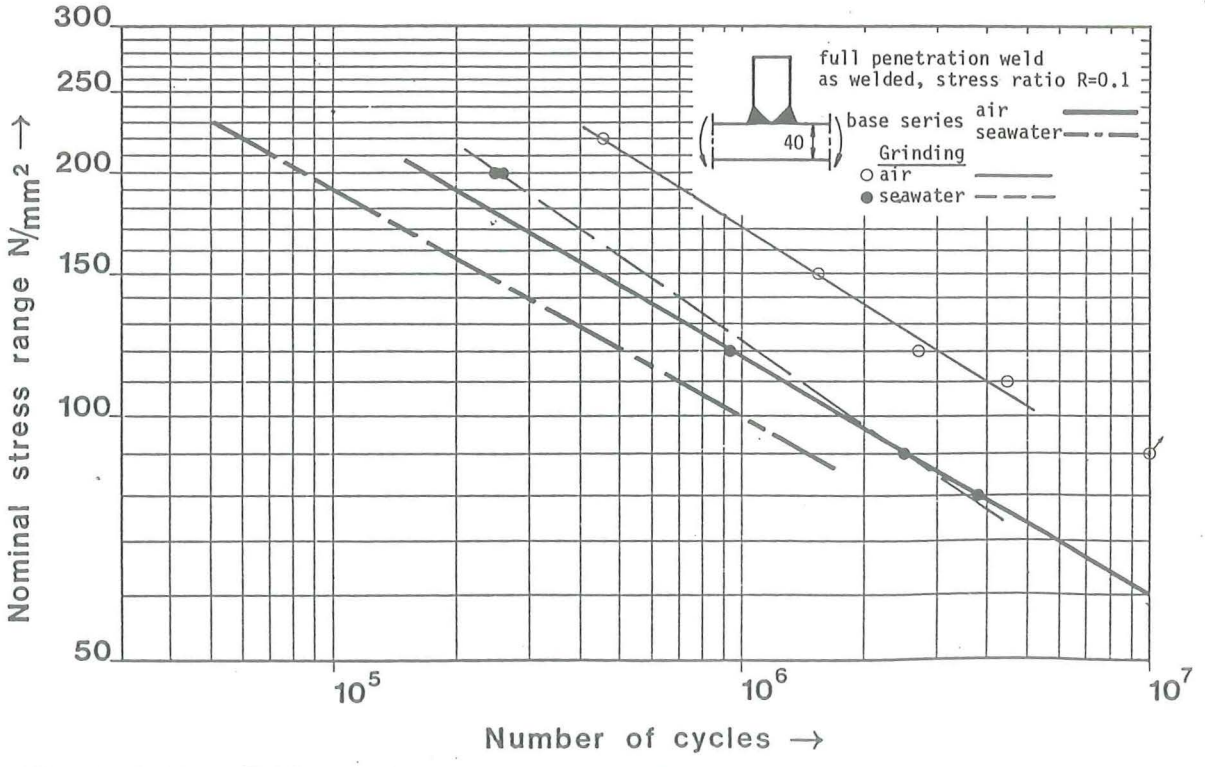

Fig. 2.2.23 Fatigue behaviour of 40 mm T-shape specimens (grinding) in air and seawater at a stress ratio R = 0.1.

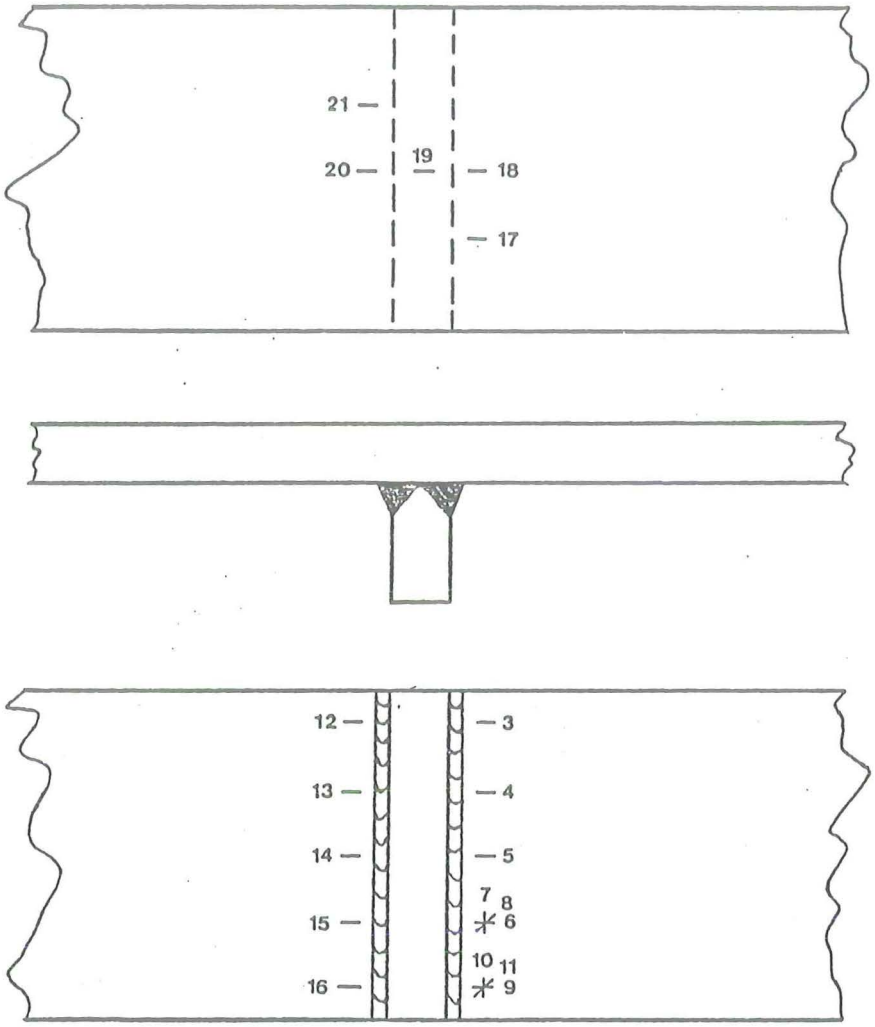

Fig. 2.2.20 Location of straingauges to a 40mm specimen

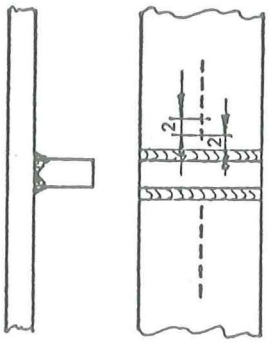

Fig. 2.2.21 Location of straingauges

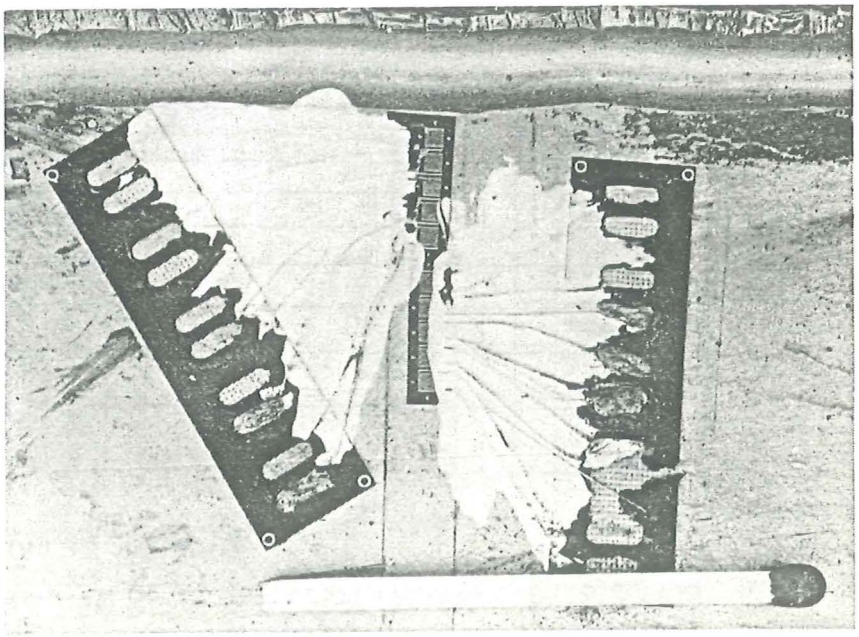

Fig. 2.2.21a appearance of a stripgauge

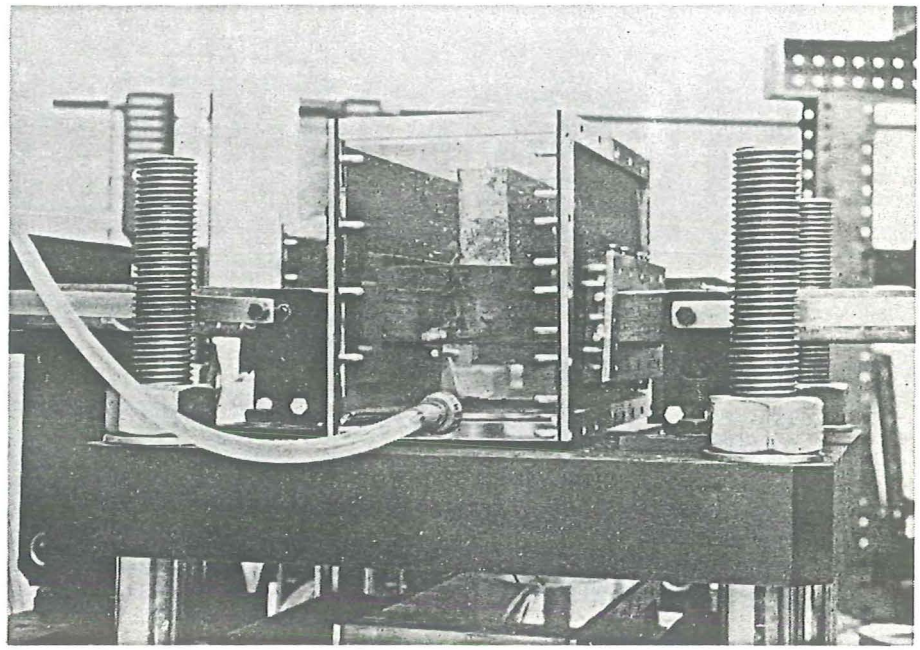

Fig. 2.2.19 Environmental chamber

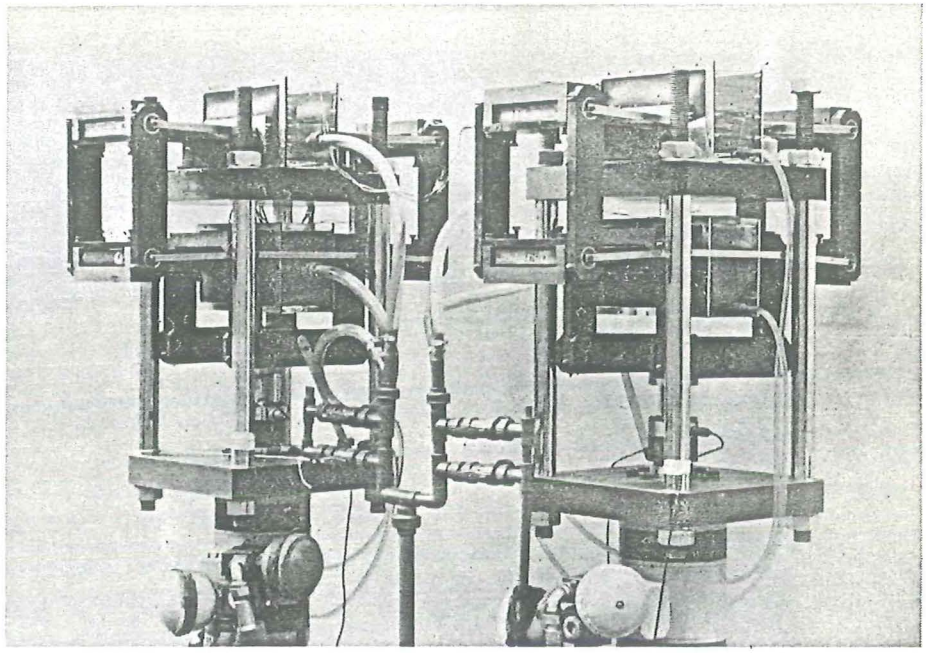

Fig. 2.2.17 100 kN twin loading machine

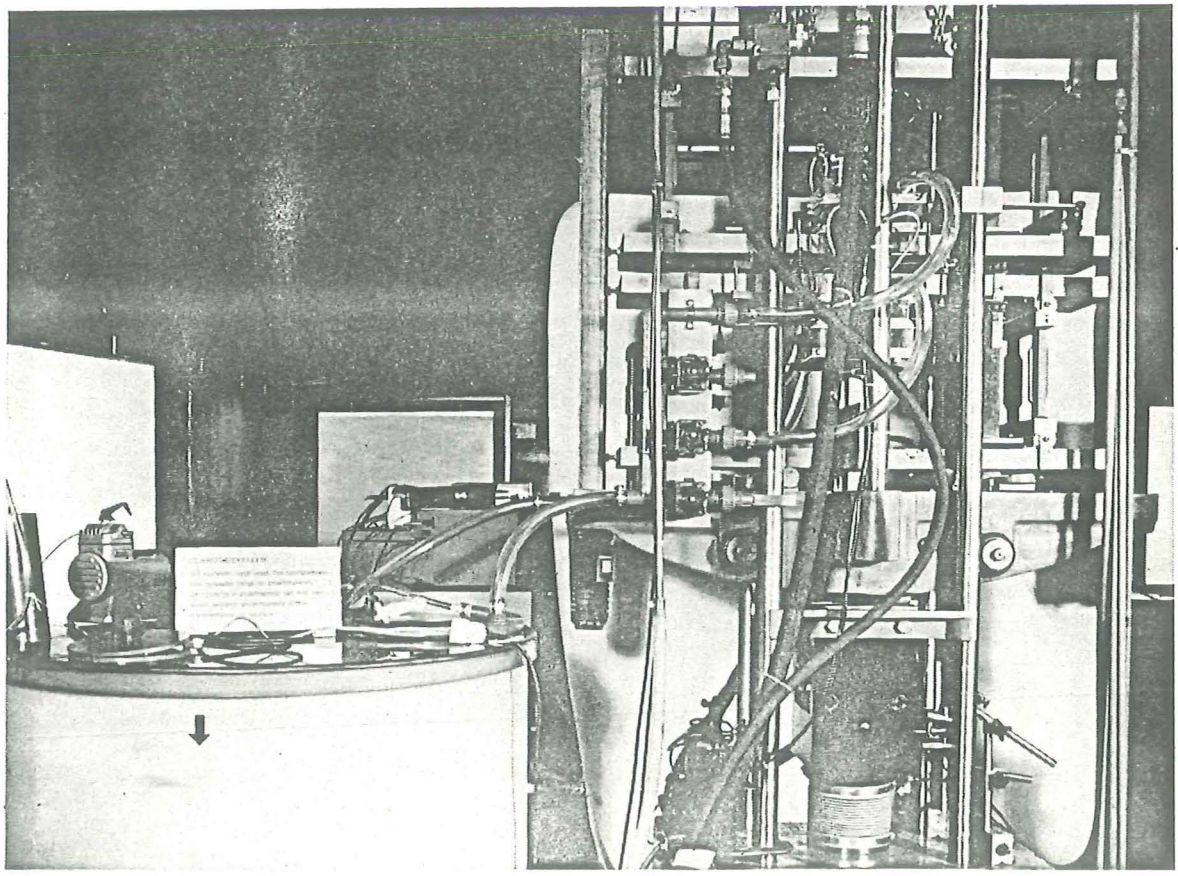

Fig. 2.2.18 500 kN loading machine for testing four specim

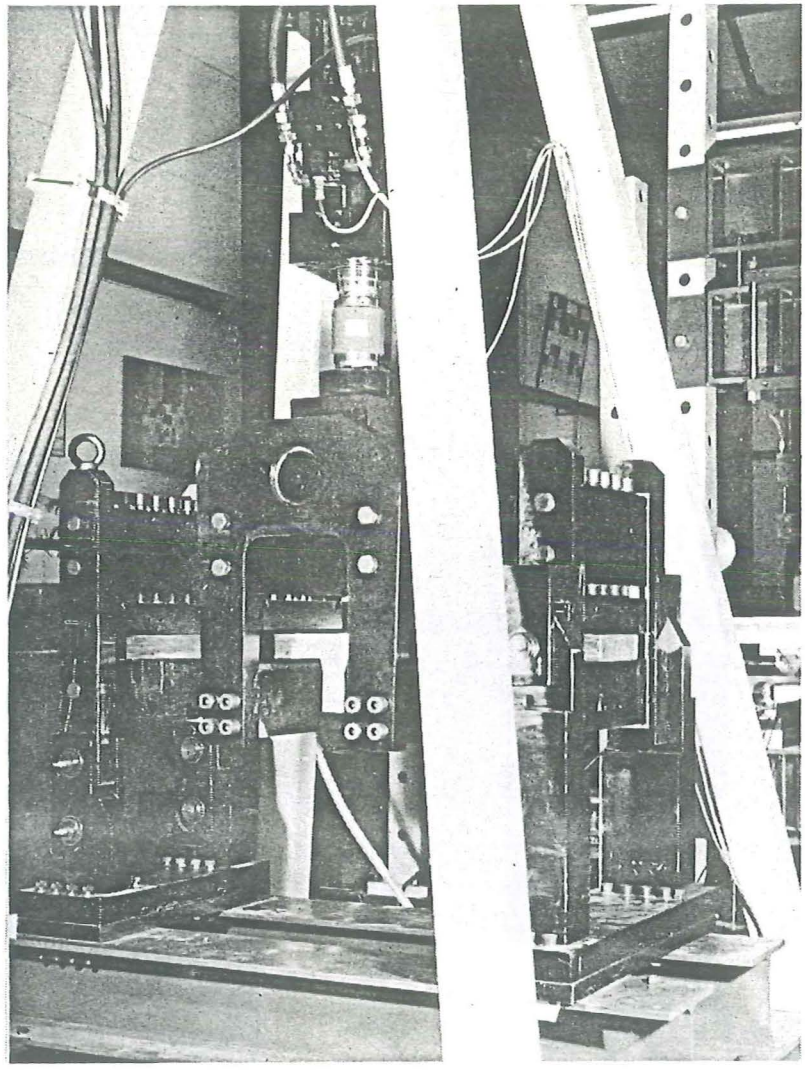

Fig. 2.2.16 500 kN loading machine

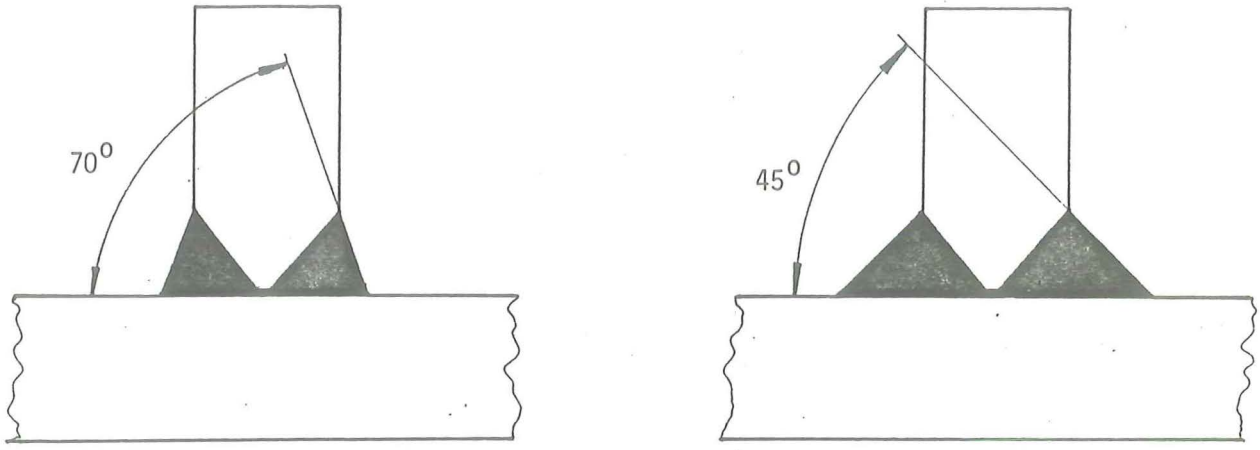

Fig. 2.2.13 Weldprofile

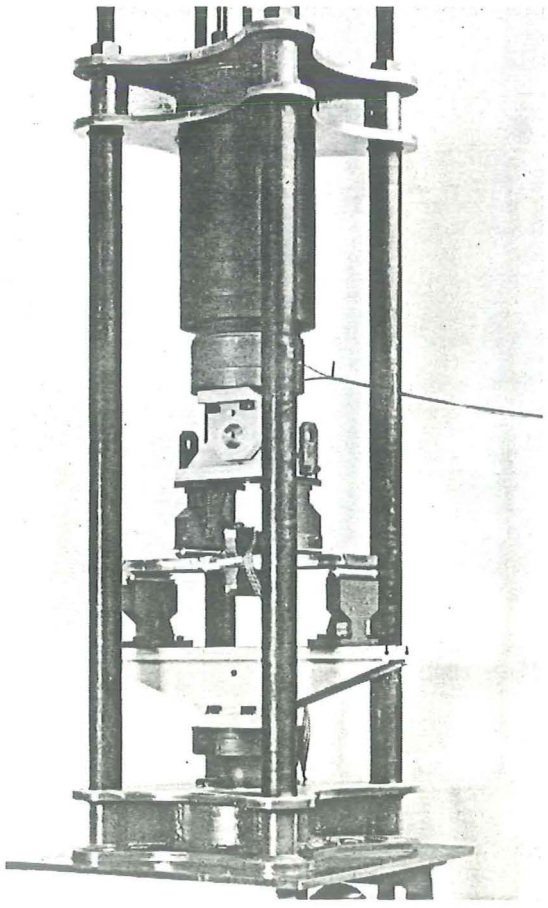

Fig. 2.2.14 250 kN loading machine

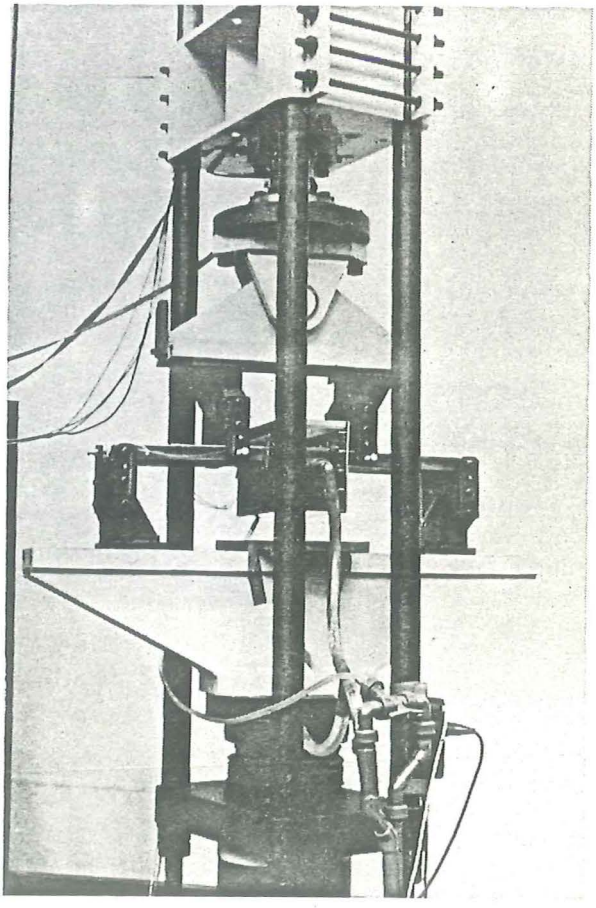

Fig. 2.2.15 250 kN loading machine

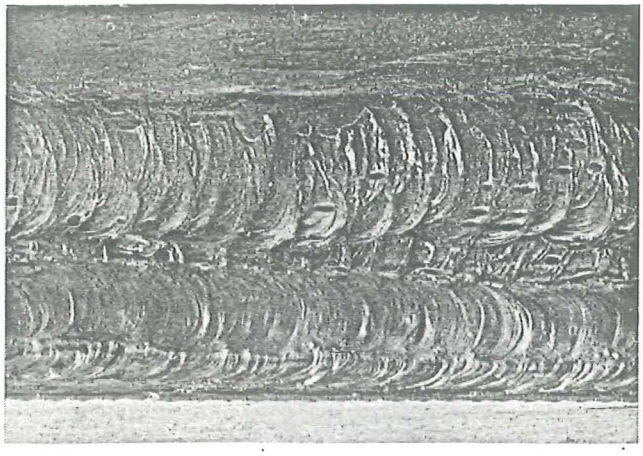

TIG-dressed

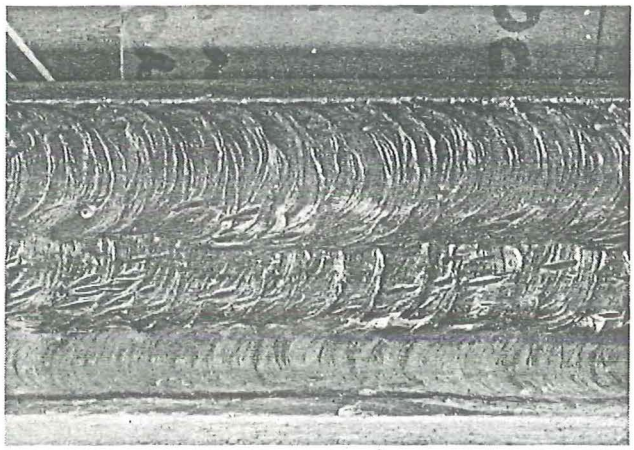

Plasma-dressed

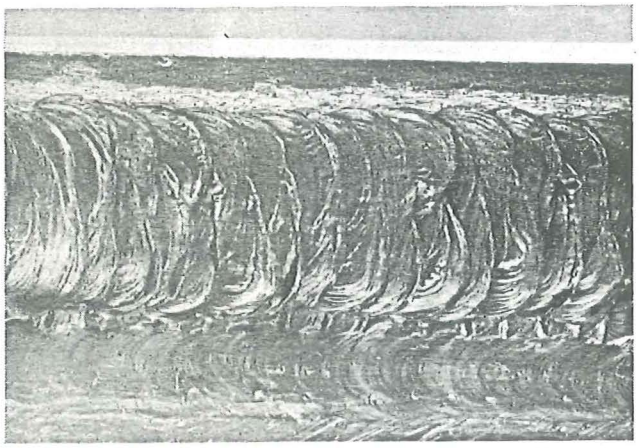

TIG-dressed (additional manufactured)

Fig.2.2.12 Surface appearance of some TIG- and Plasma-dressed specimens

Dressing : None
Number of runs : None
Welding direction : Uphill (groove weld)
Heat input run 1 - KJ/cm
run 2 - KJ/cm

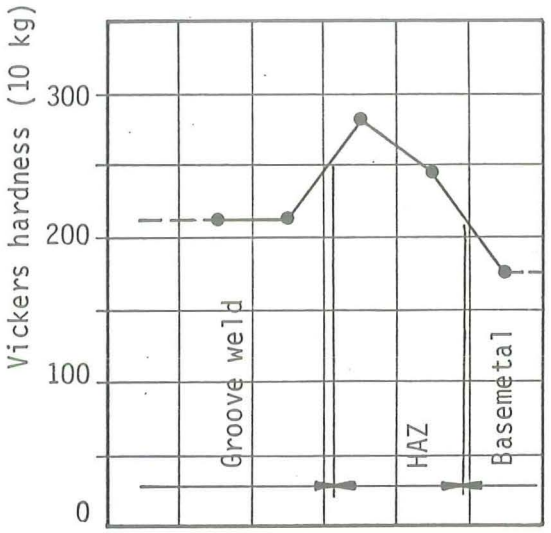

Fig. 2.2.10 - Hardness measurements at the weldtoe area (as welded)

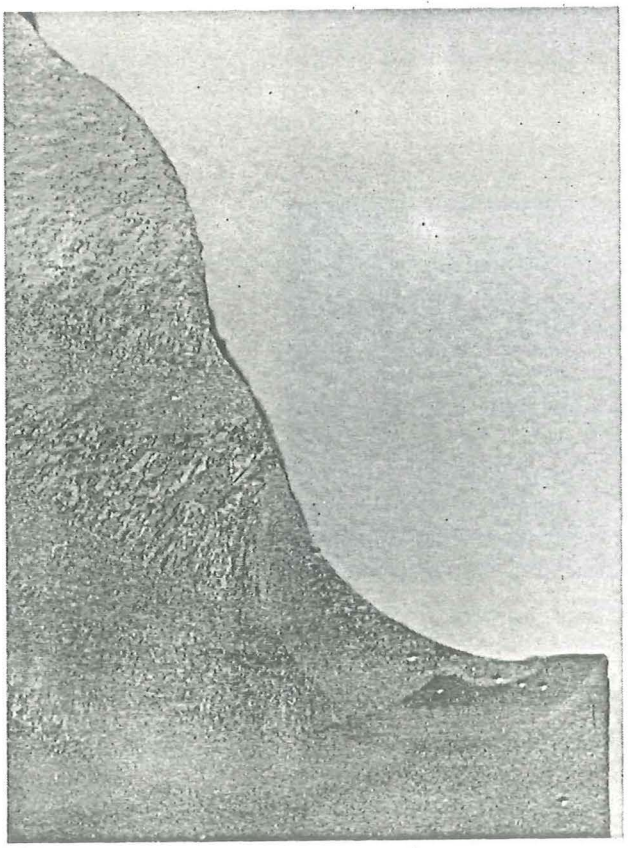

Dressing : Plasma
Number of runs : 2
Position : Vertical
Welding direction : Downhill
Heat input run 1 21.5 KJ/cm
run 2 18.1 KJ/cm

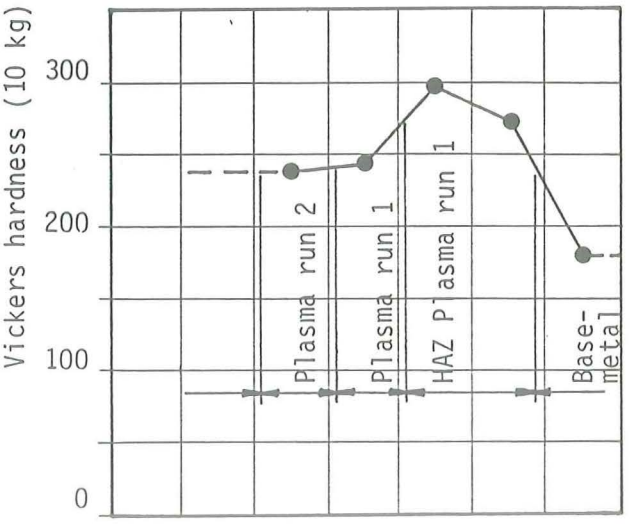

Fig.2.2.11 Hardness measurements at the weldtoe area (Plasma dressed)

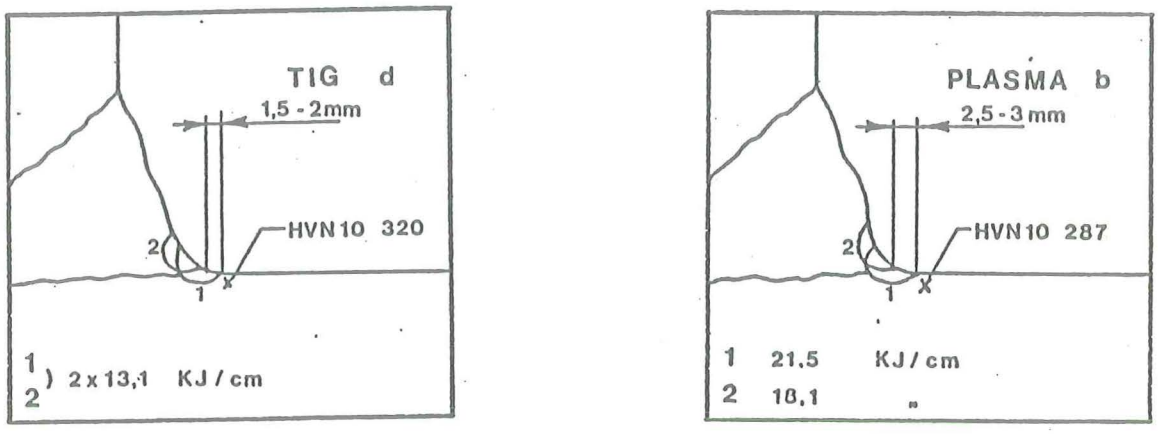

Fig. 2.2.8 The TIG- and Plasma dressing method

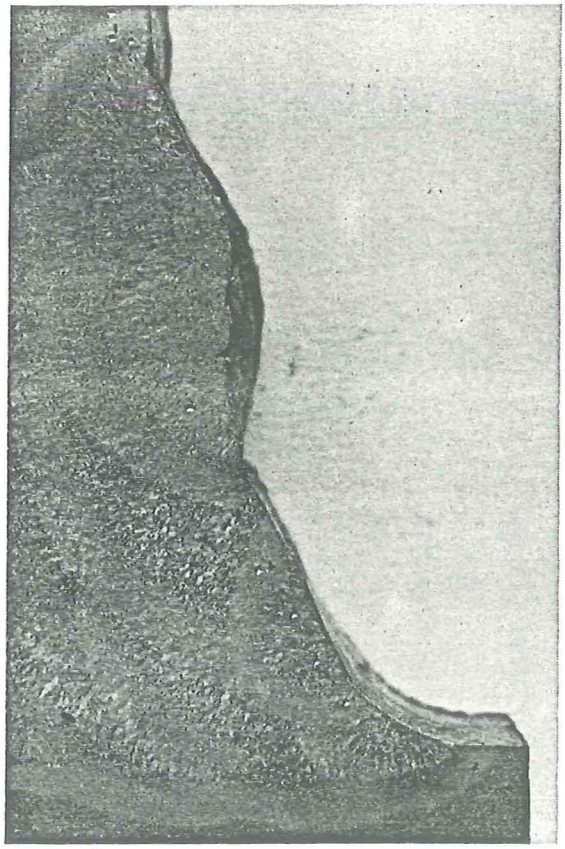

Dressing : TIG
Number of runs : 2
Position : Vertical
Welding direction : Downhill
Heat input run 1 13.1 KJ/cm
run 2 13.1 KJ/cm

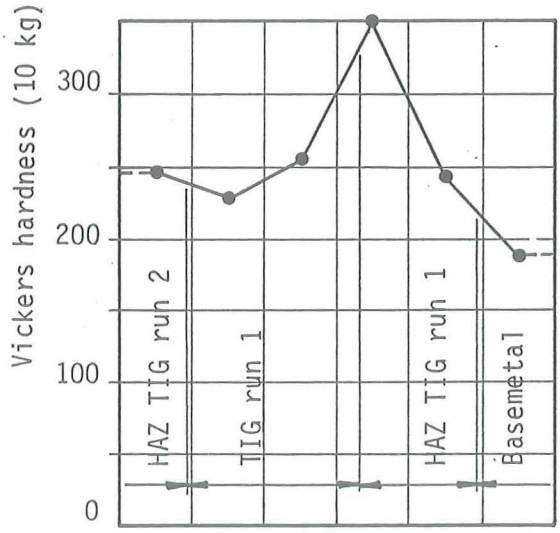

Fig. 2.2.9 Hardness measurements at the weldtoe area (TIG dressed)

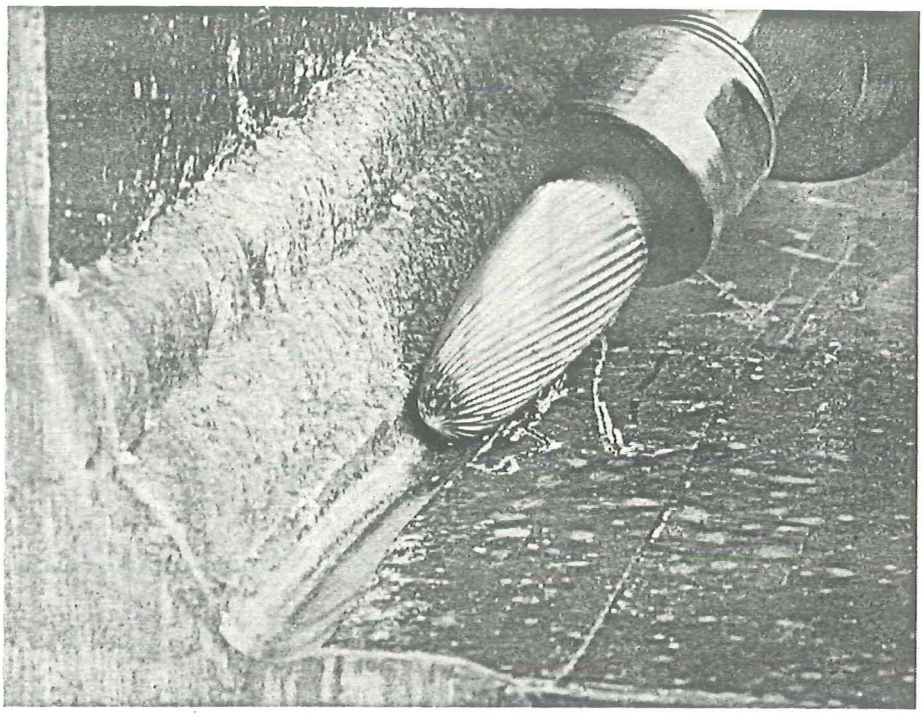

Fig. 2.2.6 Illustation of weld finishing by means of toe burr grinding.

Burr grinding

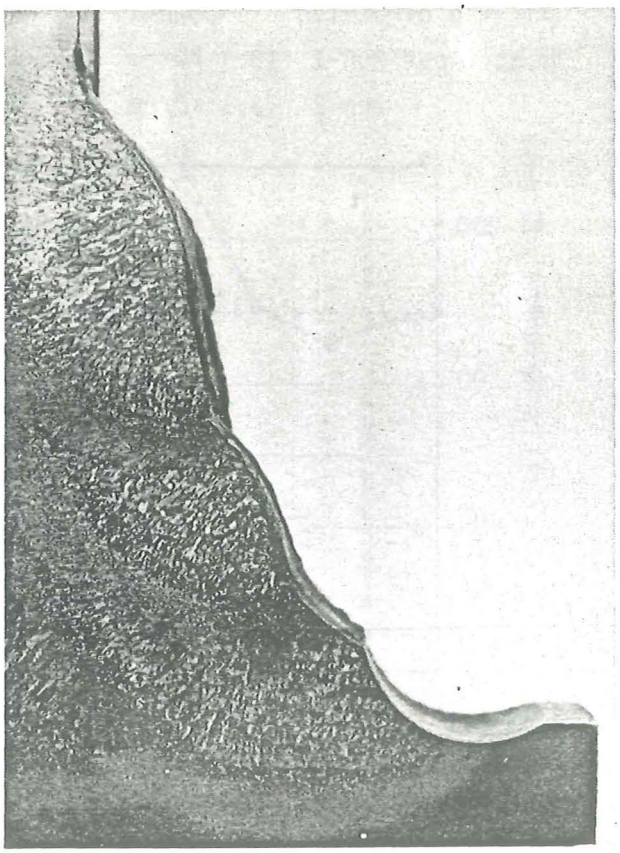

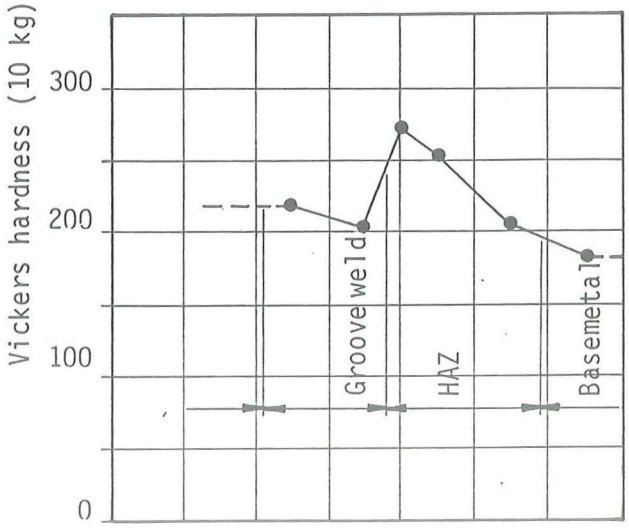

Fig. 2.2.7 Hardness measurements at the weldtoe area (Grinding)

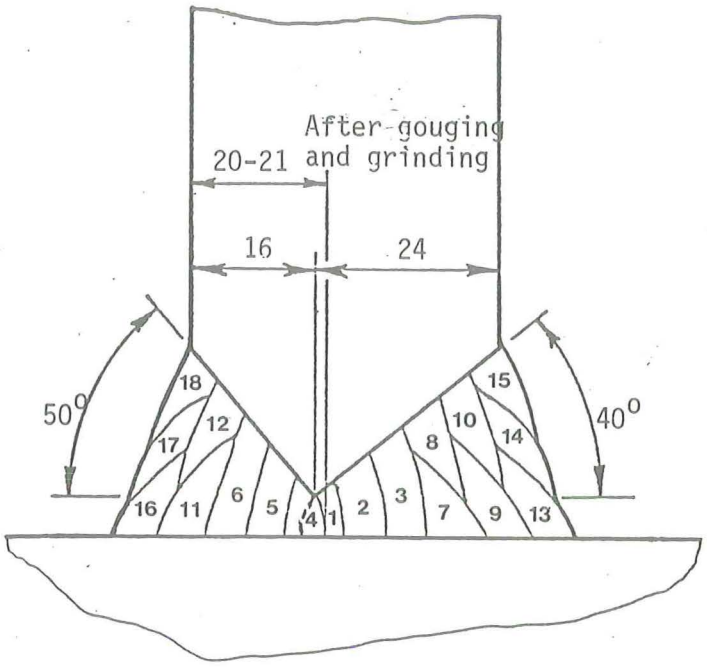

Fig. 2.2.4 Build-up sequence of 40 mm full penetration welds .

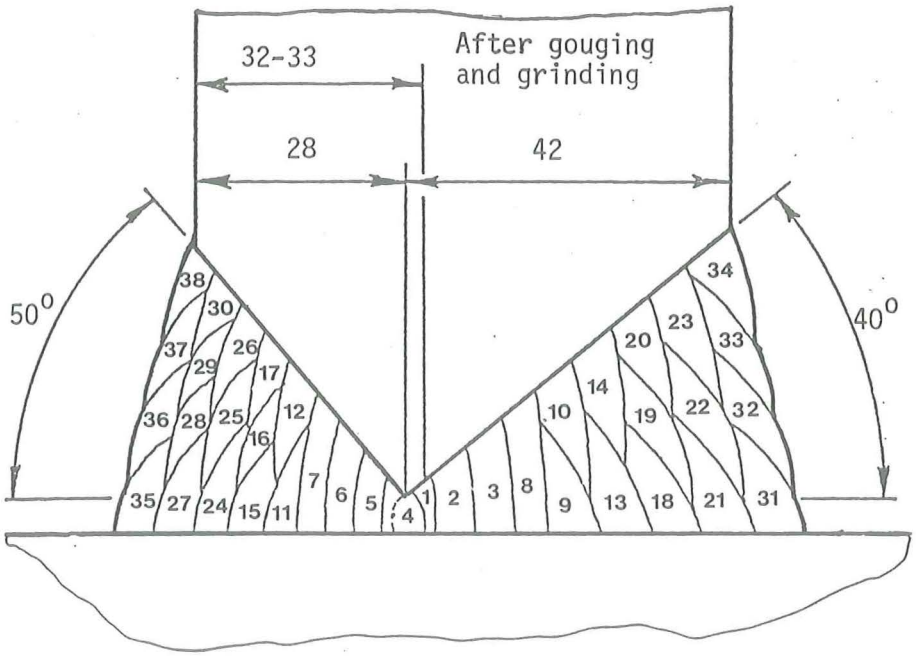

Fig. 2.2.5 Build-up sequence of 70 mm full penetration welds .

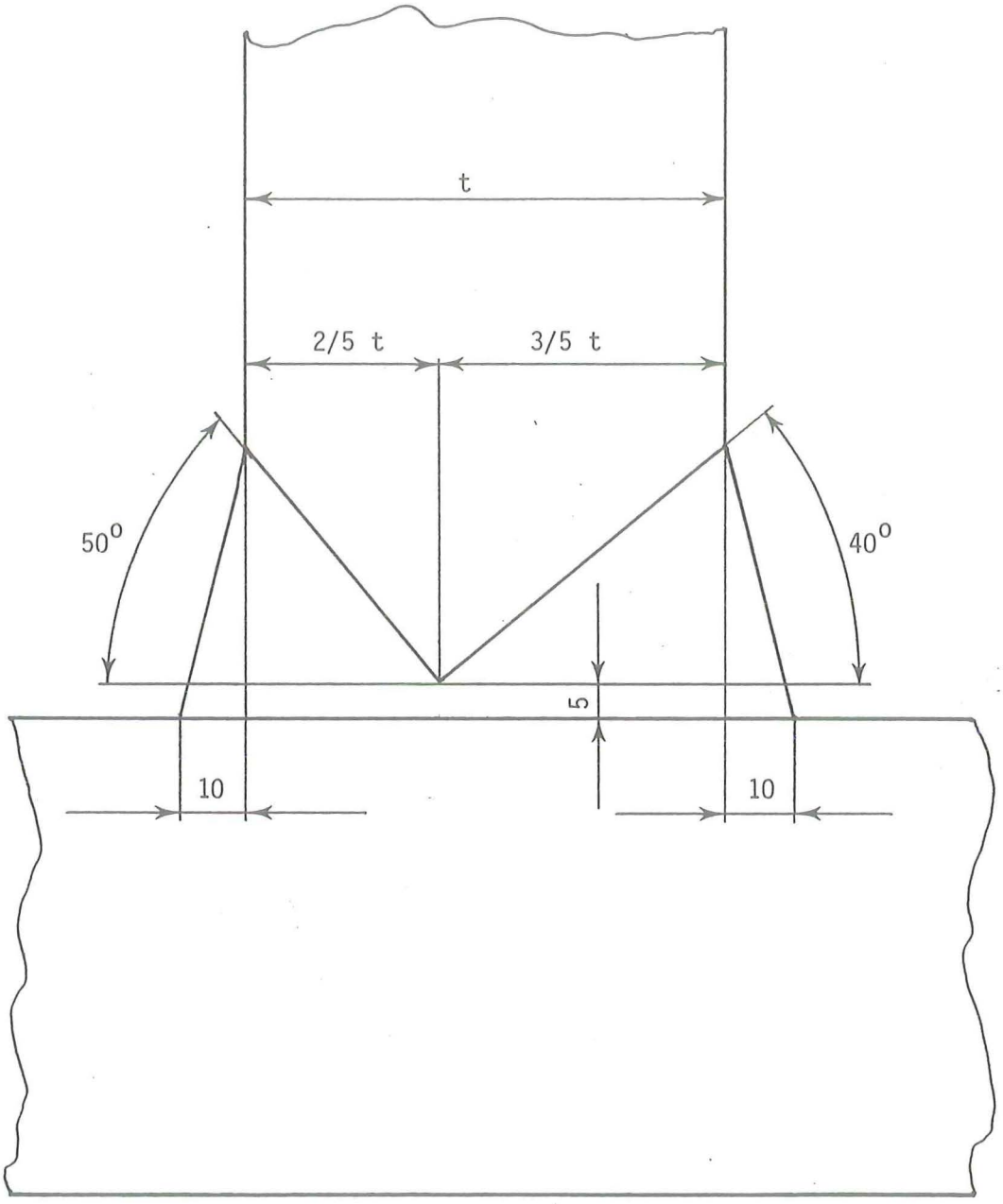

Fig. 2.2.3 Geometry of 40 mm and 70 mm full penetration welds.

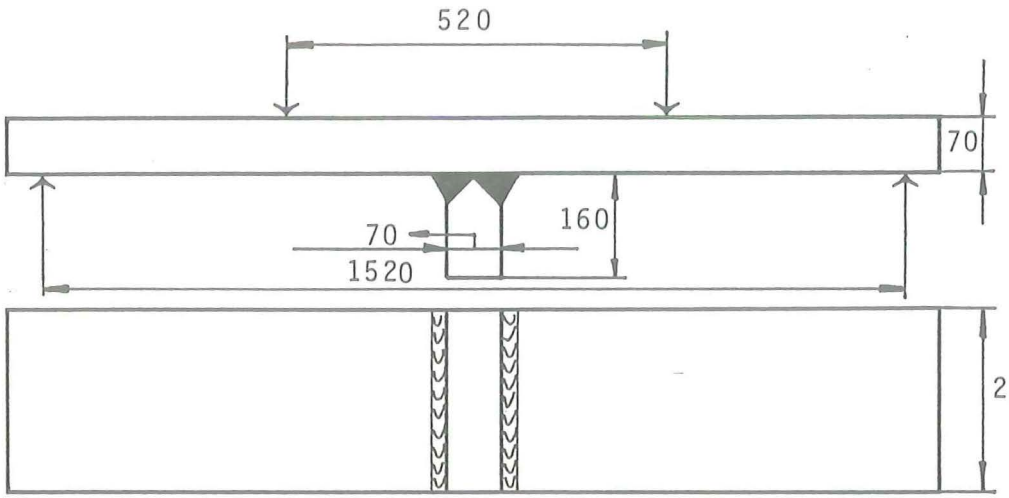

A-type:
T-shape specimen
full penetration we

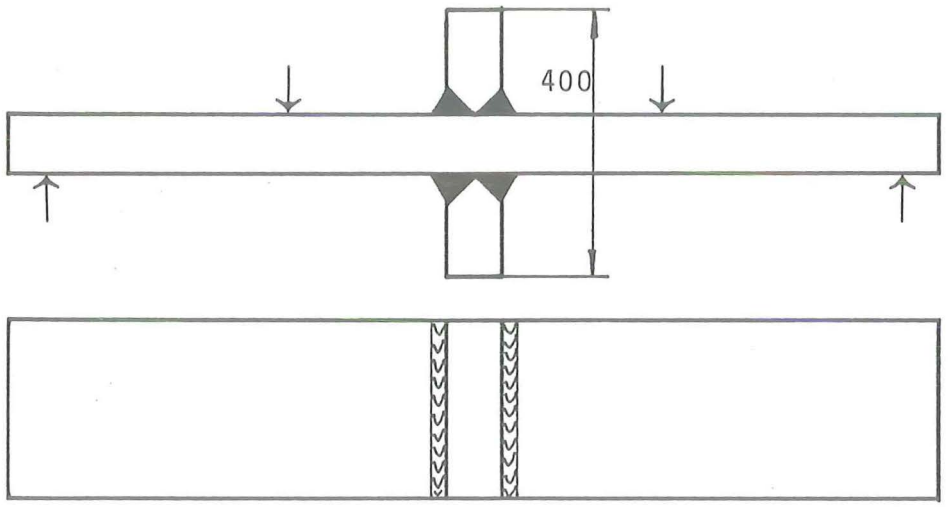

B-type:
crusiform specimen
non-load carrying
full penetration we

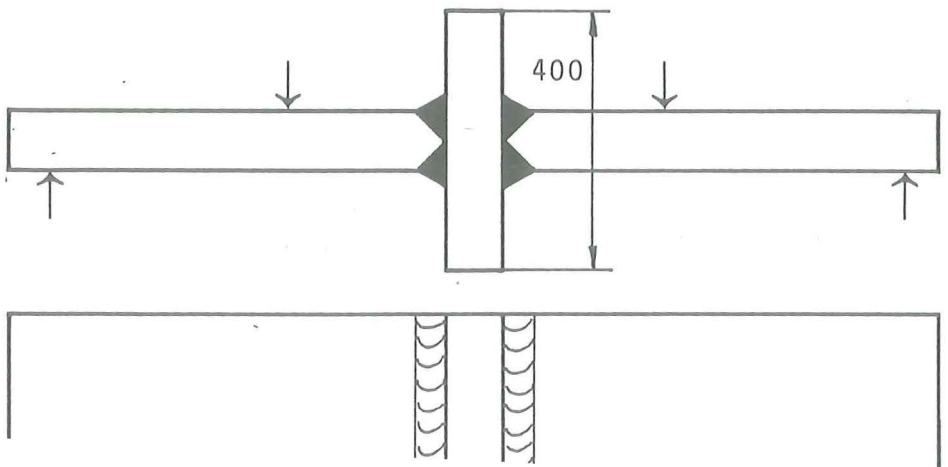

C-type:
crusiform specime
load carrying ful
pentration weld

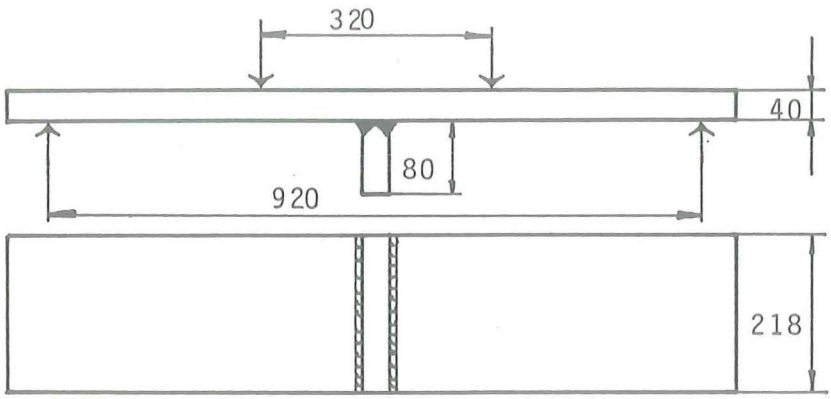

A-type: T-shape specimen
full penetration weld

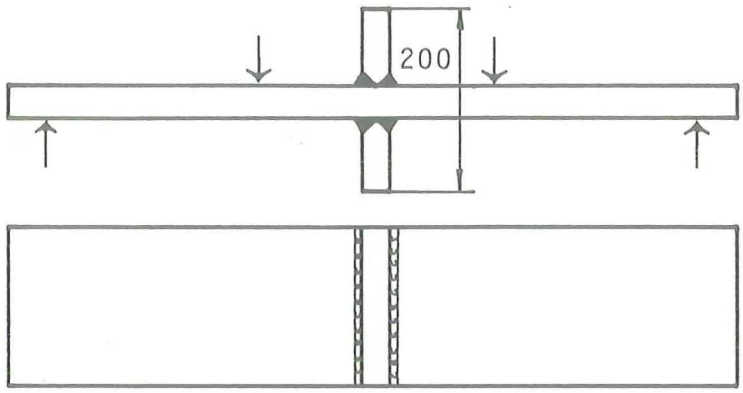

B-type: crusiform specimen
non-load carrying
full penetration weld

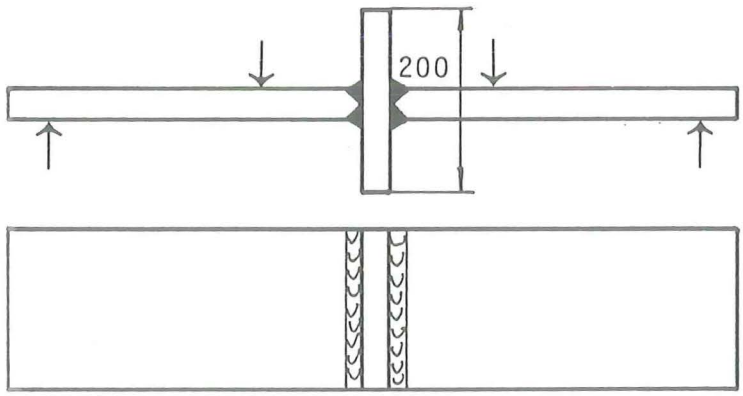

C-type: crusiform specimen
load carrying full
penetration weld

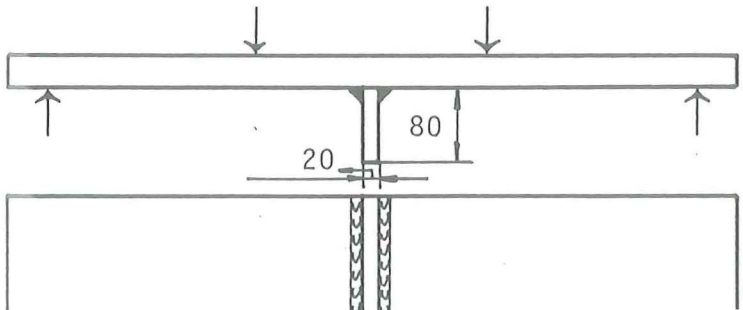

D-type: t-shape specimen
pure fillet weld

Fig. 2.2.65B A40-1-5-L-RO at 1 mm and 3 mm from crack origin.
Fig. 2.2.66 Striation spacing as a function of crack depth from specimen A40-1-5-L-RO.
Fig. 2.2.67A TEM-micrographs of the fracture surface of specimen
Fig. 2.2.67B A40-1-5-L-RO at 18 mm from the crack origin.
Fig. 2.2.68 Macrographs of secondary cracks developed near the weld at the side of the gusset opposite the main crack.
Fig. 2.2.69 Macrograph of secondary cracks developed at the side of the gusset opposite the main crack.
Fig. 2.2.70 Detail of Fig. 2.2.76.
Fig. 2.2.71 Striation spacing as a function of crack depth from specimen A40-20-3-L-RO
Fig. 2.2.72 Striation spacing as a function of crack depth from specimen A40-22-3-L-RO
Fig. 2.2.73 Striation spacing as a function of crack depth from specimen A40-24-2-L-RO.
Fig. 2.2.74 Influence of weld toe finishing on crack initiation.
Fig. 2.2.75 Effect of finishing the weld toe on the decreasing of the formation of multiple crack initiation.

Fig. 2.2.46 Variation of strain near the weld toe during testing of a 40 mm T-shape specimen.
Fig. 2.2.47 Variation of strains at the back face (opposite the weld) during testing of a 40 mm T-shape specimen.
Fig. 2.2.48 Crack front markings generated during testing of a 40mm specimen.
Fig. 2.2.49 Strain concentration factor at the weld toe of an as welded 40 mm T-shape specimen (basic testspecimen).
Fig. 2.2.50 Strain concentration factor at the weld toe of a stress relieved 40 mm T-shape specimen.
Fig. 2.2.51 Strain concentration factor at the weld toe of a 40 mm T-shape specimen of which the weld toe was finished by grinding.
Fig. 2.2.52 Strain concentration factor at the weld toe of a 40 mm T-shape specimen of which the weld toe was finished by TIG dressing.
Fig. 2.2.53 Strain concentration factor at the weld toe of a 40 mm T-shape specimen of which the weld toe was finished by Plasma dressing.
Fig. 2.2.54 Strain concentration factor at the weld toe of a 40 mm T-shape specimen performed with an improved weldprofile.
Fig. 2.2.55 Comparison of the strainconcentration factors.
Fig. 2.2.56 Striations on a fracture of a specimen, tested under corrosion fatigue.
Fig. 2.2.57 Fracture surface of specimen A40-1-5-L-RO
Fig. 2.2.58 Cross-section at the fracture surface opposite the surface as shown in Fig. 2.2.64
Fig. 2.2.59 Detail of the fracture surface shown in Fig. 2.2.64
Fig. 2.2.60 SEM-micrograph of the coarse structure indicated by the arrow in Fig. 2.2.66
Fig. 2.2.61 Detail of an area broken by cleavage (as indicated by the black arrow in Fig. 2.2.67
Fig. 2.2.62 Appearance of the fatigue fracture in the weld material
Fig. 2.2.63A SEM-micrographs of the fracture surface of specimen
Fig. 2.2.63B A40-1-5-L-RO
Fig. 2.2.64A TEM-micrographs of the fracture surface of specimen
Fig. 2.2.64B A40-1-5-L-RO at 0.4 mm from crack origin.
Fig. 2.2.65A TEM-micrographs of the fracture surface of specimen

Fig. 2.2.29 Fatigue behaviour of 70 mm T-shape specimens (stress relieved) in air and seawater at stress ratios R = 0.1 and R = -1.

Fig. 2.2.30 Fatigue behaviour of 70 mm T-shape specimens (as welded and stress relieved) in air at stress ratios R = 0.1 and R = -1.

Fig. 2.2.31 Fatigue behaviour of 70 mm T-shape specimens (as welded and stress relieved) in seawater at stress ratios R = 0.1 and R = -1.

Fig. 2.2.32 Fatigue behaviour of 40 mm and 70 mm T-shape specimens (as welded) in air and seawater at a stress ratio R = 0.1.

Fig. 2.2.33 Fatigue behaviour of 40 mm T-shape specimens (as welded and stress relieved) in air at a stress ratio R = 0.1.

Fig. 2.2.34 Fatigue behaviour of 40 mm and 70 mm T-shape specimens (as welded and stress relieved) in air at a stress ratio R = 0.1.

Fig. 2.2.35 Fatigue behaviour of 40 mm B-type specimens in air and seawater at a stress ratio R = 0.1.

Fig. 2.2.36 Fatigue behaviour of 40 mm B-type specimens in air at a stress ratio R = 0.1.

Fig. 2.2.37 Fatigue behaviour of 40 mm D-type specimens in air and seawater at a stress ratio R = 0.1.

Fig. 2.2.38 Comparison of the test on the A-type, B-type, C-type and D-type 40 mm specimens.

Fig. 2.2.39 Fatigue behaviour of 70 mm B-type specimens in air at a stress ratio R = 0.1.

Fig. 2.2.40 Angle of transition between the weld and the main plate of the four different specimen types.

Fig. 2.2.41 Fatigue behaviour of 70 mm C-type specimens in air at a stress ratio R=0.1.

Fig. 2.2.42 Comparison of the tests on the A-type, B-type and C-type 70 mm specimens.

Fig. 2.2.43 Fatigue behaviour of 40 mm , with 2.5% Ni-alloyed electrodes welded specimens in air and seawater at a stress ratio R = 0.1.

Fig. 2.2.44 Comparison of the tests of the 40 mm, with alloyed electro welded specimens and the basic tests.

Fig. 2.2.45 Fatigue behaviour of cathodically protected and over-protected 70 mm specimens in seawater at a stress ratio R = 0.1.

2.2.12. Figures

LIST OF FIGURES

Fig. 2.2.1 Dimensions of 40 mm plate specimens.
Fig. 2.2.2 Dimensions of 70 mm plate specimens.
Fig. 2.2.3 Geometry of 40 mm and 70 mm full penetration welds.
Fig. 2.2.4 Build-up sequence of 40 mm full penetration welds .
Fig. 2.2.5 Build-up sequence of 70 mm full penetration welds .
Fig. 2.2.6 Illustration of weld finishing by means of toe burr grinding.
Fig. 2.2.7 Hardness measurements at the weld toe area (grinding).
Fig. 2.2.8 The TIG-and Plasma dressing method.
Fig. 2.2.9 Hardness measurements at the weld toe area (TIG dressed).
Fig. 2.2.10 Hardness measurements at the weld toe area (as welded)
Fig. 2.2.11 Hardness measurements at the weld toe area (Plasma dressed).
Fig. 2.2.12 Surface appearance of some TIG- and Plasma dressed specimens.
Fig. 2.2.13 Weld profiles.
Fig. 2.2.14 250 k N loading machine.
Fig. 2.2.15 250 k N loading machine.
Fig. 2.2.16 500 k N loading machine.
Fig. 2.2.17 100 k N twin loading machine.
Fig. 2.2.18 500 k N loading for tested 4 specimens silmultaneously.
Fig. 2.2.19 Environmental chamber.
Fig. 2.2.20 Location of strainganges to a 40 mm specimen.
Fig. 2.2.21 Location of stripganges.
Fig. 2.2.21a Appearance of a stripgange.
Fig. 2.2.22 Fatigue behaviour of 40 mm T-shape specimens as welded in air and seawater at a stress ratio of R = 0.1 (basic tests)
Fig. 2.2.23 Fatigue behaviour of 40 mm T-shape specimens (grinding) in air and seawater at a stress ratio R = 0.1.
Fig. 2.2.24 Fatigue behaviour of 40 mm T-shape specimens (TIG dressing) in air and seawater at a stress ratio R = 0.1
Fig. 2.2.25 Fatigue behaviour of 40 mm T-shape specimens (Plasma dressing) in air and seawater at a stress ratio R = 0.1.
Fig. 2.2.26 Fatigue behaviour of 40 mm T-shape specimens (Improved profile) in air and seawater at a stress ratio R = 0.1.
Fig. 2.2.27 Comparison of the four improvement techniques.
Fig. 2.2.28 Fatigue behaviour of 70 mm T-shape specimens (as welded) in air and seawater at stress ratios R = 0.1 and R = -1.

Table 2.2.7

Testseries	Regression line	Environment	Thickness	Condition with respect to residual stresses
A40 - 1,1A	$\log N = -3.30 \log S_a + 12.85$	air	40	as welded
A40 - 2.2A	$\log N = -3.53 \log S_a + 13.02$	seawater	40	as welded
A70 - 3	$\log N = -3.09 \log S_a + 12.50$	air	70	stress relieved
A70 - 4	$\log N = -3.32 \log S_a + 12.38$	seawater	70	stress relieved

Table 2.2,8

Specimen code	Calculated initiation period %	real initiation period in %
A40-47-2	80	70
A40-1-5	80	14
A40-20-3	62	43
A40-22-3	80	59
A40-24-2	73	-

Table 2.2.9

Specimen	Weld parameter	Initiation period %	Average initiation period %
A40-1-1	As welded	31	
-2	"	26	
-3	"	27	
-4	"	26	24,75
-5	"	14	
A40-1A-1	"	28	
-2	"	21	
-3	"	25	
A40-20-2	grinding	67	
-3	"	44	53,50
-4	"	37	
-5	"	66	
A40-22-1	TIG-dressing	61	
-2	"	61	
-3	"	56	59,80
-4	"	55	
-5	"	66	
A40-24-1	Plasma dressing	74	
-4	"	60	67,00
A40-26-2	Improved profile	30	
-3	"	50	50,67
-4	"	72	

Table 2.2.6 continued

Specimen code	stress ratio R	frequency Hz	environment	influencing weld parameter	stress range N/mm^2	number of cycles until initiation N_i	number of cycles until fracture N_f
				WELD METAL COMP.			
A40-37-1-L-RO	0.1	0.2	air	as welded	200	35000	171450
A40-37-2-L-RO	0.1	0.2	air	as welded	92	668000	1521300
A40-37-3-L-RO	0.1	0.8	air	as welded	147	278000	452700
A40-37-4-L-RO	0.1	0.2	air	as welded	115	239000	803500
A40-38-1-Z-RO	0.1	0.2	sea water	as welded	139	85000	346800
A40-38-2-Z-RO	0.1	0.2	sea water	as welded	75	529000	1958000
A40-38-3-Z-RO	0.1	0.2	sea water	as welded	92	670000	1389800
A40-38-4-Z-RO,	0.1	0.2	sea water	as welded	115	330000	529500
$A40\text{-}37^{A}\text{-}1\text{-}L\text{-}RO$	0.1	0.2	air	as welded	125	221000	636000
$A40\text{-}37^{A}\text{-}2\text{-}L\text{-}RO$	0.1	0.2	air	as welded	75	1526000	4094000
$A40\text{-}38^{A}\text{-}1\text{-}Z\text{-}RO$	0.1	0.2	sea water	as welded	125	132000	441000
$A40\text{-}38^{A}\text{-}2\text{-}Z\text{-}RO$	0.1	0.2	sea water	as welded	75	475000	2211000
				CATH.PROTECTION			
A70-18-1-Z-RO-G-K	0.1	0.2	sea water	stress relieved	120	--	1505000
A70-18-6-Z-RO-G-K	0.1	0.2	sea water	stress relieved	100	--	> 2000000
A70-18-6-Z-RO-G-K	0.1	0.2	sea water	stress relieved	160	--	97700 *
A70-18-3-Z-RO-G-K	0.1	0.2	sea water	stress relieved	180	--	110200
A70-18-4-Z-RO-G-K	0.1	0.2	sea water	stress relieved	140	--	210500
A70-18-5-Z-RO-G-K	0.1	0.2	sea water	stress relieved	130	--	> 2000000
A70-19-1-Z-RO-G-K	0.1	0.2	sea water	stress relieved	120	--	357900
A70-19-2-Z-RO-G-K	0.1	0.2	sea water	stress relieved	140	--	320000
A70-19-3-Z-RO-G-K	0.1	0.2	sea water	stress relieved	120	--	307200
A70-19-4-Z-RO-G-K	0.1	0.2	sea water	stress relieved	110	--	> 2000000

* following test on the same testspecimen applied at a higher stressrange

Table 2.2.6 continued

Specimen code	stress ratio R	frequency Hz	environment	influencing weld-parameter	stress range N/mm^2	number of cycles until initiation N_i	number of cycles until fracture N_f
				WELD FINISHING			
A40-20-1-L-RO	0.1	5	air	grinding	90	-	> 10000000
A40-20-2-L-RO	0.1	5	air	grinding	150	1000000	1496800
A40-20-3-L-RO	0.1	5	air	grinding	220	197640	453240
A40-20-4-L-RO	0.1	5	air	grinding	120	1000000	2676600
A40-20-5-L-RO	0.1	5	air	grinding	110	2905000	4402400
A40-21-1-Z-RO	0.1	0.2	sea water	grinding	200	167000	254280
A40-21-2-Z-RO	0.1	0.2	sea water	grinding	200	190000	243240
A40-21-3-Z-RO	0.1	0.2	sea water	grinding	120	800000	929660
A40-21-4-Z-RO	0.1	0.2	sea water	grinding	90	1732060	2453100
A40-21-5-Z-RO	0.1	0.2	sea water	grinding	80	-	3825610
A40-22-1-L-RO	0.1	5	air	TIG dressed	180	304000	496604
A40-22-2-L-RO	0.1	5	air	TIG dressed	120	740000	1206460
A40-22-3-L-RO	0.1	5	air	TIG dressed	120	594000	1056440
A40-22-4-L-RO	0.1	5	air	TIG dressed	144	475000	858000
A40-22-5-L-RO	0.1	5	air	TIG dressed	100	3830000	5838300
A40-22-6-L-RO	0.1	5	air	TIG dressed	110		> 10000000
					130		3322100 *
A40-23-1-Z-RO	0.1	0.2	sea water	TIG dressed	100	-	1716207
A40-23-2-Z-RO	0.1	0.2	sea water	TIG dressed	150	150000	299880
A40-23-3-Z-RO	0.1	0.2	sea water	TIG dressed	120	-	640728
A40-23-4-Z-RO	0.1	0.2	sea water	TIG dressed	80	833450	2235820
A40-23-5-Z-RO	0.1	0.2	sea water	TIG dressed	70	-	2994650
A40-24-1-L-RO	0.1	5	air	plasma dressed	120	-	> 10000000
					150	-	3000000 *
					180	-	3000000 *
					200	600000	806400 *
A40-24-2-L-RO	0.1	5	air	plasma dressed	180	-	758200
A40-24-3-L-RO	0.1	5	air	plasma dressed	200	-	542000
A40-24-4-L-RO	0.1	5	air	plasma dressed	250	172300	289768
A40-25-1-Z-RO	0.1	0.2	sea water	plasma dressed	200	-	261238
A40-25-2-Z-RO	0.1	0.2	sea water	plasma dressed	160	-	563260
A40-25-3-Z-RO	0.1	0.2	sea water	plasma dressed	200	140000	257640
A40-25-4-Z-RO	0.1	0.2	sea water	plasma dressed	90	2093130	2378780
A40-26-1-L-RO	0.1	5	air	improved profile	180	-	195910
A40-26-2-L-RO	0.1	5	air	improved profile	100	600000	2022680
A40-26-3-L-RO	0.1	5	air	improved profile	160	250000	501480
A40-26-4-L-RO	0.1	5	air	improved profile	100	2000000	2782080
A40-27-1-Z-RO	0.1	0.2	sea water	improved profile	100	1372000	1887608
A40-27-2-Z-RO	0.1	0.2	sea water	improved profile	100	-	1879792
A40-27-3-Z-RO	0.1	0.2	sea water	improved profile	160	120000	227100
A40-27-4-Z-RO	0.1	0.2	sea water	improved profiel	80	2000000	2668730

*following test on the same testspecimen applied at a higher stressrange

Table 2.2.6 continued

Specimen code	stress ratio R	frequency Hz	environment	influencing weld parameter	stress range N/mm^2	number of cycles until initiation N_i	number of cycles until fracture N_f
				STRESS RELIEVING			
A40-47-1-L-RO	0.1	4	air	stress relieved	144	500000	1650000
A40-47-2-L-RO	0.1	4	air	stress relieved	180	260000	370000
A40-47-1-3-L-RO-G	0.1	5	air	stress relieved	180	90000	278883
A40-47-1-4-L-RO-G	0.1	5	air	stress relieved	120	250000	1487610
A40-48-1-L-RO-G	0.1	5	air	stress relieved	85	4000000	8850000
A40-48-5-L-RO-G	0.1	5	air	stress relieved	95	1600000	5193390
A70-28-1-L-RO	0.1	2	air	as welded	117	--	1276400
A70-28-2-L-RO	0.1	2	air	as welded	144	--	385600
A70-28-3-L-RO	0.1	3	air	as welded	126	--	690000
A70-28-4-L-RO	0.1	2	air	as welded	108	--	1389800
A70-29-1-Z-RO	0.1	0.2	sea water	as welded	171	--	142000
A70-29-2-Z-RO	0.1	0.2	sea water	as welded	144	--	152000
A70-29-3-Z-RO	0.1	0.2	sea water	as welded	110	--	401100
A70-29-4-Z-RO	0.1	0.2	sea water	as welded	126	150000	351100
A70-30-1-L-R_1-G	-1	2	air	stress relieved	160	800000	1720000
A70-30-2-L-R_1-G	-1	2	air	stress relieved	260	--	270400
A70-30-3-L-R_1-G	-1	2	air	stress relieved	220	--	370700
A70-30-4-L-R_1-G	-1	2	air	stress relieved	200	--	753600
A70-31-1-Z-R_1-G	-1	0.2	sea water	stress relieved	260	--	78600
A70-31-2-Z-R_1-G	-1	0.2	sea water	stress relieved	200	--	262500
A70-31-3-Z-R_1-G	-1	0.2	sea water	stress relieved	180	--	405100
A70-31-4-Z-R_1-G	-1	0.2	sea water	stress relieved	140	--	833600
A70-32-1-L-R_1	-1	2	air	as welded	200	--	202000
A70-32-2-L-R_1	-1	2	air	as welded	160	--	465200
A70-32-3-L-R_1	-1	2	air	as welded	120	--	1000000
A70-32-4-L-R_1	-1	2	air	as welded	140	330000	777800
A70-33-1-Z-R_1	-1	0.2	sea water	as welded	120	--	543100
A70-33-2-Z-R_1	-1	0.2	sea water	as welded	200	--	79500
A70-33-3-Z-R_1	-1	0.2	sea water	as welded	260	--	117100
A70-33-4-Z-R_1	-1	0.2	sea water	as welded	100	--	666700

Table 2.2.6 Testresults

Specimen code	stress ratio R	frequency Hz	environment	influencing weld-parameter	stress range N/mm2	number of cycles until initiation N_i	number of cycles until fracture N_f
				BASIC TESTS			
A40-1-1-L-R0	0.1	4	air	as welded	180	80000	260000
A40-1-2-L-R0	0.1	4	air	as welded	144	110000	430000
A40-1-3-L-R0	0.1	5	air	as welded	144	120000	447115
A40-1-4-L-R0	0.1	5	air	as welded	180	70000	267020
A40-1-5-L-R0	0.1	4	air	as welded	126	130000	910000
A40-1-6-L-R0	0.1	4	air	as welded	117	--	1100000
A40-48-2-L-R0	0.1	6	air	as welded	80	--	2470000
A40-48-3-L-R0	0.1	6	air	as welded	70	--	7382000
A40-48-4-L-R0	0.1	6	air	as welded	60	--	9123300
A40-1A-1-L-R0	0.1	5	air	as welded	120	290000	1029870
A40-1A-2-L-R0	0.1	5	air	as welded	100	400000	1905560
A40-1A-3-L-R0	0.1	5	air	as welded	120	240000	946640
A40-2-1-Z-R00	0.1	0.2	sea water	as welded	235	--	273000
A40-2-2-Z-R0	0.1	0.2	sea water	as welded	216	--	53300
A40-2-3-Z-R0	0.1	0.2	sea water	as welded	99	--	996500
A40-2-4-Z-R0	0.1	0.2	sea water	as welded	180	--	160000
A40-2A-1-Z-R0	0.1	0.2	sea water	as welded	180	70000	116600
A70-3-1-L-R0-G	0.1	3	air	stress relieved	144	80000	740000
A70-3-2-L-R0-G	0.1	3	air	stress relieved	126	1100000	1900000
A70-3-3-L-R0-G	0.1	2	air	stress relieved	117	--	> 2024200
A70-3-3-L-R0-G	0.1	2	air	stress relieved	216	--	149300 *
A70-3-4-L-R0-G	0.1	3	air	stress relieved	162	160000	380000
A70-3-6-L-R0-G	0.1.	3	air	stress relieved	180	--	340000
A70-3-7-L-R0-G	0.1	3	air	stress relieved	100	--	1443800
A70-3-8-L-R0-G	0.1	2	air	stress relieved	100	--	1288000
A70-4-1-Z-R0-G	0.1	0.2	sea water	stress relieved	198	--	60350
A70-4-2-Z-R0-G	0.1	0.2	sea water	stress relieved	90	--	719500
A70-4-3-Z-R0-G	0.1	0.2	sea water	stress relieved	160	--	117700
A70-4-4-Z-R0-G	0.1	0.2	sea water	stress relieved	120	--	274700
A70-4-5-Z-R0-G	0.1	0.2	sea water	stress relieved	70	--	2000000
				SPECIMEN TYPE			
B40-5-1-L-R0	0.1	4	air	as welded	180	--	465000
B40-5-2-L-R0	0.1	4	air	as welded	110	--	1718300
B40-5-3-L-R0	0.1	4	air	as welded	220	--	235300
B40-5-4-L-R0	0.1	4	air	as welded	144	--	804200
B40-6-1-Z-R0	0.1	0.2	sea water	as welded	220	--	102600
B40-6-2-Z-R0	0.1	0.2	sea water	as welded	110	--	640400
B40-6-3-Z-R0	0.1	0.2	sea water	cruciform a.w.	120	350000	536440
B40-6-4-Z-R0	0.1	0.2	sea water	cruciform a.w.	180	100000	173000
C40-8-1-L-R0	0.1	4	air	as welded	180	--	714800
C40-8-2-L-R0	0.1	4	air	as welded	150	--	1394700
C40-8-3-L-R0	0.1	3	air	as welded	234	--	416400
C40-8-4-L-R0	0.1	4	air	as welded	162	--	test cancelled
D40-10-1-L-R0	0.1	5	air	as welded	216	--	300000
D40-10-2-L-R0	0.1	5	air	as welded	144	--	1400000
D40-10-3-L-R0	0.1	5	air	as welded	180	--	485400
D40-10-4-L-R0	0.1	5	air	as welded	162	--	846000
D40-11-1-Z-R0	0.1	0.2	sea water	as welded	216	--	93800
D40-11-2-Z-R0	0.1	0.2	sea water	as welded	180	--	212400
D40-11-3-Z-R0	0.1	0.2	sea water	as welded	120	--	1003500
D40-11-4-Z-R0	0.1	0.2	sea water	as welded	144	--	411500
B70-7-1-L-R0-G	0.1	1.5	air	stress relieved	240	--	128100
B70-7-2-L-R0-G	0.1	2	air	stress relieved	160	--	458300
B70-7-3-L-R0-G	0.1	2.6	air	stress relieved	120	--	1358200
B70-7-4-L-R0-G	0.1	3	air	stress relieved	100	--	2752900
C70-9-1-L-R0-G	0.1	2	air	stress relieved	180	--	535100
C70-9-2-L-R0-G	0.1	3	air	stress relieved	216	--	380000
C70-9-3-L-R0-G	0.1	3	air	stress relieved	144	--	> 2055500
C70-9-3-L-R0-G	0.1	3	air	stress relieved	234	--	84200 *
C70-9-4-L-R0-G	0.1	3	air	stress relieved	162	--	1393000

* following test on the same testspecimen applied at a higher stressrange

Tabel 2.2.4. Chemical composition of substitute ocean water (without heavy metal ions)

Compound	Concentration mg/L
Na Cl	24.53
$Mg\ Cl_2$	5.20
Na_2So_4	4.09
$Ca\ Cl_2$	1.16
KCL	0.695
$NaHCO_3$	0.201
Kr	1.101
H_3BO_3	0.027
S_rCL_2	0.025
N_aF	0.003

Tabel 2.2.5. Range of seawater parameters

Parameter	Range
PH	7.8 to 8.2
HCO_3^-	0.08 to 0.25 mg/L
Salinity	32 to 37 mg/L
Chorinity	18 to 21 mg/L
Dissolved oxygen	92 - 95% saturated
Temperature	$20^oC \pm 1^oC$

Table 2.2.3 Testing Programme

Influencing parameter		Specimen type	Testseries	Thickness mm	Environment air	Environment seawater	Stress ratio	Frequency Hz.
Basic tests	as welded	A	A40-1	40	x		0.1	5
	as welded	A	A40-1A	40	x		0.1	5
	as welded	A	A40-2	40		x	0.1	0.2
	as welded	A	A40-2A	40		x	0.1	0.2
	stress relieved	A	A70-3	70	x		0.1	5
	stress relieved	A	A70-4	70		x	0.1	0.2
Type	B-type	B	B40-5	40	x		0.1	5
	B-type	B	B40-6	40		x	0.1	0.2
	B-type	B	B70-7	70	x		0.1	5
	C-type	C	C40-8	40	x		0.1	5
	C-type	C	C70-9	70	x		0.1	5
	D-type	D	D40-10	40	x		0.1	5
	D-type	D	D40-11	40		x	0.1	0.2
Stress-relieving	stress relieved	A	A40-47-1	40	x		0.1	5
	stress relieved	A	A40-48	40	x		0.1	5
	as welded	A	A70-28	70	x		0.1	5
	as welded	A	A70-29	70		x	0.1	0.2
	stress relieved	A	A70-30	70	x		-1	5
	stress relieved	A	A70-31	70		x	-1	0.2
	as welded	A	A70-32	70	x		-1	5
	as welded	A	A70-33	70		x	-1	0.2
Weld finishing	grinding	A	A40-20	40	x		0.1	5
	grinding	A	A40-21	40		x	0.1	0.2
	TIG-dressing	A	A40-22	40	x		0.1	5
	TIG-dressing	A	A40-23	40		x	0.1	0.2
	Plasma dressing	A	A40-24	40	x		0.1	5
	Plasma dressing	A	A40-25	40		x	0.1	0.2
	Improved profile	A	A40-26	40	x		0.1	5
	Improved profile	A	A40-27	40		x	0.1	0.2
Weldmetal composition	2.5% Ni make 2	A	A40-37	40	x		0.1	0.2
	2.5% Ni make 1	A	A40-37A	40	x		0.1	0.2
	2.5% Ni make 2	A	A40-38	40		x	0.1	0.2
	2.5% Ni make 1	A	A40-38A	40		x	0.1	0.2
Cathodic protection	cath. prot.	A	A70-18	40		x	0.1	0.2
	cath.overprot.	A	A70-19	40		x	0.1	0.2
Variable amplitude loading	Rayleigh distr.	A	A40-43	40	x		zero mean load	2.29
	Rayleigh distr.	A	A40-44	40		x	zero mean load	0.229
	Gauss distr.	A	A40-45	40	x		zero mean load	2.29
	Gauss distr.	A	A40-46	40		x	zero mean load	0.229

Table 2.2.1

TIG-dressing	
Tungsten electrode	: ø 3.2mm
polarity of electrode	: negative
shielding gas	: Ar; 7 lit/min
cup diameter	: ø 11mm
Parameters	
welding current	: 210 A (D.C.)
voltage	: 12.5 V
welding speed	: app. 12 cm/min
heat input	: first run 13.1 KJ/cm
	second run 13.1 KJ/cm

Plasma dressing	
Plasma gas	: 95% Ar + 5% H_2
flow	: 0.75 lit/min
shielding gas	: 100% Ar
flow	: 10 lit/min
nozzle	: ø 3.2 mm
Parameters	
Welding current	: 130 A (D.C.), electrode negative
voltage	: 28-30 V
welding speed	: 10.5 - 12.5 cm/min
heat input	: first run 21.5 KJ/cm
	second run 18.1 KJ/cm

Table 2.2.2

Test series	Weld parameter	Toe radius average mm	Standard deviation	Toe angle average
A40-1	As welded	1.1	0.45	65^o
A40-20	Grinding	4.0	0.00	65^o
A40-22	TIG-dressing (original)	8.2	1.70	65^o
A40-22	TIG-dressing (additional)	4.8	0.67	65^o
A40-24	Plasma-dressing	7.1	0.60	65^o
A40-26	Improved profile	0.9	0.35	45^o

2.2.11. Tables

List of tables

Table 2.2.1 TIG- and Plasma dressing parameters
Table 2.2.2 Weld toe profile measurements.
Table 2.2.3 Testing programme
Table 2.2.4 Chemical composition of substitute ocean water
Table 2.2.5 Range of seawater parameters
Table 2.2.6 Testresults
Table 2.2.7 Regressionlines of the basic tests
Table 2.2.8 Comparison of initiation periods
Table 2.2.9 Initiation periods of the basic tests and of the four dressing methods

4. A conjunction of small cracks involves relatively high local crack growth velocities, which may lead to overestimating the mean crack growth velocity at crack origins.
5. It was established that not every load cycle will cause a striation otherwise one striation is the result of only one load cycle.

cracks. It was established from striation spacing counting that in a pertinent area of the fracture surface of specimen A40-1-5-L-RO, 80% of the total lifetime was covered to generate a crack with a depth of 2mm at that very spot. This particular area was chosen for the TEM investigations because a crack was initiated at this place (see Fig. 2.2.66).
It was not possible to establish at what fraction of the lifetime this crack was initiated.
Striation-counting, systematically leads to a greater fraction of the total lifetime necessary for crack initiation (see table 2.2.8).
A possible explanation for this discrepancy might be that not every load-cycle necessarily leads to the formation of a striation in the area where counting has taken place. Another reason may be the fact that strain spacings smaller than 0.05 μm are hardly visible.
The estimation of the lifetime fraction for crack-growth is therefore too low and thus the estimation of the inition period too high. Moreover the location where straingauge measurements were carried out and the location where striation-counting had taken place were not exactly the same.
Further work has to be done in this field in order to get more information on number, orientation and other specific characteristics of these fatigue cracks. Especially so in view of welding methods, heat treatments, weld finishing techniques etc.

Conclusions

1. Crack growth measurements by means of striation counting on specimens tested in seawater are hardly feasible, because the fracture surface is attacked heavily. However, it seems possible to get valuable information on crack initiation aspects by breaking open some areas that are cracked but otherwise intact.

2. It was established that, for specimens tested in air, more than 80% of the total lifetime is involved in the formation of cracks with a depth of 2 mm.

   Nevertheless some trends on the initiation period, caused by weld parameters like PWHT and weld finishing techniques were observed.

3. On welds containing secondary fatigue cracks only, it was established that a series of small cracks (> 10) had developed.

180 N/mm^2 respectively. The fracture surfaces were examined in the SEM. The results of the striation spacing measurements are given in Fig. 2.2.78 and 2.2.80.
For these three specimens the results of the fractographic analysis in the SEM reveal smaller striation spacings than of specimens A40-1-5 and A40-47-2.
The calculated initiation periods derived from the striation spacing measurements are compared with the percentage of the real initiation periods with respect to the total fatigue life. A review of this comparison is given in table 2.2.9.

Table 2.2.8

Specimen code	Calculation initiation period %	real initiation period in %
A40-47-2	80	70
A40-1-5	80	14
A40-20-3	62	43
A40-22-3	80	59
A40-24-2	73	-

As can be seen in the table the efficiency of crack growth measurements seems to be reasonable in some cases.
However, it was not sure that the measurements were carried out at that particular location were the first crack initiation had taken place. Therefore, it was not possible to establish at what fraction of lifetime the cracks were started on the areas where was measured. This could have caused the deviation between the calculated initiation period and the real (detected during the tests) initiation period.

General discussion of the results

There are two major problems to consider in trying to estimate crack growth data from the results of striation spacing measurements. The first is the occurrence of a considerable attack on the fracture surface, when the tests are performed in seawater. The second problems is the phenomenon of multiple crack initiation at the root of the weld. These cracks will join in their growing process. This conjunction of cracks involves relatively high crack growth velocities in the unbroken material between the

0.5 µm/striation. The scatter, too was larger in this case; the narrowest striations were 0.2 µm and the broadest about 0.6 µm.
The calculated total number of cycles, derived from the local observations on the fracture surface to allow crack growth from 2 mm until whole fracture is about 70.000. The N_f is 370.000 cycles. This means that about 80% of the total lifetime was consumed in forming cracks of approximately 2 mm depth. The area with secondary cracks on the other side of the gusset was examined macroscopically. For that purpose, the remaining uncracked material was sawn through, cooled in liquid nitrogen and broken by brittle fracture. Fig. 2.2.68 gives an overall view of the fracture surface near the weld, containing 11 cracks of which some were already joined. The joining of two cracks lead to relatively high local crack growth between the two former cracks (~0.2 µm/striation).

Specimen A40-1-1-L-RO

From this specimen only the fracture surface with secondary cracks was investigated. Fig. 2.2.69 shows the fatigue crack which was developed. In this case, all formed minor cracks were already grown together, forming one closed front. The remaining part of the main plate was broken by cleavage in liquid nitrogen. The maximum crack depth of the fatigue crack was 11 mm. Fig. 2.2.70 shows a part of the fracture, photographed under an angle. The Figure shows that, in the initiation areas, cracks have grown below and above another on different planes.
During the growing in depth, these cracks were joined. This mechanism of crack growth at the beginning of the test lead to the formation of small shelves of unbroken material on the fracture surface.
Strain gauges were mounted in the vicinity where crack development was to be expected. Strain gauge no. 4 (see Fig. 2.2.69) attached in the area where the crack depth was about 8 mm, showed a substantial decrease in µstrain after 200.000 cycles. The second strain gauge (no.3 on Fig. 2.2.69), which was also attached on this side of the gusset, showed at the end of the test (~260,000 cycles) an increase in µ strain of about 25%. The tip of the growing crack had then just arrived in the area of this strain gauge. This phenomenon is described in detail in paragraph 2.2.6.7.

Specimens A40-20-3, 22-3 and 24-2

These specimens were tested in air at stress ranges of 220-, 120- and

It was to be expected that smaller striations are present in the vicinity of the crack's origin. Therefore, carbon replicas were prepared for examination in the transmission electron microscope (TEM).
Because of limitations in the preparation of the replicas, the uttermost edge of the fracture was not visible on the replicas. The distance closest to the edge was 0.4 mm. The smallest striations found in this area had a spacing of about 0.04 µm (see Figs. 2.2.64A and 2.2.64B).
Figs. 2.2.65A and 2.2.65B show fracture appearances at 1 and 3 mm depth, respectively. In these areas, the spacing is about 0.05 to 0.07µm.
A diagram showing the measured striation as a function of the actual crack-depth is given in Fig. 2.2.66. Striations smaller than 0.04-0.06 µm are often hardly visible. This might lead to overestimation of the mean striation spacing in the vicinity of crack origin. Due to coalescence of small fatigue cracks, the scatter in spacing in the welded material was relatively high.
At a crack-depth of 18 mm, striations spacings of 0.08 to 0.5 µm were found in the same area. See for example Figs. 2.2.67A and 2.2.67B which show differences in spacing at the same crack-depth. These results are at variance with the usual findings in electrical potential drop measurements, where the results suggest a very small scatter in crack growth velocity. Moreover, the macroscopic appearance suggests a homogeneous running crack front. This means that the microcrack growth rates can shift considerably, possibly depending on the local microstructure and the coincidental orientation of grains. This feature is confirmed by the fact that, on these fracture surfaces, striation-shaped areas are isolated and small.
The calculated total number of cycles derived from the local fractographic observations to allow crack growth from 2 mm until total fracture was about 150.000. The N_f was 930.000 cycles. Thus more than 80% of the total lifetime was consumed in crack formation of 2 mm depth in the area considered.

Specimen A40-47-2-L-RO-G

This specimen was tested in air (stress range = 180 N/mm^2, f = 4Hz, N_f = 370,000 cycles). The fracture surface was examined in the SEM. The results of the fractographic analysis in the SEM show somewhat larger striation spacings than in the case of specimen A40-1-5-L-RO, namely

This figure reveals the crack's origin at the toe of the weld. The crack starts in the weld toe at the top of the photograph and runs to the bottom. The arrow indicates the crack growth direction. This figure also shows that the crack originated from an undercut at the weld toe.

Fig. 2.2.59 shows a detail of the area indicated in Fig. 2.2.57.
The arrow in Fig. 2.2.59 indicates the area where a crack was initiated. This crack was growing solitarily until neighbouring cracks came in the vicinity of its tips. Then the cracks grew simultaneously, on different planes, to a certain depth, after which the two cracks grew into one crack front that grew further alone.
The fracture surface in Fig. 2.2.59 shows that, at the uttermost edge of the fracture, a coarse structure has developed. This structure correlates with the heat-affected zone near the welded area shown at the top of Fig. 2.2.58.
Figs. 2.2.60 and 2.2.61 give more details about fracture aspects in the coarse area. The arrow indicates small grain facets broken by cleavage while the fatigue crack front was passing along. Cleavage of a large grain disturbed the regularly crackfront running. This resulted in a crack growth path lying at a slightly deeper level.
Areas broken by cleavage have also been obtained in the weld material, as shown in Fig. 2.2.62. These areas are smaller due to the structure of the weld. Moreover, these areas were less frequently obtained than in the coarse structured HAZ.
Next to the coarse structure (see Fig. 2.2.59) is visible a narrow band of very fine fracture. This zone corresponds with the area in the vicinity of the weld shown in Fig. 2.2.58. This fine structure has developed after austernizing during the welding, followed by rapid cooling; the upshot is a fine ferretic perlitic structure. This band has a width of about 2 mm.

The fracture surface was examined in the scanning electron microscope (SEM) in order to get data on crack growth. Striations were observed by the SEM in an area beginning at a depth of 2 mm through the whole fracture. Striation spacings were found to be remarkably constant over a depth from 2 to 16 mm; namely 3 μm. The scatter is small.
Figs. 2.2.63A and 2.2.63B show representative SEM-micrographs of the fracture surface.

In all the specimens the cracks were started in the load carrying (main-) plate at the toe of the weld; sometimes at both sides of the gusset. For two testspieces, the crack initiation and propagation at the side of the gusset where secondary cracks had developed, were also investigated. The fracture surfaces were then released by means of sawing and breaking open the remaining area in liquid nitrogen.

Methods

All fractures were examined first macroscopically. Five fracture surfaces were examined by means of scanning electron microscopy (SEM). The fracture surface was moreover examined by transmission electron microscopy (TEM), for correlation with SEM-results. For that purpose, numerous plastic replicas were prepared of several areas of the fracture considered. The specimen tested in seawater was examined by TEM. Furthermore a comparison between the results of crack growth measurements by means of striation counting and the results of straingauge measurements has been made.

Results

Specimen A40-2-3-Z-R0

This specimen was tested in seawater (stress range = 99 N/mm^2, f = 0.2Hz, N_f = 996,500 cycles). The fracture surface was found to be heavily attacked. Of a selected area, carbon replicas were prepared and examined by TEM. In a few areas of this fracture surface, striation shaped features were found (see Fig. 2.2.56). These striations were attacked by the corrosive medium. The spacing was 0.2 μm at a distance of 15 mm from the origin of the crack. Because of the scarceness of areas with reasonably developed striations, it was hardly possible to establish crack growth data. Information on crack initiation seemed to be obtainable after breaking open some small cracks.

Specimen A40-1-5-L-R0

This specimen was tested in air (stress range = 126 N/mm^2, f = 4 Hz, N_f = 930,000 cycles). The fracture surfaces were examined extensively, Fig. 2.2.57 shows a macrograph of a fracture surface. The arrow indicates the area where on the counterpart of this fracture surface, a metallographic specimen has been prepared; it is shown in Fig. 2.2.58.

2.2.10. Appendix 2.2-I

Fractography analysis of some T-shape welded specimens, broken in endurance tests

As a part of this research programme on the corrosion fatigue behaviour of welded joints, some fractographic work has been performed in order to investigate the efficiency of crack growth measurements by means of striation counting and striation spacing measurements on welded specimens, broken in fatigue endurance tests, performed in air or in seawater. Moreover some general fractographic aspects within the scope of the ECSC corrosion fatigue project were considered.
The results of these crack-growth measurements by means of striation counting can be helpful to a proper interpretation of the fatigue endurance tests.

Experimental

Specimens

The fractographic analysis was performed on the fracture surfaces of specimens of the A-type (non load carrying T-shape welded joints). Specimens of the basic test series (as welded and stress relieved) and of the four finishing techniques were investigated.

These ten specimens were investigated:

Specimen code	Weld parameter	air	seawater	stress range N/mm^2	N_i	N_f
A40-2-3-Z-RO	as welded		x	99	-	996,500
A40-1-5-L-RO	as welded	x		126	130,000	930,000
A40-47-2-L-RO-G	stress relieved	x		180	260,000	370,000
A40-1-1-L-RO	as welded	x		180	80,000	260,000
A40-20-3-L-RO	grinding	x		220	197,640	453,240
A40-22-3-L-RO	TIG dressing	x		120	594,000	1,056,440
A40-24-2-L-RO	Plasma dressing	x		180	-	758,200
A40-26-4-L-RO	improved profile	x		100	2,000,000	2,782,080
A40-21-2-Z-RO	grinding		x	200	190,000	243,240
A40-23-2-Z-RO	TIG dressing		x	150	150,000	290,880

N_i = number of cycles until crack initiation (measured with strain gauges).
N_f = number of cycles until total fracture.

| 9| J.W. Knight
"Improving the fatigue strength of fillet welded joints by grinding and peening".
Welding Institute Members' Report 8/1976/E, 1976

|10| M. Hanzawa, H. Yokota and T. Ishiguro et al
"Improvement of fatigue strength in welded high tensile strength steel by toe treatment", IIW doc. XIII-829-77
Nippon Steel Corporation
Japan, July 1977.

|11| G.S. Booth
"A note on the influence of plate thickness on fatigue strength found in the Dutch and British tests-Draft".
The Welding Institute U.K., September 1979.

|12| S. Berge
"Fatigue crack initiation in weldments of a C-Mn Steel".
Ref. |3| , Paper 6.

2.2.9. References to chapter 2.2.

|1| American Society for Testing and Materials
"Standard specifications for substitute ocean water"
ASTM D 1141-52 (reapproved 1971).

|2| T.S. Gurney
"Fatigue design rules for welded steel joints"
Welding Institute Research Bulletin 17,
United Kingdom, May 1976.

|3| Select Seminar on European Offshore Steels Research
The Welding Institute, Abington Hall, Cambridge U.K.
27-29 November 1978

|4| O. Solli and P. Tenge
"Corrosion fatigue of welded joint in structural steels and the effect of cathodic protection", Technical Report no. 78-094
Det Norske Veritas, Norway, 30th March 1978

|5| M.Greif, W.Oberparleiter, R.olivier and W.Schütz.
"Untersuchungen zur Korrosionsermüdung an Offshore-Konstruktionen"
Abschlusbericht, EGKS-Vertrag Nr. 7210-KB/1/102
IABG-LBF, West Germany, 1981.

|6| G.S. Booth
"Constant amplitude fatigue tests performed on welded steel joints in seawater".
Ref. | 3 | , paper 9.

|7| Duquette
"Corrosion fatigue of metals and alloys"
Rensselaer polytechnic Institute, (AD-742-461)
Troy, New York, May 1972

|8| G.S. Booth
"Constant amplitude fatigue tests performed on welded steel joints in air".
Ref. | 3 | , paper 4.

results of the basic corrosion fatigue tests, no disastrous effect of overprotection was found.

9. Comparison of the results of the basic tests carried out in seawater with existing fatigue design curves, reveals that these curves are somewhat optimistic for unprotected welded steel joints under corrosion fatigue.

2.2.8. Conclusions

Constant amplitude fatigue tests were carried out in air and seawater on nonload- and load-carrying welded steel joints. The following conclusions can be drawn:

1. The S-N curves (based on stress range) obtained for air and seawater clearly reveal a deteriorating effect of the seawater on fatigue endurance. In seawater, the fatigue life was found to be at least a factor 2 to 3 shorter than in air, for lives up to 2.10^6 - 3.10^6 cycles at room temperature.
2. The plate steel thickness does not influence significantly the fatigue strength in air and seawater of the 40- and 70 mm welded steel joints.
3. The type of joint, and therefore the weldtoe angle, seems to be an influencing parameter when the toe angle is smaller than 45^o.
4. Finishing of the weld toe by means of TIG- and Plasma dressing and grinding increases the fatigue life in air as well as in seawater. TIG dressing of the weld toe was suggested to can be improved. A less steep toe angle (45^o versus 70^o) has only a slight beneficial effect. Seawater reduces the favourable effect of all finishing techniques however still a significant beneficial effect of grinding and plasma-dressing remaines.
5. Finishing the weld toe of transverse fillet welded joints subjected to bending fatigue, seems to have not only an effect on the crack initiation period based on the first observation of a visible fatigue crack, but also on the crack propagation period.
6. The stress ratio has a small influence on the fatigue strength in air and seawater of welded joints loaded in bending. An increase in stress ratio from R = -1 to R = 0.1 results in some decrease in fatigue strength. The effect was found not to depend on the environment (air or seawater) and to be more pronounced for the stress relieved specimens than for the as-welded specimens.
7. Alloying the weld electrode with 2.5% Ni, in order to obtain better fracture toughness properties of the joints, has proved to have no significant influence on fatigue behaviour.
8. Cathodic protection seems to be most effective at lower stress ranges and gives an improvement of a factor 4 in life time. Cathodic overprotection seems to have an unfavourable effect on fatigue life in comparison with cathodic protection. However, compared with the

the Dutch tests.
One variable which could have diminished the influence of plate thickness was that for the Dutch tests the overall geometry (ratio between dimensions) of the 70 mm specimens was not exactly the same as that of the 40 mm specimens.
As stated by Booth in his paper [11] further investigation on the influence of plate thickness is needed in view of the potential seriousness of the problem because existing fatigue design rules, mainly based on results of tests on relatively thin joints may not be safe for application to thick joints.

during the dressing and found that a higher heat input up to 15 KJ/cm resulted in longer fatigue lifes.
However, further increasing of the heat input up to 25 KJ/cm did not result in a further increasing of the fatigue life.
Grinding and Plasma-dressing result both in longer fatigue lifes compared with the results of specimens in as welded condition. In seawater the improvement by grinding and plasma-dressing is less pronounced. This is in agreement with the results found at the U.K. |6|
As mentioned before, seawater lowers the improvement in fatigue life as obtained in air. However, still an improvement of the fatigue life in seawater is left (compared with tests on specimens in the as welded condition of the same type). So it might be expected that corrosion protection such as for instance cathodic protection, preventing the formation of corrosion pits, could restore the improvement as obtained in air. None of the above mentioned specimens tested in seawater was subjected to cathodic protection.

2.2.7.5. Cathodic protection

As found at the U.K. |6| and West Germany |5| cathodic protection during the Dutch tests appears to result in longer fatigue lifes especially in the region of lower stress ranges. Some of the specimens, even revealed a longer fatigue life than comparable tests in air.
In the region of higher applied stress ranges this favourable effect of cathodic protection tends to disappear.
Cathodic overprotection, also studied in the Netherlands and West Germany seems to result in lower fatigue lifes than cathodically protected specimens but still somewhat higher than the fatigue lifes of the basic tests in seawater. Therefore, no disastrous effect of overprotection needs to be expected.

2.2.7.6. Effect of specimen thickness

No effect of plate thickness (40 mm versus 70 mm) was found at the Dutch tests. Tests on specimen thickness of 25 mm and 38 mm carried out at the Welding Institute U.K. however, show a slight but significant influence of thickness: the fatigue life increased when the thickness decreased from 38 to 25 mm.
A paper about this discrepancy was written by G.S. Booth |11| (The Welding Institute U.K.). In this paper it is made plausible that the findings of the Welding Institute are not necessarily conflicting with the results of

The increase in fatigue lifes was more pronounced in the case when the specimens were stress relieved.
The results from IABG/LBF (W-Germany) | 5 | , obtained from tests on 20 mm and 50 mm transverse welded specimens in air show similar increase of fatigue lifes at R = -1.
In the Netherlands the results of the tests in seawater show about the same influence of stress ratio (stress relieved- and as welded specimens respectively) as the comparative tests in air. The results from West-Germany however, indicate that the influence of stress ratio disappeared, while in the high cycle fatigue range (0.5×10^7 - 10^7 cycles) an improvement in fatigue strength has been obtained.
At the Welding Institute U.K. the results of the tests |8| on transverse welded joints(as welded), tested under bending condition in air, did not reveal any influence of R. Tests on longitudinal welded joints (as welded) under axial loading condition, indicate that no influence of stress ratio was found either. Tests on the same joint type (with longitudinal welds), however, tested under bending condition show an increase in fatigue life of a factor 1.5.
Reconsidering the testresults discussed above it might be concluded that the influence of stress ratio is believed to be significantly influenced by the condition with respect to residual stresses as found at the tests from the Netherlands.

2.2.7.4. Weld finishing techniques

A lot of work has been carried out in the past on the influence of weld finishing techniques on fatigue. It is not within the scope of this investigation to give an extensive survey of those investigations.
Therefore only a few recent investigations will be discussed.
Furthermore a literature study on this subject has started at the second half year of 1980, sponsored by the government of the Netherlands.
Grinding, TIG- and Plasmadressing of the weld toe of welded joints results in a favourable effect on fatigue life in air.
The improvement found at the Dutch tests are global in agreement with those found in other investigations| 6 , 9 , 10 |
The Dutch tests on TIG-dressed specimens, however, show only an improvement at higher stressranges, which disappears at lower stressranges.
This is at variance with the findings of the Welding Institute | 6 |
and Handrawa et al |10| who has investigated the influence of heat-input

2.2.7. Comparison with the results of other investigations on simular or related materials and specimens

Results arranged according to the parameters mentioned below.

2.2.7.1. Environment

Generally the fatigue life in seawater environment is significantly reduced, compared with the fatigue life in air.
At a temperature of 20°C and a cyclic loading frequency of 0,2 Hz the reduction in fatigue life is found to be about a factor 2-3, compared with the fatigue life in air.
Furthermore, work carried out in Norway by Solli et al | 4 | (Det Norske Veritas) and in West-Germany by Oberparleiter and Olivier | 5 | (Verein Deutscher Eisenhüttenleute LBF/IABG), also shows a reduction in fatigue life of a factor 2-3, due to the detrimental effect of seawater (20°C).
This is not in agreement with the findings of Booth et al | 6 | who had found no detrimental influence of seawater on fatigue life. However, these experiments were performed at 5°C.
The results of older research work | 7 | reveal that in an aggressive environment, temperature was found to be an influencing parameter; a higher temperature resulted in shorter fatigue lifes.
In the ECSC programme no endurance tests in seawater were carried out at different temperatures within the same laboratory.
Notwithstanding the fact that no firm conclusion can be stated with respect to the influence of temperature, it might be argued that lowering the test-temperature could have diminished the detrimental effect of seawater on fatigue life.

2.2.7.2. Post weld heat treatment

Post weld heat treatment was found to have a beneficial effect on fatigue life in air. The improvement was more pronounced at a stress ratio of R =-1 than at R = 0.1.

2.2.7.3. Stress Ratio

A comparison of the results, from different laboratories with respect to the influence of stress ratio R, shows that they are more or less inconclusive. In the Netherlands (at TNO) the tests, performed in air at a stress ratio of R = -1 show a significant increase in fatigue lifes compared with the results of the tests, carried out at R = 0.1.

respect to the different finishing techniques.
Furthermore it was established from som fracture surfaces that finishing of the weld toe has also a favourable effect with regard to decreasing of the formation of multiple crack initiation (see Fig. 2.2.75).
Reconsidering the facts that crack initiation on grinded and plasma dressed specimens had taken place at 50-60% of the total lifetime, while the improvement on total fatigue life was up to 3 times, it might be concluded that finishing has also a favourable effect on the crack propagation period of this type of specimens.

2.2.6.9. Strain concentration measurements

Fig. 2.2.49 up to and inclusive 2.2.54 give the results of the measurements of the strainconcentrationfactors. The first straingauge of the applied stripgauges (5 straingauges on a line) was bonded 2mm from the weld toe.
Therefore the theoretical SNCF at the weld toe (see the dotted line) was considered to have a value which was obtained from linear extrapolation of the results of the straingauges which were situated at a distance of 2mm and 4mm respectively from the weld toe. Fig. 2.2.55 gives a comparison of the measurements on the six different specimens. As can be seen finishing of the weld toe tends to have an influence on the SNCF (and therefore on fatigue life).

2.2.6.10. Fractography

The results of the fractographic study on fracture surfaces of specimens broken in endurance tests, are described in detail in Appendix 2.2-I
Therefore, only a summary of the results will be given here.
There are two major problems to consider in order to get reliable data for the calculation of crack growth velocities by means of the summation of striation spacings. Firstly the considerable attack on the fracture surface when the tests were performed in seawater. The second problem is the phenomenon of multiple crack initiation. These cracks will join in their growing process.
Considering the results of striation spacing measurements, as presented in Fig. 2.2.71 up to and inclusive Fig. 2.2.73, it was established that in the pertinent area of the fracture surfaces of the specimens, 60% to 80% of the total lifetime was covered to obtain a crack of 2mm depth.
However it must be emphasized that it was not possible to establish at what fraction of the lifetime the cracks were started at the particular areas where the measurements had taken place.

2.2.6.8. Crack initiation

The moment of crack initiation has been detected for many fatigue tests.
Two methods of detection were used, viz.

- Optical detection
- Straingauges (with a measuring length of 3 mm) were attached 10 mm from the weld toe of the specimens.

An advantage of the second method is the reasonable accuracy.
However, the proper detection of crack initiation is restricted to cracks initiated in the immediate vicinity of the straingauge (at a maximum distance of about 30 mm).
With the method described it was possible to detect surface cracks with a length of about 20 mm and a depth at that stage of about 1-2 mm.
A method with a much better accuracy was used by Berge et. al. |12| who had attached 1mm gauges at a distance of 1 mm from the weld toe.
With his method it was possible to detect cracks with a depth of 0.1 mm-0.2 mm. However, the area of susceptibility along the weld toe in transverse direction is very restricted. Therefore the method mentioned earlier with a moderate accuracy was chosen.
During the fatigue tests in seawater, the same method (by means of straingauges) of crackinitiation detection was used. A problem, however, was to avoid the corrosion attack of straingauges. The maximum time that could be measured was about 4 months. However, during a number of tests in seawater the straingauges were destroyed before crackinitiation could have been detected.
The above mentioned difficulties concerning the determination of crack initiation periods illustrate that the accuracy could not have been constant during all tests.
Nevertheless some trends on crack initiation time have been observed for a number of influencing welding parameters such as the basic tests, tests on specimens performed with weld toe finishing like grinding, TIG- and Plasmadressing. Table 2.2.9 gives a review of the established crack initiation periods.
In Fig. 2.2.74 the same results are given in terms of percentage of the total lifetime. The Figure shows that finishing of the weld toe result in longer initiation periods compared to the basic tests.
Generally, increase of crack initiation periods was found to be a factor 2.
As the figure indicates, no further differentiation could be made with

2.2.6.7. Strain gauge measurements

The tendencies observed during testing of all specimens were similar. Consequently the results of strain gauge measurements on only one specimen will be discussed. The location of the gauges on this specimen is indicated in Figure 2.2.20.

In Fig. 2.2.46 the strains of various gauges attached to the surface of a T-shape specimen have been plotted as a function of the number of cycles. In Fig. 2.2.47 the strains of some gauges at the back face of the specimen (opposite the gusset) have been plotted in a similar diagram. The strains were measured at the maximum value of the cyclic load. The initial value of the strains was set equal to 100%.
Fig. 2.2.46 shows that the strain of the gauges situated on the surface at the central part of the main plate at the cracked side (gauges 4, 5 and 6) began to decrease steadily after a period that the strainrange had been constant.
The strain of gauges situated on the same specimen surface in the vicinity of the side edges (gauges 3 and 9) showed a gradual increase until shortly before the end of the fatigue life of the specimen, the strain of these gauges showed a rather abrupt and steep drop.
The strain of the gauges at the back face is in fact negative; in Figure 2.2.47 the absolute value is plotted. This strain remaining constant in the initial stage, tended to increase strongly in the last stage of the test.

The steep drop of the strain at the surface near the sides occurred when the fatigue crack front at this surface passed along these gauges. As illustrated in Fig. 2.2.48 in that stage the crack depth in the centre of the width was already rather large so it is not surprising that the drop of the strain near the sides occurred just before the end of the fatigue life of the specimen.

During all experiments cracks initiated in the load carrying plate at the toe of the weld. Generally crack initiation took place at the toes at both sides of the gusset. After some time however, crack development at one of both sides became dominant.

2.2.6.6. Influence of cathodic protection

The results of the tests on cathodically protected (-900 mV) and overprotected (-1100 mV) 70 mm specimens are shown in Fig. 2.2.45.
The results indicate that cathodic protection is only effective at low(er) stress range values. This is in agreement with the findings of the Welding Institute, as presented by G.S. Booth during the European Offshore Steels Research Seminar held in Cambridge on 27-29 November 1978 |3| .
Furthermore, cathodic overprotection seems to have an unfavourable effect on fatigue life compared with the results of cathodically protected specimens. However, the lifetime of the overprotected specimens is still somewhat higher than the basic testseries in seawater. Therefore, no disastrous effect of overprotection has been observed.

The figure shows that this specimen type results in longer fatigue lifes: a factor 2.5 in air and about a factor 1.5 in seawater. The improved fatigue behaviour is considered to be the result of reduction of the strain concentration factor at the weld toe, caused by the overall geometry of this type of joint and especially the gap between the attached gusset and the main plate.
Furthermore the total heat input during the welding was lower for this joint type than for the T-shape specimen. So the unfavourable effect of residual stresses on fatigue life, especially at lower stress ranges, could have been lowered.
Fig. 2.2.38 shows the S-N curves obtained with the different types of specimens (40 mm) tested in this programme.
Reconsidering these results it should be remarked that both a more favourable shape of the weld toe of the C-type and D-type specimens and a more favourable stress distribution of the cruciform specimens under bending loading, may have caused the increase of the fatigue endurance.
In Fig. 2.2.42 a comparison is given of the S-N lines of the 70 mm A-type B-type and C-type specimens.
As the figure shows the S-N curve of the tests on B-type specimens does not differ significant with the S-N curve of the basic test, in contrast with the 40 mm results of the B-type specimens. Also the improvement of the C-type specimens is less pronounced as the increase in fatigue endurance which was found for the 40 mm C-type specimens. Both the effects found, may be attributed to the fact that the 70 mm specimens were stress relieved prior to testing.

2.2.6.5. Influence of weld metal composition

The results of the tests on specimens, welded with 2.5% Ni-alloyed electrodes of make 1 and make 2 are summarised in table 2.2.6. and presented in Fig. 2.2.43 and Fig. 2.3.44. In Fig. 2.2.43 the results are given of the tests in air and seawater.
Regarding the influence of a 2.5% Ni electrode, the application was not restricted to electrodes of one make.
In Fig. 2.2.44. a comparison is given between the S-N curves of the fatigue results of make 1 and make 2 and the S-N curves of the basic test series.
No significant influence of alloying the welding electrode with 2.5% Ni and, or, the use of electrodes from two different manufactures has been found in air and in artificial seawater.

the 40 mm T-shape specimens, tested in air at a stress ratio of R = 0.1, are given in Fig. 2.2.33.
The influence of PWHT seems to be more pronounced at lower stress ranges than at higher. Fig. 2.2.34 shows the results of the tests with as-welded and stress relieved specimen of 40 mm and 70 mm thickness. This Figure shows that the results of the stress relieved specimens of 40 mm coincide with the results of 70 mm stress relieved specimens. The S-N curve of the results of the tests on the 40 mm as welded specimens is somewhat steeper than the S-N curve of the 70 mm as welded specimens.
The results indicate no significant effect of steel plate thickness on fatigue life both for the specimens in the as welded condition as for the post weld heat treatment specimens.
The number of testresults on the 70 mm specimens is so small, however, that no definite conclusion can be drawn.

2.2.6.4. Influence of specimen type (40 mm and 70 mm thickness)

The results of the tests on different specimen types are given in Fig. 2.2.35 to 2.2.41. For comparison the regression lines of the basic test series are inserted in the figures as well.
In Fig. 2.2.35 the results of the tests on 40 mm specimens of the B-type (cruciform non-load carrying full penetration welds) are given.
The Figure indicates that the fatigue tests in air and seawater both result in longer lifes, especially at higher applied stress ranges.
However, the results of the tests on 70 mm B-type specimens in air show that no influence was found at all (Fig. 2.2.39).
This may be attributed to the fact that the 70 mm B-type specimens were stress relieved while the 40 mm B-type specimens were tested in the as-welded condition.
The testresults of the C-type specimens, only tested in air, (cruciform with load carrying full penetration welds) are given in Fig. 2.2.36 for the 40 mm specimens and in Fig. 2.2.41 for the 70 mm specimens.
Both Figures show an improvement in fatigue life of this specimen type of about a factor 3 compared to the basic test series. The improvement in fatigue life may be attributed to a better weld toe profile (angel of transition between the weld and the main plate, as outlined in Fig. 2.2.40) of this joint type.
Fig. 2.2.37 shows the results of the tests on 40 mm D-type specimens (performed with pure fillet welds).

The fatigue data of the basic test series (air- and seawater results) have been compared with relevant fatigue design curves for the joint geometry under consideration (Class F |2|).
The testresults of 40 mm and 70 mm (as welded specimens) have been used.
The mean design curve and the most commonly used design curve, the mean minus two standard deviations curve, have been used (Fig. 2.2.32).
In comparing the data obtained, it should be remembered that the design curves are intended to be applied primarily to axially loaded joints and that the present results have been obtained under four point bending.
As shown in Fig. 2.2.32 the mean air fatigue results correspond well with the class F_2 mean S-N curve of the design curve; the mean fatigue life of tests in seawater with the class F_2 minus two standard deviation S-N curve of the design curve. However, it should be mentioned that BS 153 does not make distinction between tension and bending.
In considering that the mean value of the seawater results correspond with the class F_2 minus two standard deviation S-N curve, and that the testresults have been obtained under bending loading, this design curve seems to be somewhat optimistic for unprotected welded steel joints under corrosion fatigue conditions.

- Influence of stress ratio: the results of the experiments on the 70 mm T-shape specimens, tested at stress ratios R = 0.1 and R = -1, indicate that the stress ratio can have a significant effect on the fatigue strength.
It may be observed that with the as-welded specimens under bending loading, an increase in stress ratio from R = -1 to R = 0.1 tends to result in a small decrease in the fatigue strength (Fig. 2.2.28).
Fig. 2.2.29 indicates that for the stress relieved specimen this effect is very significant in air and even more in seawater.
This may be explained on the basis of the fact that, in the as-welded joints high tensile residual stresses exist.
Under the applied loading (R = 0.1 and R = -1) the stresses near the weld in the as-welded specimens will largely remain tensile, even under compressive loading (R = -1). Under these circumstances, the stress range can be assumed to be the major variable determining fatigue, and no large effect of stress ratio can be expected when the results are expressed in terms of the applied stress range.

- Influence of PWHT and steel plate thickness: the results of the tests on

- Improved profile: As shown in Fig. 2.2.26 changing the weld angle from 70^{o} to 45^{o} seems to increase the fatigue life in air as well as in seawater only at a high number of cycles. The improvement is not very significant. The overall geometry of the weld seems not to be an important influencing parameter at this specimen configuration under four points bending loading.

  Fig. 2.2.27 gives the best fit curves of the testresults in air and seawater of the four finishing techniques together. The S-N curves of the base testseries (air and seawater) are inserted as well. As can be seen in air, grinding and plasma dressing give significant improvement in fatigue strength while TIG dressing and changing the weld geometry in a more favourable shape give only a slight beneficial influence. Fatigue tests on additional manufactured TIG dressed specimens show that this dressing technique could be optimized.
  In seawater also, grinding and plasma dressing give the best improvement, which is at high stress ranges almost the same as in air while at relatively low stress ranges, these techniques are less effective in improving the fatigue life.

2.2.6.3. Influence of post weld heat treatment and R-ratio (specimen thickness 70 mm)

- Effect of seawater: Fig. 2.2.28 gives the results of the tests in air and seawater on specimens in as-welded condition.
  Fig. 2.2.29 shows the testresults obtained with the stress relieved specimens. The testspecimens have been tested, both the as-welded and the stress relieved specimens, at two different stress ratios, viz. $R = 0.1$ and $R = -1$.
  Fig. 2.2.28 and Fig. 2.2.29 show that the fatigue lifetime is at least a factor 2 to 3 shorter in seawater than in air when the same stress range is applied. The seawater effect on the fatigue behaviour of the welded steel joints seems to be more pronounced for the stress relieved specimens than for the as-welded specimens. Stress relieving has a favourable effect on air fatigue endurance (Fig. 2.2.30 and Fig. 2.2.31).
  In air this effect is larger at $R = -1$ than at $R = 0$ 1 (see Fig. 2.2.30), which can be explained on the basis of crack closure effects. In seawater however, the favourable effect of stress relieving is less pronounced (see Fig. 2.2.31), or even negligible at $R = 0.1$, due to a more detrimental effect of seawater on the fatigue endurance of the stress relieved specimens.

2.2.6.2. Influence of fatigue improvement techniques

- Grinding: Fig. 2.2.23 gives the results of the tests of which the weld toes of the specimens were finished by grinding. As can be seen this finishing technique appears to have a favourable effect, in terms of fatigue life, of 3 times in air and 2 times in seawater. In air the improvement seems to be equal in the short term fatigue life as well as in the high cycle range. In seawater however, the improvement is more pronounced at higher stress levels than at the lower. This can be explained by the fact that a defect on microscale which remained after the dressing run, may accelerate the moment of crack initiation more at relatively low stress levels than at higher stress levels.
  Another effect which affects the crack initiation more during long term corrosion fatigue is the corrosion-time itself which is more effective at low stress range/high cycle fatigue.

- TIG dressing: Fig. 2.2.24 shows that the results of the tests in air of the original specimens, finished by TIG-dressing, indicate that this finishing technique seems to be favourable only in short lifes. However the supplementary tests, manufactured and finished by another welder(within the same welding specifications) shows a greater influence than have been obtained in the original tests.
  Close examination of the improved weld transitions (TIG dressing) shows that the two supplementary testspecimens were provided with better improved weld toe profiles, in terms of surface quality and number of small imperfections (see Fig. 2.2.12), than the four original specimens. Therefore these supplementary testresults are difficult to compare with the original tests.
  The improvement of TIG-dressing on welded specimens tested in seawater seems to be small. One supplementary manufactured and TIG dressed specimen, tested in seawater, seems to have no "manufacturing influence" at all.

- Plasma dressing: Fig. 2.2.25 shows the results of tests on plasma dressed specimens. This finishing technique gives an important improvement on fatigue life: a factor 3 in air and a factor 2 in seawater.
  Obviously, as with the grinded versus the as-welded specimens, dressing of the weld toe seems to be less effective when tested in seawater.

same specifications, coincides with the testresults of the specimens welded with electrodes of make 1 (with which most of the specimens were welded).
Fig. 2.2.22 shows a detrimental influence of seawater on fatigue life of a factor 2 which is normal.
The experiments on 40 mm T-shape specimens with non-load carrying full penetration welds in as welded condition are considered to be the basic tests. Linear regression lines have been computed on a double logarithmic scale.
The regression lines of the 40 mm basic testresults are considered to be a reference for the 40 mm experiments in air and seawater.
Therefore these regression lines of the basic tests in air and seawater are inserted, in other figures, for comparison.
Table 2.2.7 gives a review of the regression lines of the 40 mm basic testseries. The regression lines of the 70 mm basic testseries are also given.

Table 2.2.7.

Testseries	Regression line	Environment	Thickness	Condition with respect to residual stresses
A40 - 1,1A	$\log N = -3.30 \log S_a + 12.85$	air	40	as welded
A40 - 2.2A	$\log N = -3.53 \log S_a + 13.02$	seawater	40	as welded
A70 - 3	$\log N = -3.09 \log S_a + 12.50$	air	70	stress relieved
A70 - 4	$\log N = -3.32 \log S_a + 12.38$	seawater	70	stress relieved

The testresults of the 70 mm stress relieved specimens, tested in air and seawater, are given in Fig. 2.2.29 . These tests are considered to be the basic tests for the 70 mm testseries. The detrimental effect of the seawater on fatigue life appears to be somewhat greater than found at the tests on 40 mm specimens, namely a factor 3 to 4. This will be discussed later on (at the influence of post weld heat treatments).

gauges was 2, the highest about 20. The strain of all gauges was measured periodically during the fatigue life.
Furthermore, measurements of the strainconcentration near the weld toe were carried out on some specimens of the basic test series and for some specimens after weld finishing. For these measurements, special stripgauges were applied. These stripgauges consist of 5 straingauges in line, with a gauge length of 1.3 mm, at a distance of 2 mm from each other.
These stripgauges were bonded in the longitudinal direction along the centerline of the mainplate at a distance of 2 mm from the toe of the weld (see Fig. 2.2.21).

2.2.5.5. Fractography

A fractographic analysis has been performed on ten T-shape specimens. Seven of them were tested in air and three in seawater. The major aim of this work was to investigate the efficiency of crack growth measurements by means of striation counting and striation spacing measurements on fracture surfaces of welded specimens, broken in endurence tests. Moreover, some general fractographic aspects fitting within the scope of the ECSC corrosion fatigue were examined.
All cracks and fracture surfaces were first examined macroscopically. Five fracture surfaces were partly examined by a scanning electron microscope; one of these surfaces was examined by a transmission electron microscope, after preparation of numerous plastic replicas from several areas of the fracture surface in question. In two specimens the weld at the side of the gusset where only secondary cracks were observed has been examined macroscopically. This was achieved by removing the major part of the surrounding uncracked material by saw cutting, and fracturing the remaining ligaments in liquid nitrogen.

2.2.6. Testresults and discussion

The results of all tests are summarised in table 2.2.6 and presented by plotting in S-N curves, in Fig. 2.2.22 up to and inclusive Fig. 2.2.45.

2.2.6.1. Basic testseries

The testresults of the 40 mm basic testseries, carried out in air as well as in seawater, are given in Fig. 2.2.22.
As can be seen from the testresults in air, no endurance limit has been determined up to 10^7 cycles. The testresults of the specimens, welded with an unalloyed electrode of another manufacturer (make 2) with the

The temperature and the PH were controlled continuously. The chemical composition (salinity, bi-carbonate concentration, chlorinity etc.) was controlled periodically. Acceptable ranges for each of these parameters are given in table 2.2.5. A fresh mix of seawater was substituted periodically (about every 3 months).

Table 2.2.5. Range of seawater parameters

Parameter	Range
PH	7.8 to 8.2
HCO_3^-	0.08 to 0.25 mg/l
Salinity	32 to 37 mg/l
Chlorinity	18 to 21 mg/l
Dissolved oxygen	92 - 95% saturated
Temperature	$20^oC \pm 1^oC$

The free corrosion potential was found to be approximately -0.750V with respect to an Ag/AgCl reference electrode.
The tests under cathodic protection were performed at a potential of -0.900V and under overprotection at -1.100V with respect to an Ag/Agcl reference electrode. For both series under cathodic protection an impressed current system was used.
For the corrosion fatigue experiments the central part of the specimens was surrounded by a transparant box of about 10 l (see Fig. 2.2.19) through which the seawater was pumped from a reservoir of 1000 l with a flow rate of about 1 l/min. During all these tests the "solution volume-to-specimen area" ratio was 3 to 6 times the minimum as recommended in ASTM specification G31-72.

2.2.5.4. Straingauge measurements

Straingauge measurements were carried out during a limited number of tests. The straingauges were attached to the surface of the main plate adjacent to the weld toe, and sometimes to the plate surface opposite the gusset as well (see Fig. 2.2.20). These measurements were envisaged to obtain a general impression of the initial strain distribution over the specimen width and information about the time (number of cycles) and the location(s) of crack initiation. The lowest number of strain-

The experiments in air were tested at loading frequencies between 2 and 10 Hz; in aerated seawater the loading frequency was 0.2 Hz.
The T-shape specimens (A- and D-type) were inserted in the loading machine in such a way that at R = 0.1 the weld toe was loaded in tension.
Final failure of a fatigue test was defined when the fatigue crack had extended over more than half the specimen thickness, measured on the side edge of the specimen. Moreover, when a fatigue test in air had reached a lifetime of 10^7 cycles without any indication of crack initiation the test was stopped.

2.2.5.3. Environmental conditions

The fatigue tests have been performed in:
- laboratory air
- artificial seawater (under freely corroding conditions and with cathodic-over-protection).

All tests were carried out at a temperature of 20°C (air and seawater).

The artificial seawater was prepared according to the specification for substitute ocean water (ASTM specification number D1141-52), without addition of stock solution nr. 3.|1|
During all tests clean air was blowing continually into the supply of seawater to maintain the amount of dissolved oxygen within its specification (92 - 95% saturated).
Chemical composition of the -aerated- seawater is given in table 2.2.4.

Table 2.2.4: Chemical composition

Compound	Concentration mg/L
Na Cl	24.53
$Mg\ Cl_2$	5.20
Na_2SO_4	4.09
$Ca\ Cl_2$	1.16
KCL	0.695
$NaHCO_3$	0.201
Kr	1.101
H_3BO_3	0.027
S_rCL_2	0.025
N_aF	0.003

replicas of the weld toe area. The small ripple at the toe surface, if present, was neglected.
The measurements were done by using a magnifying glass. The results are given in table 2.2.2 (including the average value and the standard deviation).

2.2.4. Loading equipment

During the tests eight test fixtures in three participating laboratories were available.
At the Metal Research Institute in Apeldoorn three test fixtures with capacities of 100, 350 and 500 kN were used simultaneously.
All of them were suitable to test the specimens under R = -1 condition.
In Fig. 2.2.16 one of these test fixtures is shown.
At the Stevinlaboratory (University of Technology, Delft) four test fixtures with capacities of 100 and 250 kN were used. Two of them had the configuration of a common four-point bending fixture as shown in Fig. 2.2.14 and Fig. 2.2.15.
Two of the four other machines were able to test two specimens simultaneously in a twin-loading testing system resulting in normal four-point bending fatigue (see Fig. 2.2.17).
In the test fixture of the Ship Structures Laboratory (University of Technology, Delft) it was possible to test four specimens simultaneously as shown in Fig. 2.2.18.
The fatigue machines discussed above were all equiped with hydraulic actuators, operating in closed loop control with load feed back.

2.2.5. Experimental

2.2.5.1. Influencing parameters, number of tests

Detailed information about the testing programme is given in table 2.2.3. As can be seen, most of the influencing parameters have been investigated under two environmental conditions (air and seawater). The number of tests per series was generally four. For the basic test series, however, six or more experiments were carried out.

2.2.5.2. Details about the test condition

The experiments were carried out under constant amplitude loading (sine wave form) in pure bending condition. Most of the tests were carried out at a stress ratio of R = 0.1. Tests at R = -1 were also performed.

Fig. 2.2.8. shows schematically the TIG dressing procedure. Table 2.2.1. gives detailed information of the method. Fig. 2.2.9. shows a cross section of a TIG-dressed weld toe area together with the results of hardness measurements.

III. The manual Plasma dressing method involved , as with TIG dressing, remelting of the weld toe without addition of filler material. The plasma dressing procedure consisted also of two remelting runs. The second-tempering-run had nearly the same heat input as the first one and was located 2.5 to 3 mm from the first run in the direction of the original groove weld (see Fig. 2.2.8.) In. Fig. 2.2.11. a cross section and results of hardness measurements are given.
Visual inspection of the weld toe profile was applied during and after the dressing.
Fig. 2.2.12 shows the surface of some dressed weld toe areas by a:TIG dressing; b: Plasma dressing; c: TIG dressing of additional manufactured testspecimens (dressed by another welder).
For both the TIG- and the Plasma method the dressing was performed in vertical position in downhill direction with standard equipment.
Preheat and interpass temerature: 100-150^{o}C.

IV. Improved profile is achieved by increasing the flank angle of the weld as shown in Fig. 2.2.13.

2.2.3.5. Maximum hardness numbers

Figs. 2.2.7, 2.2.9, 2.2.10 and 2.2.12 show the cross sections as of the three finishing methods and, for comparison, one of an as welded specimen.
Results of hardness measurements are also given (HVN 10).
As can be seen in Fig. 2.2.10 the maximum hardness numbers in the heat affected zone of the base metal of specimen in the as welded condition are about 250-275 HVN 10.
Fig. 2.2.9. and Fig.2.2.11. show that the TIG-and Plasma dressing by means of two runs give acceptable maximum hardness numbers in the HAZ of the base metal.

2.2.3.6. Weld toe profile

The weld toe geometry (radius and flank angle) achieved by each of the four dressing methods was measured by means of measurements on cross sections of

2.2.3.3. Post weld heat treatment

The majority of the specimens with a thickness of 70 mm were stress relieved prior to testing. The 40 mm specimens were generally tested in the as welded (non-stressrelieved) condition. In some cases this general rule was abandoned in order to investigate the influence of applying/omitting stress relieving.

Stress relieving has been performed by heating up to 580°C ($\pm$ 20°C) at a mean rate of 200°C/hour (above 300°), holding time 2½ hours, followed by furnace cooling at a rate of 100°C/hour to below 300°C, after which air cooling was applied.

2.2.3.4. Finishing techniques

The influence of four finishing techniques was studied and these are designated as follows:

I Toe burr grinding
II TIG dressing
III Plasma dressing
IV Improved profile (which is not actually a weld finishing technique)

I. Toe burr grinding is achieved by grinding the weld toe with the burr tool as illustrated in Fig. 2.2.6.
This technique effectively removes undercuts and defects which occur at the weld toe region. The average depth of grinding at the weld toe was approximately 0.6 mm although depths of up to 0.9 mm have also been observed.
Fig. 2.2.7. shows a cross section of a weld toe region which was finished by grinding. An advantage of this finishing technique is that the surface score marks are parallel to the direction of the applied bending stress.

II. The manual TIG dressing procedure involved remelting of the weld toe using standard equipment for TIG welding without the addition of filler material. The method of TIG dressing consists of one single run on the melting line, followed by a second-tempering-dressing run with nearly the same heat input to avoid high local harndness values in the weld toe region. The second weld run was located 1.5 to 2.0 mm from the first run (see Fig. 2.2.8).

2.2.3.2. Details about welding

General information

Welding process : Manual metal arc welding
Welding position : Vertical
Welding direction : Uphill

Filler metals

Electrodes : Covered basic electrodes AWS code E 7016
Electrode diameters : ø 3¼ mm for the first two welds beads on each side of the root of the joint.
ø 4 mm for the following weld runs.

Preheat temperature : 110 - 150°C
Interpass temperature : 125 - 150°C
These temperatures were measured and recorded continuously by thermo-couples

Build up sequence

In Fig. 2.2.4 and Fig. 2.2.5 the build-up sequences are given of the 40 mm- and 70 mm full penetration welds respectively, as applied for the A-, B- and C-type specimens.
The pure fillet welds (no penetration) as applied for the D-type specimens were single pass welds (welding: vertical uphill) with a throat length of 10 mm.

Welding parameters

Welding current: ø 3¼ mm electrodes 110-125 A,
ø 4 mm electrodes 140-155 A.
Voltage : 24 - 27 V.

Cooling time of the weldbeads

The cooling time from 800 to 500°C of the welds beads was between 10 and 20 seconds. These values apply to both 40 mm and 70 mm weldments and were measured at the interpass temperatures mentioned earlier.

The three different configurations of the 70 mm transverse welded specimens are given in Figure 2.2.2.
Most of the specimens (A-, B- and C- types) were performed with full penetration welds. The thickness of the gusset(s) was the same as that of the main plate (40 mm and 70 mm).
Figure 2.2.3 gives schematically the geometry of the full penetration welds.
The groove preparation was performed by means of oxygen cutting.
Furthermore, T-shape specimens were manufactured with pure fillet welds (no penetration). This specimen type (designated as D-type in Figure 2.2.1) was only fabricated with a plate thickness of the main plate of 40 mm.

Each specimen was manufactured such that the longitudinal direction of the main plate was aligned parallel to the rolling direction of the plate.
The T-shape specimens (A-type) were manufactured by attaching a gusset transversely to the surface of the main plate by full penetration welding.
The cruciform specimens of the B-type (with non-load carrying welds) were manufactured by attaching two gussets transversely to the surface on both sides of the main plate by full penetration welding.
The cruciform specimens with load carrying welds (C-type) were manufactured by full penetration welding of two plates forming the main part of the specimens, to a short transverse plate with the same thickness as the main plate as shown in Figs. 2.2.1. and 2.2.2. (40 mm and 70 mm thickness respectively).

The specimens of all testseries were manufactured according to one general method, namely:
Three specimens were welded simultaneously without restraint.
The specimens were situated above each other, maintaining a gap between the individual mainplates of about 10 mm.
This gap was filled up with strips at the central part of the specimens, in order to avoid starts and stops at the specimens, during the welding.
After the welding the specimens were separated by removing the intersection at the central part of the specimen by means of oxygen cutting.

2.2.1. Introduction

This part of the programme involves the (corrosion-)fatigue testing (bending under constant amplitude loading) of welded plate specimens. For these tests, joints with transverse load-carrying and non-load carrying full penetration welds were selected because of their similarity with the weldgeometry of a typical brace to chord tubular joint. The variables being considered in this endurance part of the small scale testing are:

- Environment: - air
  - seawater (unprotected and cathodically (over)protected)

- Loading condition: - stress ratio R = 0,1 and R = -1
- Welding parameters: - as welded versus stress relieving
  - weld finishing (grinding, TIG- and Plasma dressing)
  - weld metal composition
  - type of welded joint
- Plate thickness : - 40 mm and 70 mm

The results of the experimental work are being presented in the form of S-N curves.
In addition to the fatigue testing, attention has been paid to strain gauge measurements and to fractography.
The straingauge measurements were envisaged to detect the time (number of cycles) and the location(s) of crack initiation, and to obtain information about crack development/crack growth.
The above mentioned (corrosion-)fatigue endurance tests were carried out at the Metal Research Institute NTO in Apeldoorn and the University of Technology in Delft; Ship structures Laboratory/Stevin Laboratory.

2.2.2. Material

The material of the specimens satisfied Euronorm 113-72, Grade FeE 355 KT requirements as described in detail in paragraph 2.2.1.

2.2.3. Specimens

2.2.3.1. Fabrication of testspecimens

Figure 2.2.1 illustrates the four specimen configurations of the transverse joints with a plate thickness of 40 mm.

Delft University of Technology
Department of Civil Engineering
Stevin Laboratory

2.2 ENDURANCE TESTS ON PLATE SPECIMENS

Delft, April 1981.

J.L.v.Leeuwen

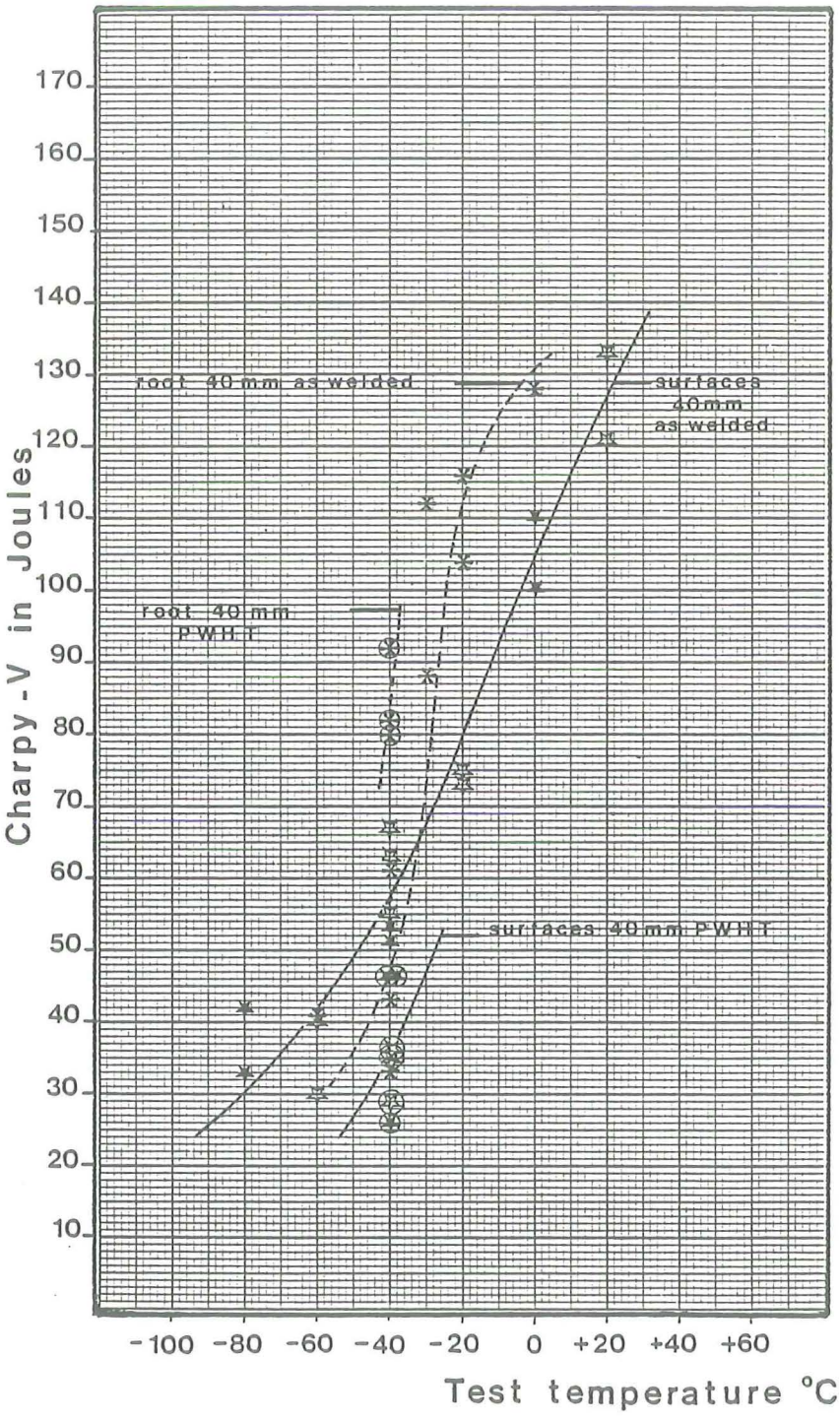

Electrode B2

AWS code E 8016 C1

position in weld	as welded	P.W.H.T.
S1	☆	⊛
S2	✶	⊛
R	*	⊛

Fig. 2.1.10 Charpy-V transition curves.

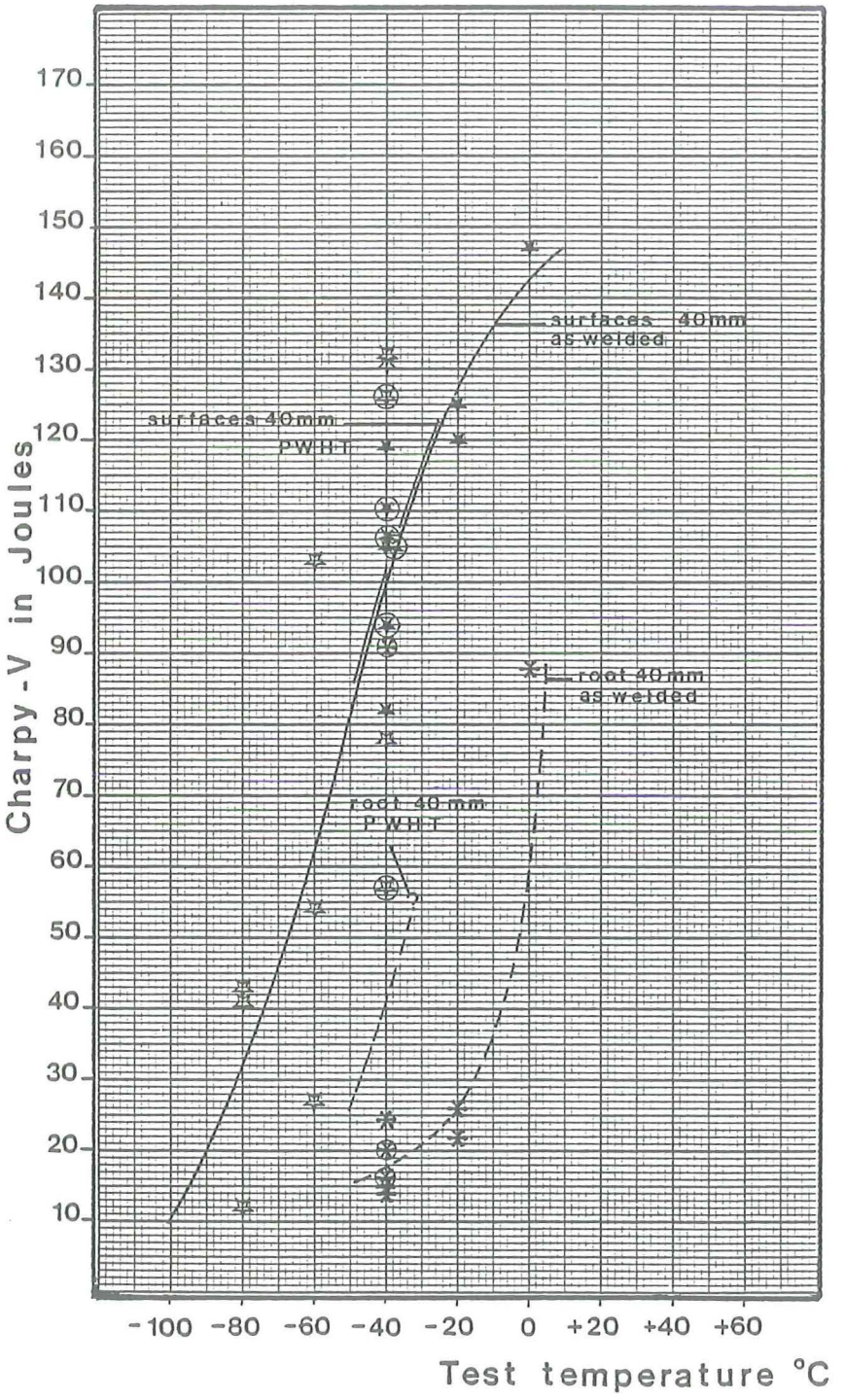

Electrode B1

AWS code E8016 C1

position in weld	as welded	P.W.H.T.
S1	☆	⊛
S2	✶	⊛
R	*	⊛

Fig. 2.1.9 Charpy-V transition curves.

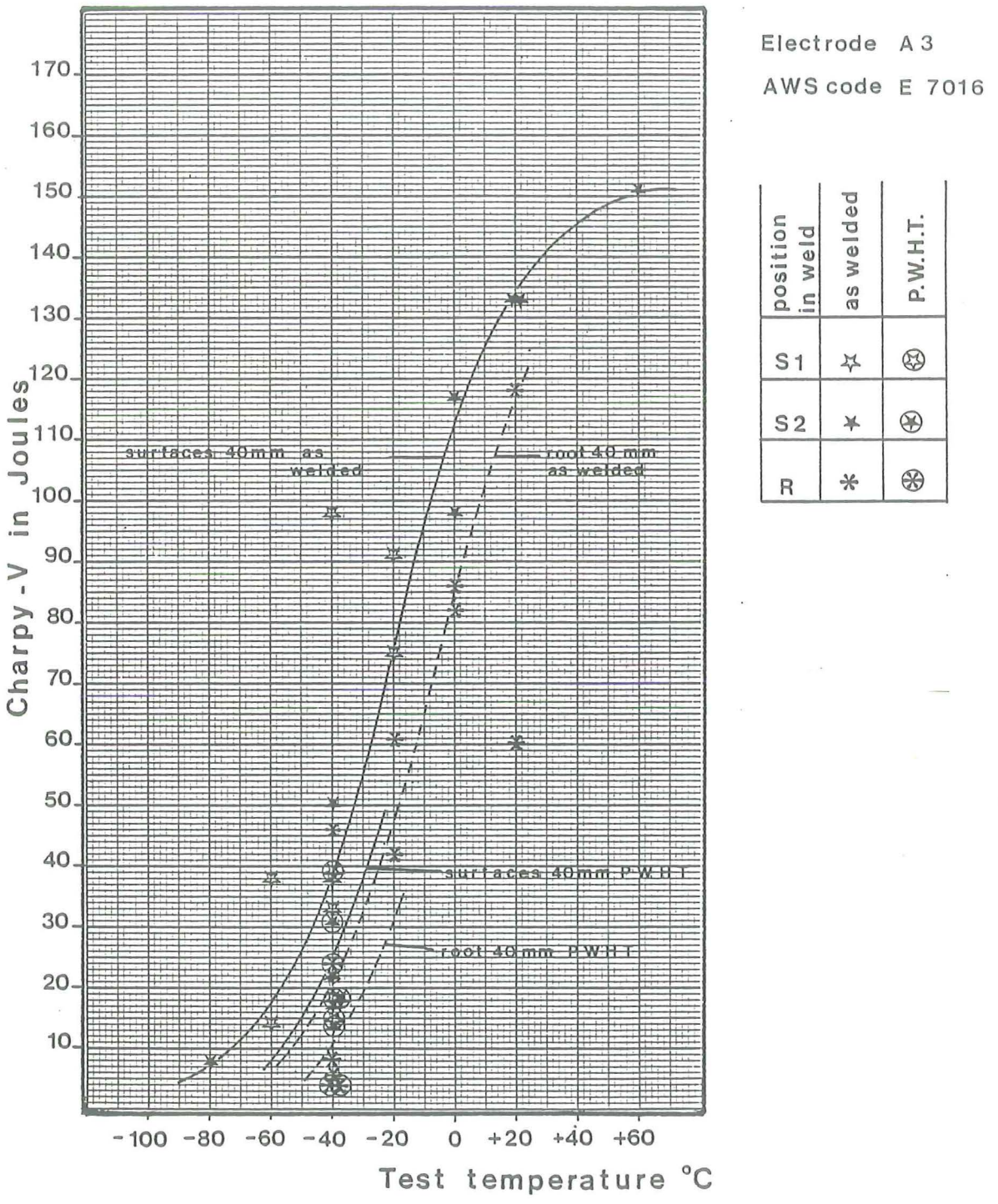

Fig. 2.1.8 Charpy-V transition curves.

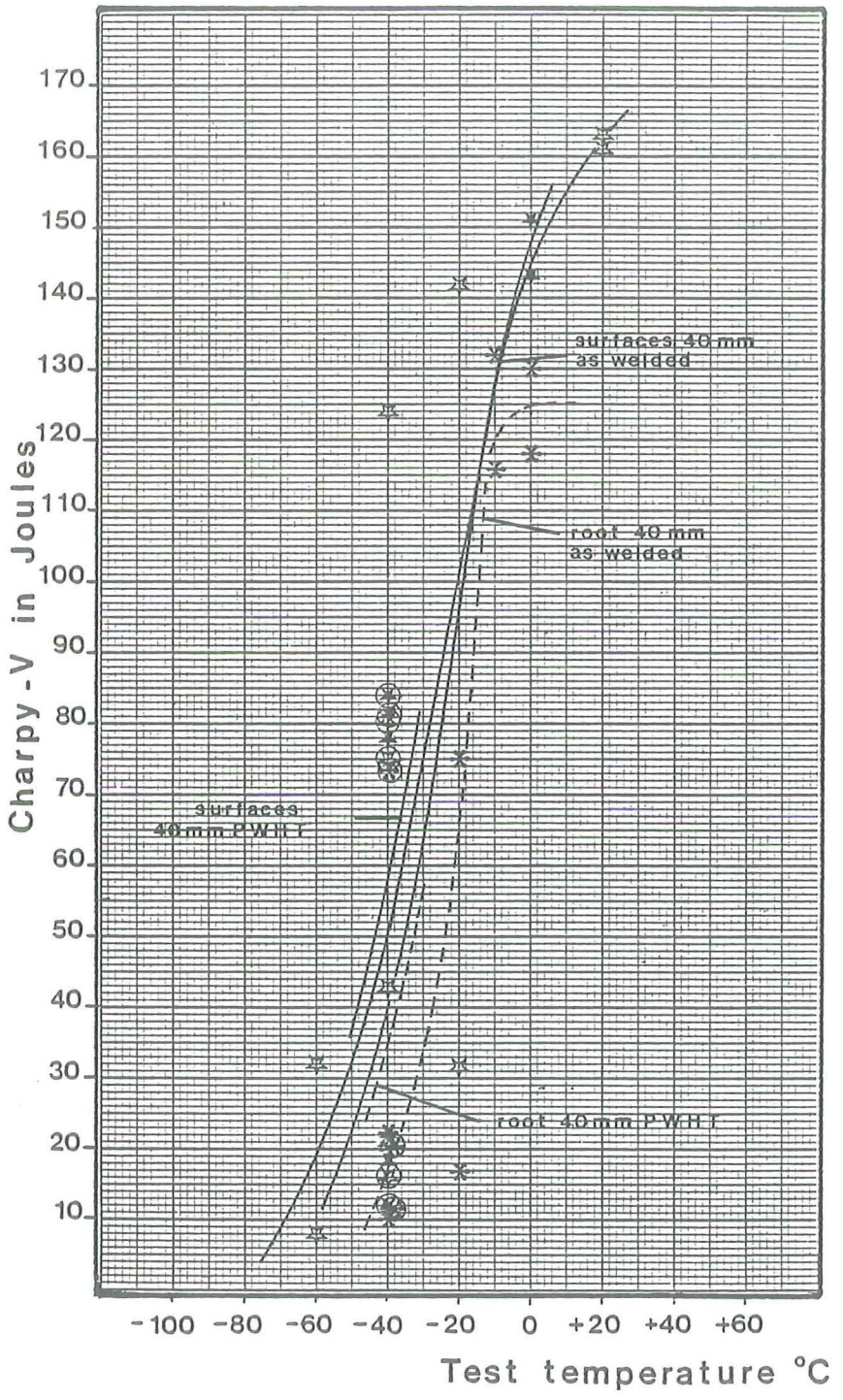

Electrode A2

AWS code E 7016

position in weld	as welded	P.W.H.T.
S1	☆	⊛
S2	✶	⊛
R	*	⊛

Fig. 2.1.7 Charpy-V transition curves.

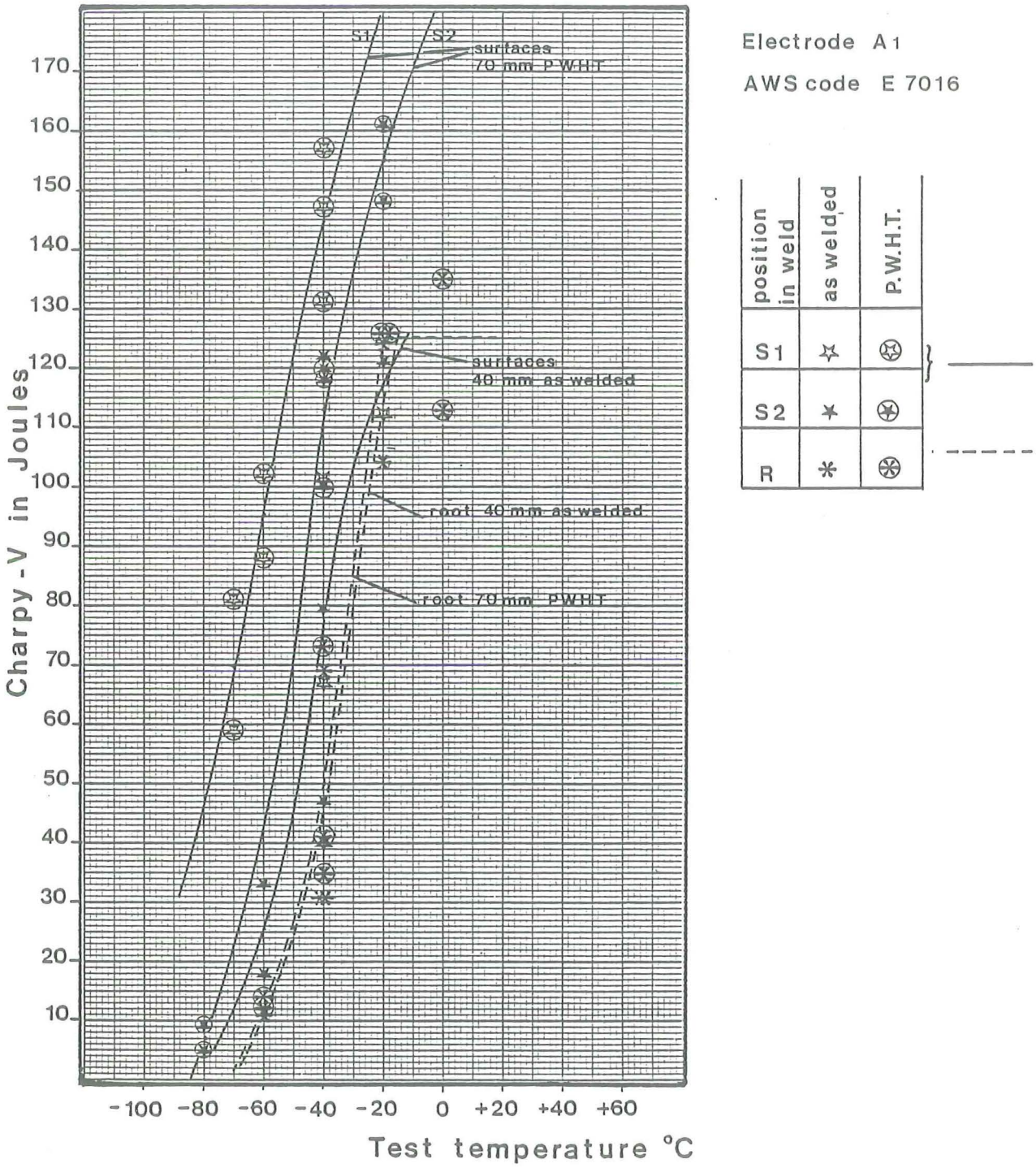

Fig. 2.1.6 Charpy-V transition curves.

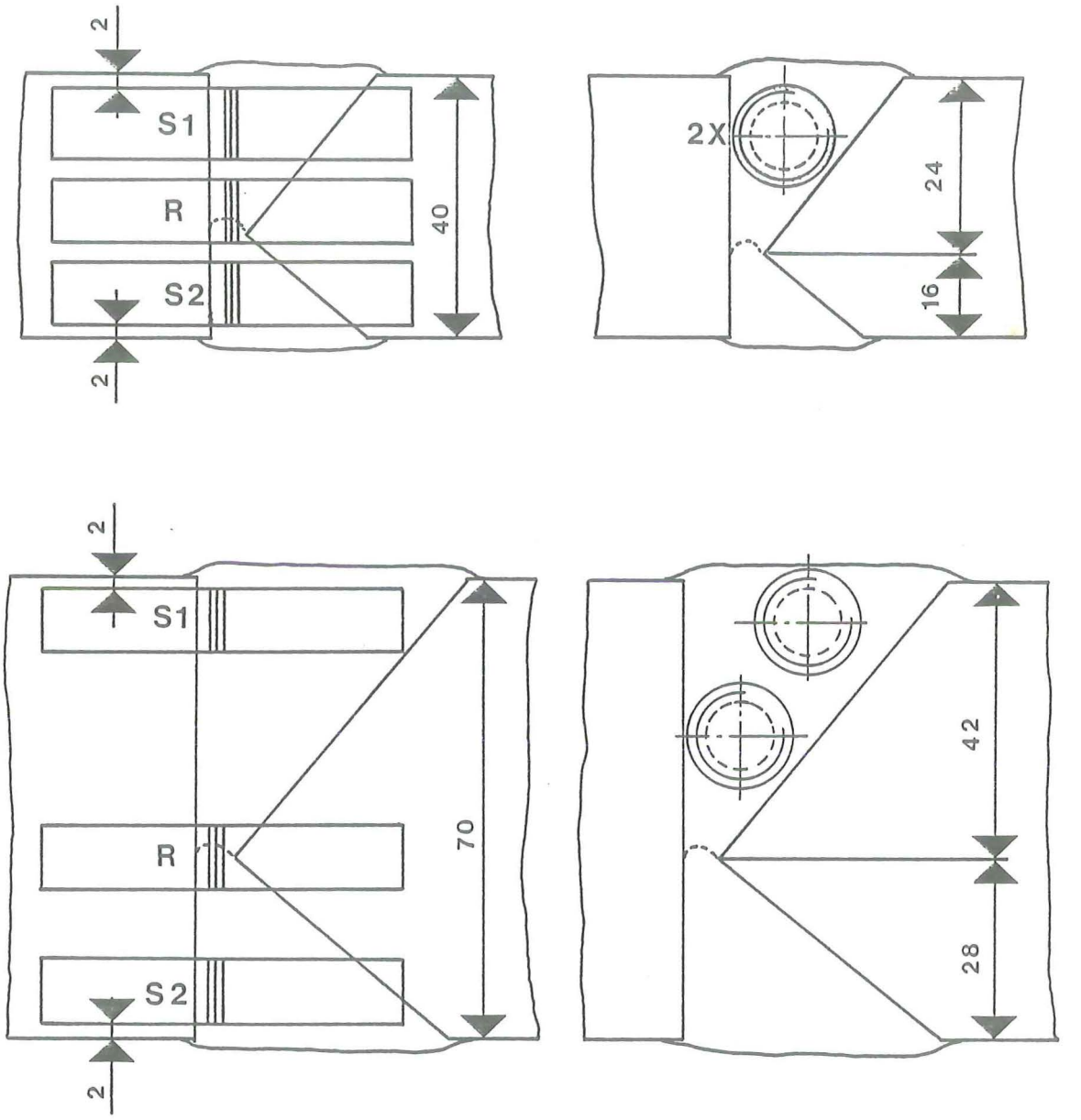

Fig. 2.1.5 Position of the Charpy-V specimens and the tensile bars in weld metal.

As deposited microstructure of weld metal B1.
(C-Mn 2½% Ni basic-electrode)
Average lineas intercept grain diameter ($d^{-\frac{1}{2}}$) for as deposited and heat affected regions: 11.5
Microstructural constituents: proeutectoid ferrite, ferrite side plates with aligned carbides and ferrite carbide aggregates.

Magnification: 200x
Nital etch

L 1333

As deposited microstructure of weld metal B2.
(C-Mn 2½% Ni basic electrode)
Average linear intercept grain diameter ($d^{-\frac{1}{2}}$) for as deposited and heat affected regions: 15.1
Microstructural constituents:
Fine acicular ferrite, proeutectoid ferrite and side plates ferrite.

Magnification: x 200
Nital etch.

L 1332

Fig. 2.1.4

As deposited microstructure of weld metal A1.
(C-Mn basic electrode)
Average linear intercept grain diameter ($d^{-\frac{1}{2}}$) for as deposited and heat affected regions: 13.0
Microstructural constituents: acicular ferrite, proeutectoid ferrite and side plates ferrite.

Magnification: x 200
Nital etch

L 1331

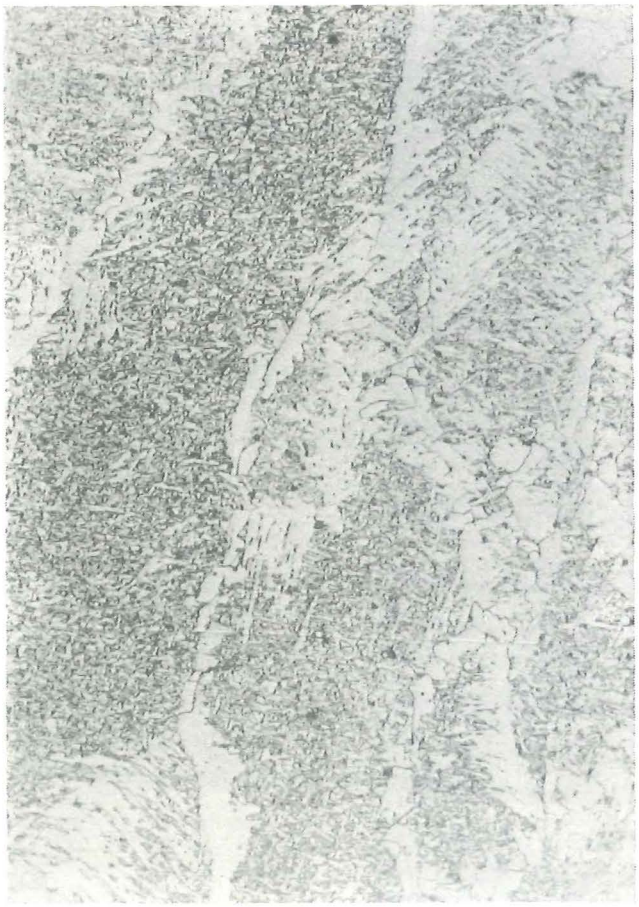

As deposited microstructure of weld metal A2.
(C-Mn basic electrode)
Average linear intercept. grain diameter ($d^{-\frac{1}{2}}$) for as deposited and heat affected regions: 13.0
Microstructural constituents acicular ferrite, proeutectoid ferrite and side plates ferrite.

Magnification: x 200
Nital etch

L 1330 Fig. 2.1.3

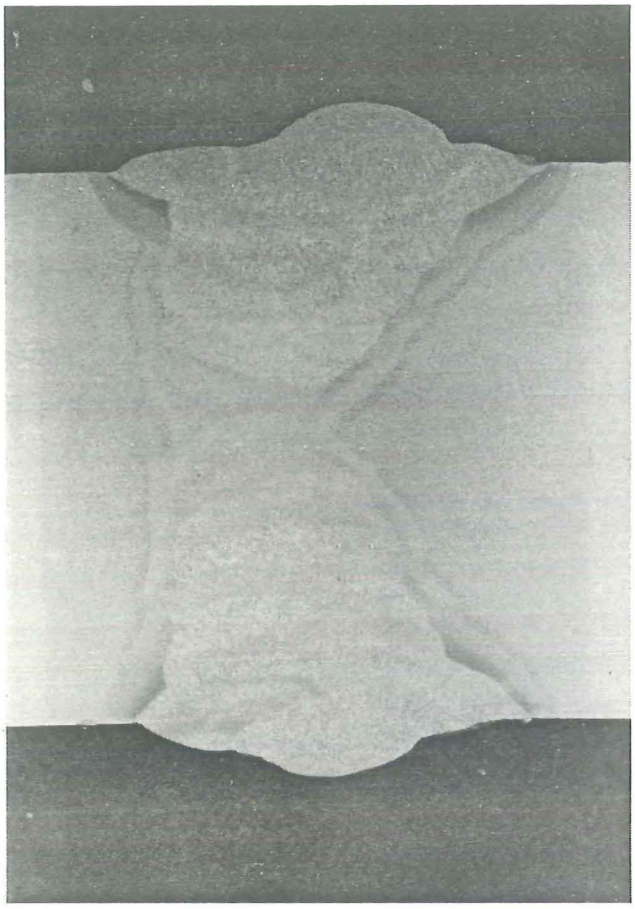

Transverse section of a 40 mm double bevel groove weld showing the weld building.

Electrode: A1
AWS: E 7016

L 1335

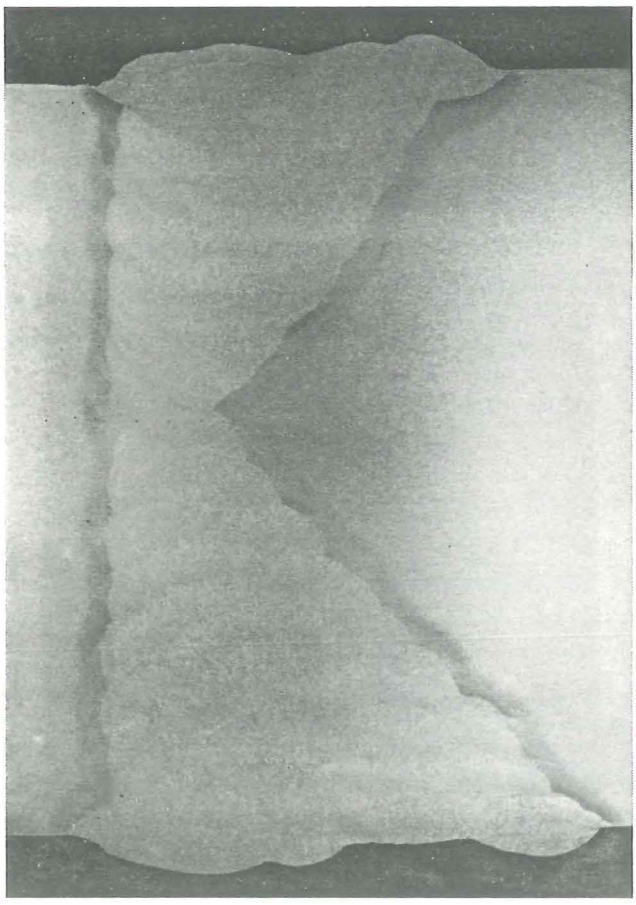

Transverse section of a 70 mm double bevel groove weld showing the weldbuilding.
Electrode: A1
AWS: 7016

L 1336

Fig. 2.1.2

2.1.5. Figures

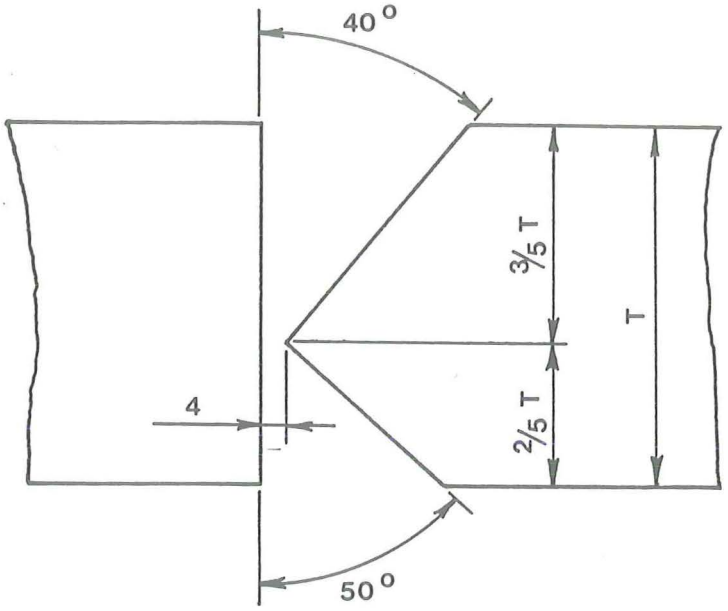

Fig. 2.1.1 Weld preparations in 40- and 70 mm steel plate.

Table 2.1.7 Results of tensile-, Charpy V- and COD tests.

Code electrode (see table 2.1.3)	Plate steel thickness	Condition*	Tensile tests****				COD-tests at -10°C		Charpy-V tests ** (J) (temperatures °C)								Weld position C_v tests
			Ra N/mm²	Rm N/mm²	A5 %	Z %	δci mm (init)	δc mm (max)	-80	-60	-40	-30	-20	-10	0	+20	
A1							0.067	0.067			69		112				S1
E 7016	40 mm	A.W.					0.041	0.041		25	83		121				S2
			484	585	25	73	0.231	0.236		11	44		114				R
id.								1.8		95	145					215	S1
	70 mm	PWHT						>1.8	7		113		156				S2
			428	540	26	71	-	1.6		13	50		126		124		R
A2							0.10	0.10		20	63		86			162	S1
E 70 16	40 mm	A.W.					0.03	0.03			39				147		S2
			479	580	24	70	0.06	0.03			17		46	124	124		R
							0.25	0.25			57						S1
id.	40 mm	PWHT	430	520	24	70	0.31	0.31			59						S2
							0.77	0.77			35						R
A3							0.16	0.16		26	56		83				S1
E 70 16	40 mm	A.W.					0.07	0.07	8		30				107	133	S2
			463	557	24	66	0.19	0.19			20		52		84	89	R
							0.15	0.15			24						S1
id.	40 mm	PWHT					0.10	0.10			21						S2
							0.33	0.33			14						R
B1							0.10	0.10	32	61	114						S1
E 80 16 C1	40 mm	A.W.					0.25	0.25			102		122		147		S2
			471	550	27	71	0.03	0.03			18		24		88		R
							0.41	0.41			96						S1
id.	40 mm	PWHT	430	520	27	70	0.69	0.69			103						S2
							0,61	1.13			42						R
B2							0.36	0.36		35	62		74			127	S1
E 80 16 C1	40 mm	A.W.					0.36	1.47	37		53				105		S2
			560	665	24	67				41	46	100	110		128		R
							-										
id.	40 mm	PWHT					0.39	1.44			39						S2
							0.67	2.06			85						R

* AW (as welded)
PWHT (post welded heat treated)

** Mean values (usually 3 test results)

*** S = surface 1 = first side
R = root 2 = second side

**** mean values (2 test results)

Table 2.1.5 Chemical composition of MMA weld metals

Type electrode	Chemical composition								
	C%	Mn%	Si%	P%	S%	Ni%	Mo%	N%	O%
A1	0.09	1.3	0.60	0.013	0.008	0.1	0.05	0.009	0.024
A2	0.07	1.0	0.57	0.016	0.008	0.1	0.05	0.012	0.030
A3	0.05	0.93	0.16	0.010	0.012	0.28	0.15	0.016	0.057
B1	0.06	0.53	0.27	0.013	0.008	2.3	0.05	0.012	0.042
B2	0.08	0.94	0.40	0.021	0.012	2.4	0.05	0.011	0.034

Table 2.1.6 Results of hardness measurements on AW welded test panels

Plate steel thickness	Position in welded joint	parent plate	Hardness survey (Hv 10)			
			HAZ1	weld metal	HAZ2	parent plate
40 mm	surface	175	260	210-190	275	175
	root	175	260	220-230	225	190
70 mm	surface	180	295	190-225	270	180
	root	180	225	220-240	240	210

Table 2·1.3 Characterisation of MMA electrodes

Code	Class (AWS)	Type electrode
A1	E 7016	C-Mn basic electrode
A2	E 7016	C-Mn basic electrode
A3	E 7016	C-Mn basic electrode (with about 0.5% Ni and 0.2% Mo)
B1	E 8016 C1	C-Mn 2½% Ni basic electrode
B2	E 8016 C1	C-Mn 2½% Ni basic electrode

Table 2.1.4 MMA welding details for 40- and 70 mm thick welded steel panels

Welding parameters	40 mm	70 mm
geometry	K	K
weaving	restricted (3x diameter)	restricted (3x diameter)
arc energy	1.8 kJ/mm	1.8 kJ/mm
welding current (Ac)	110-125 Amps[1)] 140-155 Amps[2)]	110-125 Amps[1)] 140-155 Amps[2)]
arc voltage	24 - 27 V	24 - 27 V
number of layers	18 - 21	40
preheat temperature	110 - 150 °C	110 - 150°C
interpass temperature	125 - 150°C	125 - 150°C

1) Ø 3¼ mm electrodes 2) Ø 4 mm electrodes

TABLE 2.1.2

Mechanical properties of steel plates [1]

Steel plate[2] (code)	Plate dimensions l(length) x w(width) x t(thickness) mm	Tensile tests				Charpy V (J) at -30°C -length direction[4]
		Ro.2 (N/mm^2)	Rm (N/mm^2)	Elongation % (d p 5)	Reduction in area (%) in thickness direction[3]	
71214	7000 x 2250 x 40	413	560	31.0	44.7	143
		403	540	31.0	-	-
71215	7000 x 2250 x 40	412	560	31.0	25.6	160
		415	564	33.0	44.3	-
71216	7000 x 2250 x 40	400	552	30.5	52.0	169
		406	561	30.0	28.6	-
71217	7000 x 2250 x 40	400	550	32.0	45.8	170
		418	554	29.0	46.8	-
V 9159	~ 5000 x 2100 x 70	383	535	32.0	61.7	164
		393	546	32.0	62.1	-
V 9160	5000 x 2100 x 70	379	541	33.0	46.6	146
		377	525	28.0	28.2	-
V 9161	5000 x 2100 x 70	382	537	32.0	61.9	153
		358	515	31.0	-	-
V 9162	5000 x 2100 x 70	382	539	30.0	58.4	161
		370	521	31.0	36.6	-
V 9163	5000 x 2100 x 70	388	541	30.5	62.3	152
		367	530	32.0	61.2	-

1) Mechanical properties at both sides of the steel plates

2) Steel plates have been ultrasonically tested and bend tests (with bend radii $1\frac{1}{2}$ t; t = thickness) have been performed.

3) Ø 8 mm bars with 40 mm thick steel plates, Ø 10 mm bars with 70 mm thick steel plates.

4) Average values of $3C_V$ tests.

TABLE 2.1.1

CHEMICAL COMPOSITION

Chemical composition in % x 10^{-3}												
	C	Mn	P	S	Si	Al tot	Cu	Sn	Cr	Ni	Nb	C.eq
Product analysis	170	1450	15	4	310	40	n.d	n.d	n.d	n.d	38	< 0.45%
Plate 71214**	177	1443	16	4	349	n.d	19	6	39	17	46	0.45

n.d. = not determined

** See Table 2.1.2

. The highest hardness values in welded steel joints can usually be observed in the weld root region.

. The lowest Charpy V values can usually be observed in the weld root region.PWHT can influence the transition temperature in both a positive and negative way.

. The COD weldmetal toughness requirements, often stipulated by certifying authorities for welded joints in offshore structures, for as deposited weld metals, can usually not be satisfied with C-Mn filler materials.

. Nickel bearing electrodes to the AWS E 80 18 - C1 type often give in as-deposited weld metals a superior low temperature weld metal toughness in COD terms than C-Mn electrodes (e.g. to the AWS E 7016 or E 7018 type). Work conducted by UKOSRP and TNO confirmed that it is true for some, but not all electrodes conforming to the E 8018 - C1 classification (Ref. 1).

. Post weld heat treatment (PWHT) usually has a beneficial effect on weld metal toughness in terms of COD (Ref. 1).

. The evaluation of weld metal toughness, on the basis of COD measurements, often shows high scattering results.
High scatter appears to be an inherent problem encountered in testing materials at temperatures within the brittle to ductile transition regime. The reasons for the scatter are not fully understood, but they are probably partly related to - local - weld microstructure variations (Ref. 1).

. No clearcut - simple - correlation exists between Charpy V and COD.

2.1.3. References to chapter 2.1.

|1| H.G. Pisarski
"A summary of fracture research conducted within the ECSC Marien Technology Exucutive Working Group II", Doc. WG-II-79 (November).

decrease as a result of postweld heat treatment (PWHT). Elongation and reduction of area were not significantly influenced by PWHT. Charpy V transition temperature curves have been determined for the weld metal in the root- and sub-surface region (see Figure 2.1.5) of all weldments and for some weldments also for the heat affected zone (Figures 2.1.6 till 2.1.10). The fracture path in the Charpy V test specimens was always in the direction of welding and the notch position perpendicular to the plate surface. The results of the Charpy V tests are tabulated in Table 2.1.7.
COD values have been determined for the various welded panels in AW and PWHT condition. The COD tests have been performed at -10 ^{o}C. The COD tests were carried out with 1 x 1 type specimens (subsidiary testpieces) according to BS Draft for Development DD19 "Methods for COD testing" with a through thickness crack perpendicular to the plate surface.
The effect of post weld heat treatment (PWHT) on fracture toughness has been studied by comparing COD values for AW condition and after PWHT.
It was necessary to use the technique of prepressing (2% deformation) for the AW-COD specimens to redistribute residual stresses in order to obtain a straight crack front after fatigue cracking.
COD values were always determined at maximum load plateau or maximum obtained load and in most cases also at the onset of stable crack growth (by PD technique). The results of the COD tests are tabulated in Table 2.1.7.

Discussion and evaluation

The welding procedure used for the fabrication of the welded steel panels has also been applied for the fabrication of the small scale test fatigue specimens. The fabrication of the small scale test fatigue specimens has usually been performed with a C-Mn electrode (code A1), some specimens have been made with another C-Mn electrode (code A2) and with a 2½ % Ni containing electrode (code B2). The fabrication procedure has been described more extensively in par. 2.2. It is impossible on basis of the present work to draw any definitive conclusions.
However, in considering the results of other characterization programmes some pertinent conclusions can be drawn.

. With tensile testing both yield and ultimate tensile strength of weld metals tend to decrease with post-weld heat treatment (PWHT). Elongation and reduction in area are usually not significantly influenced by PWHT.

The test panels were manual metal arc (MMA) welded. All welding (without restraint) was performed in the vertical-up position (3G position).
The consumables used for the fabrication of the test panels were basic-coated low-hydrogen type electrodes, produced by different manufacturers (Table 2.1.3). Welding details have been tabulated in Table 2.1.4. Back gouging together with some grinding was carried out on all welds. In order to diminish the risk of hydrogen cracking, a preheat temperature of 110-150 ^{o}C was maintained during gouging and welding. Interpass temperatures were limited between 125-150 ^{o}C. The arc-energy for the vertical up manual welds was about 1.8 kJ/mm. All electrodes were dried before use during one hour at 300 ^{o}C and stored at 100 ^{o}C.
Post weld heat treatment (PWHT) involved heating to 580 ^{o}C ($\pm$ 20 ^{o}C) at a mean rate of 200 ^{o}C/hr (above 300 ^{o}C) holding 1 hr/25 mm thickness at 580 ^{o}C, with afterwards furnace cooling at a rate of 100 ^{o}C/hr to 300 ^{o}C followed by air cooling.

Test procedure/test results

The welded test panels showed no significant defects on ultrasonic inspection (ASME code).
Chemical compositions of the MMA weld metals in the different welded steel panels are shown in Table 2.1.5.
Macrophotographs of both polished and etched transverse sections were taken from the welded test panels, to illustrate the weld run configuration. Characteristic macrophotographs are shown in Figure 2.1.2.
The microstructure of the weldments was studied with an optical microscope. The weld metal microstructure appeared to depend strongly on the type of electrode used (Figs 2.1.3 and Figs 2.1.4).
Hardness profiles were determined for some welded test panels with a Vickers pyramidal indenter with a load of 5 kg. The microhardness has been determined on both the root- and sub-surface positions. Table 2.1.6 shows the results of hardness surveys on two test panels viz.
- 40 mm test panel (as welded, E 70 16 - code A1 type electrode)
- 70 mm test panel (as welded, E 70 16 - code A1 type electrode)

The highest microhardness values were found to occur in the root region of a weld, as indicated by Table 2.1.6. The tensile properties (of full material) have been determined for all welded test panels (Table 2.1.7). Ultimate tensile stress and yield strength of the weld metals were found to

2.1.1 Steel (plate material)

The steel used for the fabrication of the welded panels for the fracture toughness characterization programme and for the fabrication of the small scale test specimens for the fatigue programme has been supplied by Hoogovens-ESTEL B.V. (Holland).
The steel, a normalized carbon-manganese steel, satisfied Euronorm 113-72, GRADE Fe E 355 KT requirements.
The steel was delivered in 2 plate thicknesses viz 40- and 70 mm.
The 40- and 70 mm steel plates came from the same steel heat.
Chemical composition and mechanical properties of the steel plates are described in Table 2.1.1 and Table 2.1.2.
The various steel plates had similar microstructures (pearlite varied between 20 and 25%, ASTM grain size (ferrite) varied between 10.5 and 11).

2.1.2 Weld procedure/weldment characterization

A characterization programme on welded test panels was performed for the selection of a welding procedure for the fabrication of the small scale test fatigue specimens.
The characterization programme involved the following:

- Fabrication of welded test panels
- NDT of welded test panels
- Chemical analysis and microstructural investigation (inclusive micro-hardness measurements) of weld metals
- Mechanical properties and fracture toughness properties (tensile tests, Charpy V tests, COD tests) of weldments.

Fabrication of welded test panels

The characterization programme was performed on 40- and 70 mm thick welded steel panels.
All welds in the 40- and 70 mm steel plates were made on plates with a length of 800 - 1000 mm and of about 300 mm width to produce test panels with overall dimensions of (800 - 1000) x 600 mm. The weld preparations used for the 40- and 70 mm steel plates are shown in figure 2.1.1.

Metal Research Institute TNO
Apeldoorn

2.1 MATERIAL

Apeldoorn, April 1981.

ir. G.H.G.Vaessen

CONTENTS

	Page
2.3. Random load tests on plate specimens	2-123
2.3.1. Introduction	2-125
2.3.2. Material and specimens	2-125
2.3.3. Environment and test frequency	2-125
2.3.4. Equipment	2-126
2.3.4.1. Testing machines	2-126
2.3.4.2. Machine input signal	2-127
2.3.5. Test conditions and results	2-128
2.3.5.1. Testconditions	2-128
2.3.5.2. Testresults	2-129
2.3.6. Discussion of results	2-130
2.3.6.1. Load spectra	2-130
2.3.6.2. Cumulative damage	2-130
2.3.6.3. The use of σ_{rms}	2-131
2.3.7. Conclusions	2-132
2.3.8. References to chapter 2.3.	2-133
2.3.9. Appendix 2.3.-I	2-134
2.3.10 Tables	2-138
2.3.11 Figures	2-140
2.4. Fatigue crack propagation tests	2-147
2.4.1. Introduction	2-149
2.4.2. Material; Welding consumables	2-149
2.4.3. Specimens	2-150
2.4.4. Equipment	2-151
2.4.4.1. Loading equipment	2-151
2.4.4.2. Measuring equipment	2-151
2.4.5. Programme	2-152
2.4.6. Discussion of results	2-153
2.4.6.1. Evaluation and presentation	2-153
2.4.6.2. Base metal in air	2-154
2.4.6.3. Base metal in seawater	2-157
2.4.6.4. Heat affected zone	2-157
2.4.6.5. Weld metal	2-159
2.4.6.6. Separate discussion of the results of some tests	2-160
2.4.7. Comparison with the results of other investigations on similar or related materials	2-161
2.4.8. Conclusions	2-164
2.4.9. References to chapter 2.4.	2-166
2.4.10 Tables	2-168
2.4.11 Figures	2-170

CONTENTS

	Page
2.1. Material	2-5
2.1.1. Steel (plate material)	2-7
2.1.2. Weld procedure/weldment characterization	2-7
2.1.3. References to chapter 2.1.	2-10
2.1.4. Tables	2-11
2.1.5. Figures	2-16
2.2. Endurance tests on plate specimens	2-27
2.2.1. Introduction	2-29
2.2.2. Material	2-29
2.2.3. Specimens	2-29
2.2.3.1. Fabrication of specimens	2-29
2.2.3.2. Details about welding	2-31
2.2.3.3. Post weld heat treatment	2-32
2.2.3.4. Finishing techniques	2-32
2.2.3.5. Maximum hardness numbers	2-33
2.2.3.6. Weld toe profile	2-33
2.2.4. Loading equipment	2-34
2.2.5. Experimental	2-34
2.2.5.1. Influencing parameters, number of tests	2-34
2.2.5.2. Details about the test condition	2-34
2.2.5.3. Environmental conditions	2-35
2.2.5.4. Straingauge measurements	2-36
2.2.5.5. Fractography	2-37
2.2.6. Testresults and discussion	2-37
2.2.6.1. Basic testseries	2-37
2.2.6.2. Influence of fatigue improvement techniques	2-39
2.2.6.3. Influence of post weld heat treatment and R-ratio	2-40
2.2.6.4. Influence of specimen type	2-42
2.2.6.5. Influence of weld metal composition	2-43
2.2.6.6. Influence of cathodic protection	2-44
2.2.6.7. Straingauge measurements	2-45
2.2.6.8. Crack initiation	2-46
2.2.6.9. Strain concentration measurements	2-47
2.2.6.10 Fractography	2-47
2.2.7. Comparison with the results of other investigations	2-48
2.2.7.1. Environment	2-48
2.2.7.2. Post weld heat treatment	2-48
2.2.7.3. Stress ratio	2-48
2.2.7.4. Weld finishing techniques	2-49
2.2.7.5 Cathodic protection	2-50
2.2.7.6. Effect of specimen thickness	2-50
2.2.8. Conclusions	2-52
2.2.9. References to chapter 2.2.	2-54
2.2.10 Appendix 2.2.-I "Fractographic analysis"	2-56
2.2.11 Tables	2-64
2.2.12 Figures	2-73

2. BASIC TEST

In these directions the growth rates can vary with the geometry of the joint and even with the load level.
This highlights the necessity to obtain data about crack depth.
The crack measurements reported here have been made along the weld toe but effort is going on to measure also crack depth in future.

Chapter 4 gives a general discussion of the results and a summary of the conclusions.

Environment	- air, seawater, cathodic protection
Loading condition	- constant amplitude tests, stress ratio, variable amplitude tests
Welding parameters	- Stress relieving Weld finishing techniques Weld metal composition Type of welded joints
Plate thickness	- 40 and 70 mm,

Chapter 2.1. gives information about the material used for fabrication and weld characterization and in chapter 2.2. the testprogramme, the fabrication of the test specimens, the test conditions and the results of the endurance tests have been described.

Complimentary to these endurance tests, crack propagation studies have been carried out (chapter 2.3.) to provide necessary information for the alternative method of fatigue analysis using linear fracture mechanics.

All these tests provide valuable information about the investigated parameters, however, the complex stress distribution which exists at the weld toe around the intersection welds between tubular members made it necessary to study the fatigue behaviour of real tubular joints.
For that reason a part of the programme deals with the corrosion fatigue testing of tubular T- and X joints of different sizes (chapter 3).
The first aim of this part is to provide more data from which a reliable S-N curve based upon hot spot strain or stress can be derived.
Strain measurements were therefore made and compared with finite element (FE) calculations and/or parametric equations for stress or strain concentration factors (SCF's or SNCF's).
Besides hot spot strain and number of cycles to failure, crack propagation was observed in all tests.
However, the application of linear fracture mechanics is complicated by the fact that the cracks grow in two directions:

- along the weld toe (and sometimes growing away from the weld toe in several directions).
- and through the thickness of the parent material.

1. Introduction

The shortage of world oil reserves together with the complex political and financial situation in the Middle East has led to an ever increasing demand for the exploitation of offshore oil and gasfields.

The movement of these offshore exploitations to deeper and rougher areas, for instance the North Sea, requires very large structures and the use of thick plate steels and constitutes special problems in designing fabrication (e.g. welding), material-selection, steelmaking etc.
This and the large amount of steel being used in these structures justified further research-work.
Essential for a safe design of new structures and the recertification of existing structures are reliable criteria for the fatigue analysis of welded tubular joints to avoid localized cracking at the nodes.
This means that the designer needs information about:

a) The fatigue behaviour of relevant joints (under the relevant environmental conditions).
b) The loading spectrum, the structure will see in service.
c) The stress analysis of the joints of the structure.

In calculating fatigue life, these three sources of information should be intergrated with the aid of an appropriate life prediction method.
Especially the knowledge about the fatigue behaviour of tubular joints in marine environment was very restricted.
Existing data on the fatigue cracking of steel structures were usually confined to those appropriate to land-based structures, constructed principally from flat plate elements and obtained from rather small size specimens.
However offshore structures are fabricated almost entirely from large tubular steel sections and are operating in a salt water environment.
Therefore an ECSC research programme has been carried out to extend the current knowledge about the (corrosion) fatigue behaviour of critical joints in offshore structures.
In this programme, conducted with financial aid of the ECSC, the UK, France, Germany, Italy and the Netherlands were participating.
This report describes the results of the Dutch part of this investigation.
Tests on real size tubular joints are complicated and expensive, so a number of important parameters were studied on plate specimens e.g.:

1. INTRODUCTION

0. Summary

This report deals with the Dutch part of the ECSC-Offshore Steels Research Programme. The aim of this investigation was to provide the designer of offshore structures with relevant data about the (corrosion) fatigue behaviour of tubular joints.
A number of parameters influencing the fatigue strength, such as:

environment, loading, loading condition, welding parameters and plate thickness, has been studied on 40 and 70 mm thick plate specimens.

Tests in seawater of 20^{o}C showed a reduction in fatigue life with a factor of 2-3 compared with the fatigue life in air.
Post weld heat treatment and weld finishing techniques were found to have a benificial effect on the fatigue life in air, however in seawater this beneficial effect is smaller. Cathodic protection results in longer fatigue lifes in the region of lower stress ranges.
In the region of higher applied stress ranges this favourable effect tends to disappear. No effect of the plate thickness was found for the tested specimen of 40 and 70 mm.

A number of variable amplitude tests were carried out. From these tests the validity of Miner's rule seems to be satisfactory.
To provide the necessary data for a fatigue analysis, using linear elastic fracture mechanics, crack growth studies have been carried out.
The complex stress distribution which exists at the weld toe around the intersection welds between tubular members made it necessary also to carry out (corrosion) fatigue tests on tubular T- and X joints of different sizes.
The results show a very significant size effect. The fatigue strength of large tubular joints is considerably lower than that of small joints. The influence of seawater is of the same order as found in testing plate specimens (a reduction in fatigue life with a factor 2-3). The test with cathodic protection does not show an improvement in fatigue life compared with seawater tests.
The fatigue strength of large joints at long lives is lower than expected.
It seems advisable to rotate the AWS-X design curve, in such a way that the slope will be steeper, the design lives at low stress levels shorter and at high levels longer.
How far the results of the other studied parameters on plate tests are valid for tubular joints will be checked in a second phase investigation.

ECSC CONVENTION 7210-KB/6/602 (J.7. 1 f/76)
FINAL REPORT

FATIGUE AND CORROSION FATIGUE BEHAVIOUR OF OFFSHORE STEEL STRUCTURES

By: J. de Back' and
G.H.G. Vaessen" et al.

Delft/Apeldoorn, April 1981

Investigation with financial aid of the
European Community of Steel and Coal.

' Delft University of Technology
Stevin Laboratory
Department of Civil Engineering

" Metal Research Institute TNO
Apeldoorn

Contents

0. Summaries

1. Introduction

2. Basic tests
   2.1. Material
   2.2. Endurance tests on plate specimens
   2.3. Random load tests on plate specimens
   2.4. Fatigue crack propagation tests

3. Tubular joint testing

4. General discussion of the results

5. Appendices